Battelle
Columbus Laboratories

Report

FINAL POST-FLIGHT REPORT

on

SPAR V
EXPERIMENT NO. 74-30
AGGLOMERATION IN IMMISCIBLE LIQUIDS
(Contract No. N58 31543)

to

NATIONAL AERONAUTICS AND
SPACE ADMINISTRATION
GEORGE C MARSHALL SPACE FLIGHT CENTER
ALABAMA

July, 1979

Principal Investigators:

S. H. Gelles and
A. J. Markworth

BATTELLE
Columbus Laboratories
505 King Avenue
Columbus, Ohio 43201

Battelle
Columbus Laboratories
505 King Avenue
Columbus, Ohio 43201
Telephone (614) 424-6424
Telex 24-5454

March 7, 1980

George C. Marshall Space Flight Center
National Aeronautics and Space Administration
Marshall Space Flight Center, Alabama 35812

Attention: PF11/Mr. Roger Chassay

Gentlemen:

Enclosed you will find eight copies and one reproducible copy of the approved final report on Contract NAS 8-31543, "Rocket Experiment 74-30: Agglomeration in Immiscible Liquids at Low G". This report covers all work conducted under the subject contract.

Additional distribution of this report was made as follows:

AP29F	0*
AS24D	3
AT01	1
EM63-12	1
DCAS	0*
PF11	8**

*Copy of letter of transmittal only.

**Plus a reproducible (Camera - Ready)

Should you have any questions or comments regarding this report, please call me at (614) 424-7603.

Very truly yours,

Kenneth E. Meiners
Manager
Materials Processing

KEM:klh

xc: Stan Gelles
S.H. Gelles Associates
2840 Fisher Road
Columbus, Ohio 43204

FOREWARD

This report was prepared by Battelle's Columbus Laboratories under NASA Contract No. NAS8-31543 entitled "Rocket Experiment 74-30: "Agglomeration in Immiscible Liquids at Low G" for the George C. Marshall Space Flight Center of the National Aeronautics and Space Administration. Mr. Roger Chassay is the principal COR. Data on this program are recorded in Battelle's Columbus Laboratories Research Notebook 32085 and 33314.

ABSTRACT

This report describes a research effort, the overall objective of which is to understand the influence of gravity, cooling rate, and composition on the macro- and microstructure of liquid-phase immiscible alloys. Al-In alloys of compositions 30, 40, 70, and 90 weight percent indium have been processed aboard two sounding rocket flights, SPAR II, and SPAR V. The SPAR II flight experiment capsule included the 40 and 70 weight percent indium alloys and was processed by heating to 970 C, holding at this temperature for 15 minutes, and then rapdily cooling through the miscibility gap and solidification temperatures while in the microgravity environment. Comparative ground-base samples were similarly processed.

Radiographic and metallographic examination of the SPAR II flight and ground-base samples showed the expected separation at 1-g of the ground-base alloys into indium-rich and aluminum-rich layers. The flight alloys, however, produced unexpected results. Instead of the fine uniform structures expected, an aluminum-rich core surrounded by indium-rich metal was found.

A number of possible mechanisms were suggested to explain the origin of the massive separation. One of these, namely the possibility that the alloys were not homogeneous at the start of the cool-down, was made the subject of an extensive ground-base program and the prime motivation for the SPAR V experiments.

The Post-SPAR II ground-base experiments included spin-up/despin simulations and liquid-phase interdiffusion measurements and analyses. The spin-up/despin tests demonstrated the ineffectiveness of this motion in providing measureable mixing and thus supported the inhomogeneity hypothesis. The liquid-phase diffusion measurements and analyses indicated that if diffusion were the only mechanism available for homogenization, the holding time of 15 minutes used in the SPAR II experiment was insufficient.

The SPAR V experiment was primarily design to determine whether suspected inhomogeneity in the liquid phase contributed to the observed

segregation. SPAR V was conducted in a manner similar to SPAR II but incorporated a hold-time of 16 hours at the homogenizing temperature. Four Al-In alloys; 30, 40, 70, and 90 weight percent indium, were processing in this flight and on the ground but with a somewhat slower cooling rate. The results obtained from the SPAR V 40 and 70 weight percent indium alloys were essentially identical to those from SPAR II. The 30 and 90 weight percent indium alloys also showed massive separation into configuration similar to the 40 and 70 weight percent indium alloys. The 90 weight percent indium alloy showed additional mportant evidence that surface-tension induced droplet migration had occurred in this alloy which could at least in part account for the observed structures.

Because of the similarity between the SPAR II and SPAR V results, it was concluded that the SPAR II specimens must have been homogeneous at the start of cool-down. This conclusion, coupled with observation of wave-like structures and oscillatory convection occurring during DTA experiments, indicate that surface-tension drive fluid motion was probably present during the processing of these alloys. Recommendations for further work to confirm some of the suggested mechanisms are included in the report.

TABLE OF CONTENTS

TABLE OF CONTENTS
(Continued)

LIST OF FIGURES

LIST OF FIGURES
(Continued)

LIST OF TABLES

LIST OF TABLES
(Continued)

FINAL POST-FLIGHT REPORT

on

SPAR-V EXPERIMENT NO. 74-30
AGGLOMERATION IN IMMISCIBLE LIQUIDS

to

NATIONAL AERONAUTICS AND SPACE ADMINISTRATION

from

BATTELLE
Columbus Laboratories

by

S. H. Gelles and A. J. Markworth

July, 1979

INTRODUCTION AND SUMMARY

Background

Immiscible liquid systems as defined in this study are those material systems containing a liquid-phase misicibility gap, i.e., a field in the phase diagram representing an equilibrium between two liquids of different composition. At a sufficiently high temperature, the two-phase equilibrium is replaced by a single-phase liquid field. The present study is primarily devoted to metallic liquid immiscible systems and in particular to a model system, Al-In.

The Al-In phase diagram as determined by Predel[1] and checked in the present study is shown in Figure 1. The miscibility gap extends from above the monotectic temperature of 640 C to the upper consolute temperature of ∿820 C. The composition extremes range from the monotectic composition of 17.5 to 96.8 weight percent indium.

There are a large number of liquid-phase immiscible materials. Reger[2], for example, has listed over 500 systems which contain or were suspected of containing liquid-phase miscibility gaps. A number of these

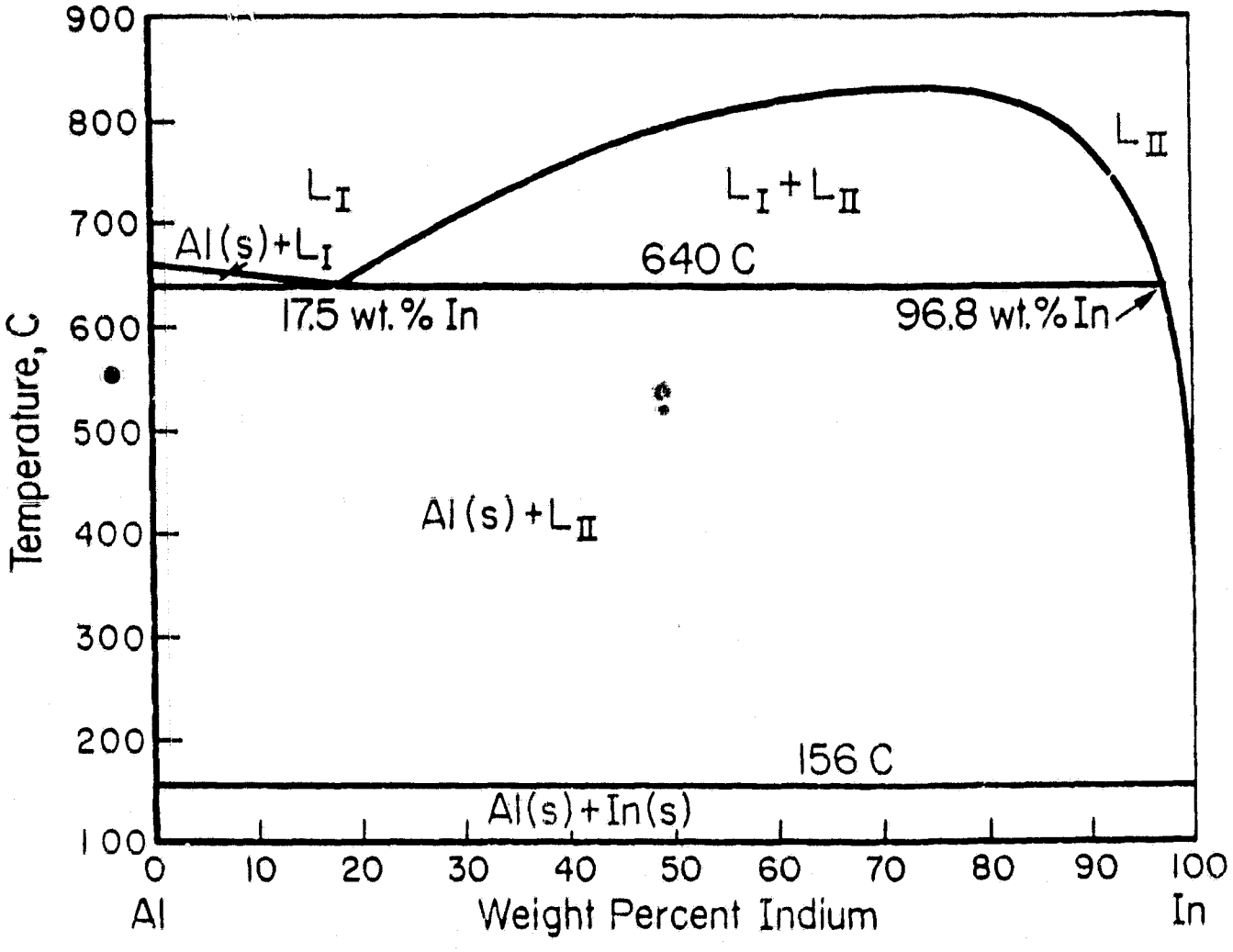

FIGURE 1. Al-In EQUILIBRIUM DIAGRAM[1]

systems are presently being used in such applications as electrical contacts, permanent magnets, and bearings. There are many other potential applications, for example, superconductors, superplastic materials, and catalysts. These applications and the role of processing these materials in space have been the subject of NASA sponsored programs at Battelle's Columbus Laboratories.[3,4]

If the coexisting liquids present within the miscibility gap have measurable density differences, there will be a great tendency for the materials to segregate and coalesce. Since Stoke's flow and convection are minimized in the absence of gravity, it was anticipated that droplet coalescence and segregation resulting from these movements would be virtually eliminated at low g.[5] This fact should, at least in theory, allow the production of materials containing a fine distribution of one phase contained within a matrix of a second phase.

The low-gravity environment also offers an opportunity to study the phase separation process without a major influence from gravitational effects. Thus, effects that may be masked by gravity on earth can likely be studied more efficiently at low g.

Overall Objective

The overall objective of this study is to gain an understanding of the influence of gravity, cooling, rate, and composition on the structure of liquid-phase immiscible systems.

Program Outline

Experiments involving four alloy compositions in the Al-In system were conducted on Sounding Rocket Flights SPAR II and SPAR V. A detailed description of the SPAR II flight and ground base experiments has been previously published[6,7] and is summarized in the present report for the sake of completeness and for the purposes of comparison with the SPAR V results. During the experiments, all of the flight and ground-base specimens were subjected to a homogenizing treatment at 970 C and were then rapidly cooled to room temperature.

The SPAR II experiments provided unexpected results in the form of massive separation of the aluminum-rich and indium-rich phases. After careful analysis of the SPAR II experiments, it was concluded that in all likelihood, the alloys were not homogeneous at the start of cool-down. The suspicion prompted a detailed ground-base study dealing with such subjects as the degree of mixing to be expected from rocket spin-up and despin and the liquid-phase diffusion characteristics of Al-In alloys. The results of these ground-base investigations have shown that little mixing is expected from rocket spin-up and despin. Furthermore, it was determined that the homogenizing time used in SPAR II was insufficient to produce a uniform composition if it is assumed that the only mechanism for available homogenization is diffusion. Accordingly, the SPAR V experiment was designed to insure that the alloys were homogeneous before cool-down by increasing the holding time at 970 C. A summary of the SPAR II and SPAR V experiments as well as the intermediate ground-base research follows.

Review of the SPAR II Experiment

The specific objective of this experiment was to determine the effect of gravitational acceleration on the macro- and microstructure of an Al-40 and Al-70 In alloy cooled through the miscibility gap at a rate of approximately 15 C/second.

The flight experiment, which was processed May 17, 1976, incorporated both alloy samples contained in separate crucibles within a single cartridge. The samples were held at 970 C for 15 minutes on the ground prior to launch. Approximately 154 seconds after launch, the flight samples were cooled at a rate of ∿14.7 C/second. A comparative ground-based sample was processed in a similar way but with an average cooling rate of 17.9 C/second. The flight sample was solidified completely while still at low g.

Post-flight analysis of the macro- and microstructures of the Al-40 and -70 In alloys showed rather unexpected results. Instead of the expected fine dispersion of indium-rich particles within an aluminum-rich matrix, the structures consisted of a massive aluminum-rich core surrounded by indium-rich metal. In the case of the -40 In alloy, the shape of the aluminum-rich phase was constrained by the crucible dimensions. However,

in the -70 In alloy, the aluminum-rich core assumed a roughly spherical geometry. The microstructure of the aluminum-rich portion of the alloys consisted of large drops of indium-rich metal contained in the aluminum-rich host as well as a fine distribution of indium-rich particles (presumably the result of the monotectic decomposition). In the indium-rich material, two types of aluminum-rich phases were found; aluminum-rich spheres which result from droplet precipitation within the miscibility gap and aluminum-rich dendrites which result from the precipitation of solid aluminum within an indium-rich liquid.

A number of mechanisms were suggested and some analyzed to explain how the massive separation might have occurred. Among these were residual fluid motion, conventional convection, surface tension driven flows and non-homogeneous starting material. The last of these items appeared to be highly probable, and was thus made the subject of extensive ground-base research and the SPAR V flight experiment.

Post-SPAR II Ground-Base Experiments

Three types of experiments were carried out for the purpose of assessing the degree of mixing and homogenization that might be expected after a 15-minute hold at 970 C and the spin-up/despin motion occurring during rocket flight. The following experiments were conducted:

(1) Spin-up/despin experiments
(2) Differential thermal analysis (DTA) measurements of equilibrium kinetics
(3) Direct measurements of interdiffusion coefficients in liquid Al-In alloys.

Spin-Up/Despin Experiments

The spin-up/despin experiments simulated the action of the rocket on a single phase liquid having a sharp concentration gradient above the consolute temperature. A layer of water saturated with copper sulphate set below a layer of pure water contained in a transparent vial made up the

system used to simulate the single phase liquid Al-In alloys. The samples were spun-up on a turntable to speeds of 246 RPM (simulating the spin-up to 240 RPM of the rocket while being photographed. The compositional changes occurring during this motion were qualitatively followed by the color variation imparted by the blue copper sulfate solution. The parameters varied in the experiments were (1) the relative amounts of copper sulfate solution and water, and (2) the presence or absence of an air gap or wetting agent.

A major conclusion from the spin-up/despin simulation is that little in the way of mixing occurs as a result of this motion. The major disturbance is confined to the region of highest concentration gradient adjacent to the original interface between the copper sulfate solution and water.

DTA Experiments - Approach to Equilibrium

Differential thermal analysis was used to determine the rate of homogenization of liquid Al-In alloys by measurement of the apparent consolute temperature as a function of holding time at 970 C. These studies were carried out on three alloys, Al-40.1, -70.1, and -76.0 In. The most extensive series of measurements was conducted on the Al -40.1 In alloy. The results show that a holding period of 8 hours is required to produce an equilibrium value of the consolute temperature. This observation corresponds to a value for the interdiffusion coefficient of 8×10^{-5} cm^2/second. Equilibrium values of the consolute temperatures were obtained for the Al- 40.1 and - 76.0 In alloys and were found to agree reasonably well with the values obtained by Predel.[1] It should be noted that some of the DTA curves obtained for these alloys displayed oscillatory behavior which has been attributed to the presence of oscillatory convective flows in the melt.

Liquid Phase Interdiffusion Considerations

A series of computations have been made of the product of interdiffusion coefficient, D, and time, t, to produce a uniform composition for

the geometrical configuration of the SPAR alloys. These calculations are based upon a solution of Fick's diffusion equations for the applicable boundary conditions.[8] Values of Dt equal to 0.5 have been computed for producing homogeneity within 1 percent (absolute) of the intended compositions in the 40 and 70 weight percent indium alloys.

A series of direct measurements of the interdiffusion coefficients of liquid Al-In alloys have been carried out at 970 C in 1 mm inside diameter capillary tubes. Samples have been held at this temperature for 1 or 4 hours and then rapidly cooled. They have then been metallographically polished along a central longitudinal plane and subjected to electron beam microprobe analysis in order to obtain composition as a function of distance along the length of the diffusion couple. The interdiffusion coefficients have been determined from a least-square fit of the data with computed composition-distance curves for various values of D. The computer codes used account for the changes in dimension on cooling from 970 C, where the diffusion occurs, to room temperature, where the electron beam probe measurements are made.

The average obtained from these measurements is 8.1×10^{-5} cm^2/second. This compares reasonably well with the average values of 4.8×10^{-5} cm^2/second calculated from the in situ measurements made by Dr. L. Lacy of Marshall Space Flight Center by a radiographic technique and with the $\sim 8 \times 10^{-5}$ cm^2/second value obtained from DTA measurements. Based on an average value for the diffusion coefficient of 6.4×10^{-5} cm^2/second (average value of present measurements and those of Lacy) and the calculated value for Dt equal to 0.5, a time period of 2.2 hours is anticipated as the required duration for producing homogeniety in the SPAR Al-In alloy samples assuming diffusion is the only process by which homogenization can take place. Hence, it was concluded that an insufficient hold time was used on the SPAR II experiment.

SPAR V Flight Experiment 74-30

The objective of this experiment was to determine whether the concentration gradients thought to be present in the SPAR II samples at the start of cool-down were the cause of the observed massive separation. The hold time of 16 hours at 970 C was chosen as a reasonable homogenizing

time. This represents a safety factor of ∿7 over the 2.2 hour time period calculated on the basis of the measured diffusion coefficient and the solutions to Fick's equations.

Beside the 40 and 70 weight percent In alloys, which were the same composition as used in the SPAR II experiment, two other alloy compositions were processed; 30 and 90 weight percent In. The 30 weight percent In alloy was chosen in order to investigate the effect of lower indium droplet concentrations on phase separation whereas the 90 weight percent In alloy was selected to investigate the propensity of the primary phase to precipitate at the crucible walls.

The cartridge design used in the SPAR V samples was basically the same as that used in SPAR II. The 40 and 70 weight percent In alloys were contained in one capsule while the 30 and 90 weight percent In alloys were contained in a second one. The only deviation in the design was the absence of an internal thermocouple within the capsule containing the 30 and 90 weight percent In alloys.

The SPAR V flight samples were processed on September 11, 1978, but not without some deviations from the original plan in the form of a failed internal thermocouple in the capsule containing the 40 and 70 weight percent In alloys and in a somewhat lower cooling rate (10 C/sec versus the desired 15 C/sec). The latter deviation provided the complication that the alloys were not completely solidified within the lower gravity time period.

After processing, the flight and comparably prepared ground control samples were examined radiographically and by optical microscopy. The results obtained for the 40 and 70 weight percent In alloys were very similar to those previously obtained in the SPAR II experiments. The flight samples, once again, have a structure consisting of a macroscopically sized aluminum-rich core surrounded by an indium-rich alloy. Likewise, the ground control samples had typical layered structures. Some subtle differences in the microstructures of the SPAR II and SPAR V ground control samples could be attributed to differences in cooling rate.

The structures of the 30 weight percent In alloys were quite similar to those of the 40 weight percent In alloys and thus provided little further understanding of the phase separation process. The 90 weight percent In alloy, however, did provide some new insight into the mechanisms that may be contributing to massive phase separation. Most notable among the observations made on the alloy is the presence of an annular zone denuded of aluminum-rich spheres around the massively separated aluminum-rich core. This observation, coupled with the fact that there is an increasing concentration of aluminum-rich spheres close to the central core, has provided evidence supporting the theory that the aluminum-rich spheres have migrated from the outer regions of the alloy into the interior, presumably under the action of surface tension gradients. These observations have been analyzed according to a formulation previously used by Bewersdorff[9] and found to be consistent with that mechanism. An alternative interpretation, that of particle pushing by an advancing indium solidification front, has been ruled out on the grounds that the observed coalescence of the aluminum-rich spheres would not be expected for solid aluminum spheres at the melting point of indium ($\sim$ 155 C). Evidence for particle pushing, however, has been observed elsewhere in the SPAR samples. In this case, agglomeration of the particles has been observed but not coalescence. The particle pushing mechanism does not appear to have contributed significantly to the massive coalescence that has been observed in all the Al-In SPAR II and SPAR V samples.

In addition to the surface tension driven migration of the aluminum-rich spheres, there is mounting evidence to indicate that surface tension driven fluid flows arising at the liquid-gas or liquid-liquid interfaces induce appreciable convection currents within the alloys during the homogenization and phase separation processes. Such flows can originate from temperature or concentration gradients and would contribute significantly to the observed massive separation. Evidence for this behavior has been obtained in the following forms.

(1) A number of wave-like structures have been observed both in the flight and ground base samples.

(2) Oscillatory temperature fluctuations have been observed in DTA samples undergoing phase separation.

(3) The SPAR II samples appear to have been homogenized after a 15-minute hold time even though the theoretical hold time necessary as calculated from diffusion considerations is 2.2 hours.

A number of experiments have been suggested to follow-up on these suggested mechanisms.

DETAILED PROGRAM DESCRIPTION

Review of the SPAR II Experiment

The SPAR II experiment which was flown May 17, 1976, has been described in detail in a Post Flight Summary Report[6] and in an AIAA publication[7]. For the sake of completion, we will include here a brief description of the SPAR II flight and ground-base experiments and a summary of the results.

The specific objective of the SPAR II experiment was to determine the effect of gravitational acceleration on the macro- and microstructure of an Al-40 and an Al-70 weight percent In alloy cooled through the miscibility gap at a rate of $\sim$ 15 C per second.

Sample Configuration

The sample configuration used in the SPAR II experiments (and later used in one of the SPAR V samples) is schematically shown in Figure 2. The alloy components in proper proportion were contained in separate aluminum oxide crucibles especially machined for a close fit with the internal dimensions of the stainless steel cartridge. The samples were carefully prepared by initially melting the components in high vacuum and then by sealing them in the cartridge under a partial pressure of helium. The

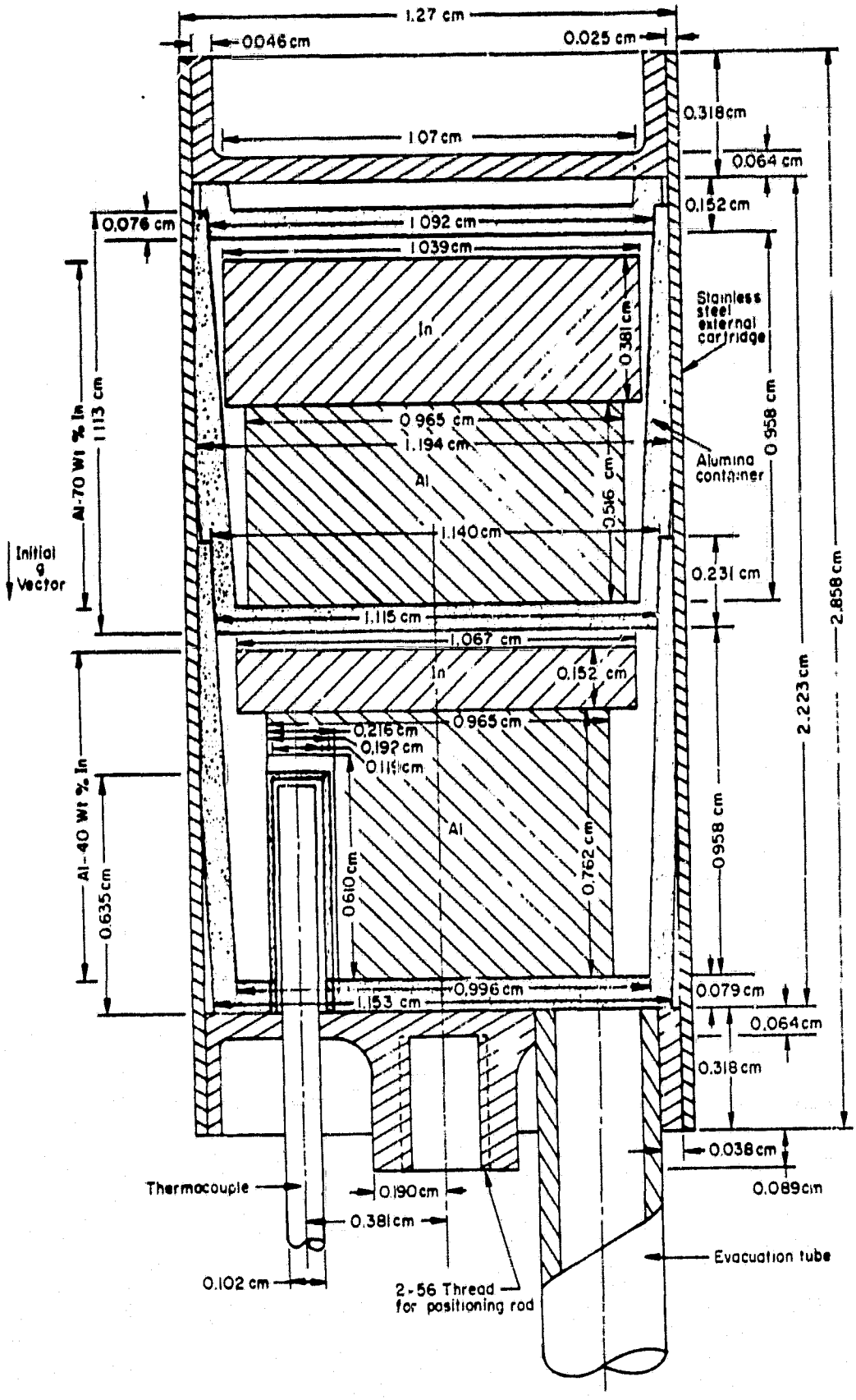

FIGURE 2. SCHEMATIC DIAGRAM OF EXPERIMENT CARTRIDGE

helium pressure level was chosen so that the cartridge contained slightly less than one atmosphere (0.1 MN/m^2) of pressure at the maximum temperature, 970 C. Provision was made for measurement of the sample temperature through introduction of an internal inconel sheathed chromel-alumel thermocouple into the capsule.

Flight Procedure

The stainless steel cartridge containing the two alloys was heated to $\sim$ 950 C in the rocket for 15 minutes before launch. This temperature corresponds to positions in the Al-In equilibrium diagram within the homogeneous single phase liquid field above the miscibility gap (See Figure 1). The alloys were allowed to remain at this temperature during launch and for $\sim$ 154 seconds after launch. Accelerations decreased to $< 4 \times 10^{-5}$ g $\sim$ 91 seconds after launch so that a time period of $\sim$ 63 seconds was available for the damping of any residual fluid motion in the specimen. At the end of this stabilization period, the samples were rapidly cooled by means of helium gas which was allowed to flow around the periphery of the stainless steel cartridge. A complete cooling curve was successfully telemetered from the rocket and indicated that the average cooling rate through the miscibility gas was 14.7 C/second. A thermal arrest of approximately 9-second duration corresponding to the monotectic transformation was clearly visible on the cooling curve. Complete solidification at $\sim$ 156 C, as indicated by the internal temperature of the alloy, took place well within the microgravity time frame. All in all, the experiment appears to have been conducted successfully and according to the original plan.

Ground Base Samples

Prior to the SPAR II flight, two ground base samples had been processed in the General Purpose Rocket Furnace for the purpose of obtaining terrestrial standards for comparison with the flight samples. One of the samples was run in exactly the same way as the flight

sample and had an average cooling rate through the miscibility gap of 17.9 C/second, reasonably close to that of the flight sample. The other ground-base sample which was considered to be a secondary standard was actually subjected to the thermal cycle twice and in an orientation anti-parallel to that of the other two samples. Average cooling rates through the miscibility for the two cycles conducted on this sample were 12.2 and 12.9 C/second.

The flight and ground base samples were examined by X-radiography and by metallographic techniques on a macroscopic and microscopic level.

Results of the SPAR II Experiments

As previously delineated, we expected that the 40 weight percent In alloy flight sample would show a fine dispersion of indium-rich droplets within an aluminum-rich matrix. The expected structure of the 70 weight percent In alloy flight sample was not as clearly defined. One possibility was an interlacing network of aluminum-rich and indium-rich phases on a microscopic level. Alternatively, the expected structure of this alloy might be that resulting from the spinodal decomposition of the homogeneous liquid. If this latter structure was retained during solidification, the sample would be expected to have modulated structure consisting of composition fluctuations having a wavelength on the order of 0.01 to 0.1 μ. The spinodal structures, however, may be extremely unstable in the liquid owing to the relatively high liquid phase diffusion coefficients.

As shown in Figure 3, the expected macro- and microstructures were not observed on the flight sample. Instead the structure of the space processed alloys as determined by X-radiography and macro-examination consisted of an aluminum-rich core surrounded by indium-rich metal. For the Al-70 weight percent In alloy, the aluminum-rich core was approximately spherical; whereas, in the Al-40 weight percent alloy, the aluminum-rich core occupied a larger fraction of the container volume and was roughly the shape of the container. There was a great tendency for the indium-rich material to wet the aluminum container walls.

The expected layering of the indium-rich and aluminum-rich materials in the alloys processed terrestrially was observed.

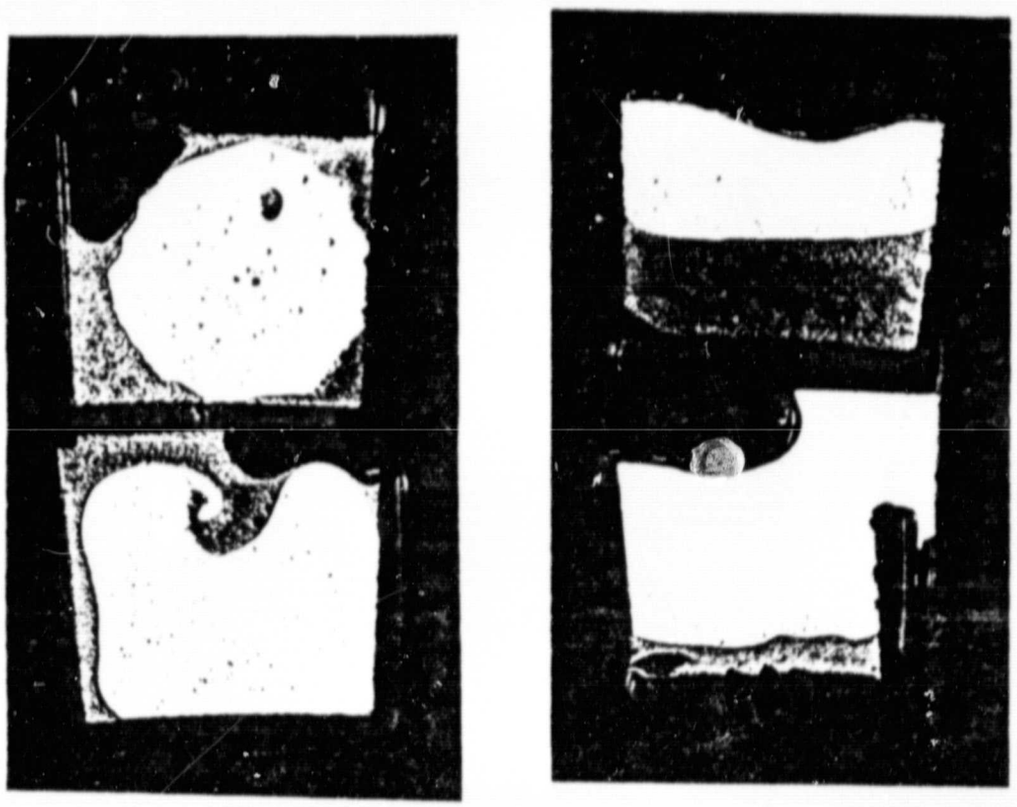

FIGURE 3. MACROPHOTOGRAPHS OF SPAR II FLIGHT AND GROUND BASE ALLOYS

The microstructural features of all the samples were similar and consisted of the following phases:

(1) Indium-rich droplets in an aluminum-rich matrix
(2) Aluminum-rich spheres showing evidence of the monotectic transformation and aluminum-rich dendrites in an indium-rich matrix

A great difference in the distribution of the dispersed phases was seen between the samples processed at 1-g and those processed in space. In the 1-g processed samples, the effect of gravity could be easily seen by the settling of the indium-rich droplets in the aluminum-rich matrix and by the floating of the aluminum-rich spheres and dendrites in the indium-rich matrix. The same type of particles were seen in the flight sample, and although they were relatively coarse, their distribution was much more uniform than it was in the samples processed on the earth.

Interpretation of SPAR II Results

The unusual distribution of phases in the SPAR II flight sample was considered to have resulted from two causes:

(1) The tendency to form the configuration which has the lowest combination of surface and interfacial energies
(2) Fluid flow mechanisms that provide the means to achieve the lower energy configurations.

As part of the SPAR II analysis, calculations were made to determine the configurations expected at low gravity for mixtures of molten aluminum and indium as a function of the volume fraction of aluminum. The two liquids are assumed to be of spherical geometry and are in a containerless configuration. The results show an overwhelming tendency for the liquid indium to surround the liquid aluminum when the interfacial energy between the aluminum and indium is < 350 ergs/cm^2 as expected.

Insight into the case in which a container is involved was also obtained from published analyses and experiments conducted on liquid-gas mixtures at low g (10,11). Based on these results, the observed macro-

structure of a wetting indium-rich material surrounding an aluminum-rich core is expected.

During the analysis of the SPAR II results, a number of possible mechanisms by which massive separation might occur were suggested. These are summarized in Table 1. Most of them involve fluid motion leading to droplet collisions and subsequent coalescence. Only the first three mechanisms listed in Table 1 were analyzed in any detail and are summarized in the following discussion.

Calculations dealing with residual motion from the rocket spin and despin have shown that the time available at micro-g levels before the quenching operation (94 seconds) is appreciably longer than that required to dampen the residual motion to a very small level (30 seconds for the 40 weight percent In alloy, 55 seconds for 70 weight percent alloy). It was concluded that this source of potential fluid motion can be neglected.

Analysis of conventional convection at low-g arising from density differences in the single phase alloy led to the conclusion that fluid velocities on the order of 0.1 cm/second are possible. Thus, in the 10-second period between initial phase separation and monotectic solidification, fairly substantial fluid flows are possible. Although this was a "worse case" computation since the density differences assumed were those between pure aluminum and pure indium, it was concluded that this mechanism is a probable contributor to the observed massive separation.

An estimate of the likelihood for thermocapillary flow (surface tension drive fluid motion arising from temperature gradients) was obtained through calculation of Marangoni numbers for the Al-In alloys studied. The high values of the Marangoni numbers (Ma = 229 for Al-40 weight percent In, Ma = 500 for Al-70 weight percent In) indicated that at a cooling rate of 15 C/second and with the resulting temperature gradient of 10 C/cm, fluid motion due to surface tension gradients are likely. Another manifestation of the Marangoni effect, the migration of droplets under a thermal or solutal gradient was not considered in the SPAR II post-flight analysis. However, some evidence that this effect may be present in this system is presented in the second of the report "SPAR V Flight Experiment 74-30".

TABLE 1. POSSIBLE MECHANISMS FOR MASSIVE PHASE SEPARATION

Residual Fluid Motion
Surface Tension Drive Flow (Marangoni effect)
Conventional Convection
Capillarity (spreading)
Transformation Segregation
Transformation Volume changes
Nonuniform Starting Composition

Another suggested source of the observed massive separation, the spreading of a liquid onto a solid or another liquid surface was not analyzed. Droplet spreading is usually rapid and thus, could also play a major role in the evolution of the observed structure of SPAR II flight samples.

Another contributor to the observed macrostructure was hypothesised in terms of directional cooling effects during specimen quenching and their relation to phase separation. In this mechanism, the separating phase (indium, in the SPAR II samples) would initially precipitate preferentially at the container walls since this part of the melt is the first to reach theconsolute temperature during cool-down. The local precipitation may be coupled with the spreading phenomenon described above and could, in addition, be associated with the rejection of aluminum into the specimen interior. This mechanism, however, was not a part of the SPAR II post-flight analysis.

Still another source of fluid motion was considered but not analyzed; namely transformational volume changes as a result of the liquid-liquid phase separation or due to the monotectic transformation. It is possible that these volume changes could lead to fluid motion sufficiently large to effect droplet coalescence. Some evidence of volume changes accompanying phase separation has recently been presented by Potard[12].

The agglomeration process itself, wherein two colliding droplets unite to become one larger droplet could also lead to localized fluid motions due to the expulsion of host liquid from between the droplets and due to the shape change from dumb-bell to spherical. It is expected that the more rapid this coalescence process is the more wide-spread will be the fluid motion.

At the conclusion of the SPAR II experimental analyses, the most suspicious source of the unanticipated structures observed was the possible lack of homogeneity in the single phase liquid alloy at the start of cool-down after the relatively short 15-minute hold at 950 C. Accordingly, an extensive ground-base program was initiated to analyze this possibility. The analysis culminated in the design and execution of the SPAR V experiment.

Post-SPAR II Ground Based Experiments

Purpose and Overall Description

In order to explore the possibility that the SPAR II flight and ground base samples were not homogeneous at the time of the cool-down (after the 15-minute hold time), three types of experiments were conducted for the purpose of assessing the degree of mixing that might have occurred during rocket spin-up and despin and to determine the rate of homogenization of the liquid alloy assuming that this process is controlled strictly by diffusion. A simple ground base simulation of the rocket spin-up and despin was conducted to determine the degree of mixing expected from this motion. In addition, two types of experiments were conducted to determine the diffusion characteristics of liquid phase Al-In alloys. The first used a differential thermal analysis (DTA) technique to assess the rate of homogenization of a liquid melt at a temperature above the miscibility gap by monitoring the apparent consolute temperature as a function of hold time. The second set of experiments was designed to provide a direct measurement of the interdiffusion coefficients in the liquid Al-In alloys at 970°C, the approximate hold temperature used on SPAR II and later used on SPAR V.

Spin-up and Despin Experiments

In order to simulate the action of spin-up and despin in a single phase liquid containing a concentration gradient, the apparatus shown in Figures 4 and 5 was fabricated. This equipment consisted of a 61 cm diameter lucite "spin" platform mounted on a two-speed (163 and 246 RPM) polishing wheel. The apparatus included a fixture for holding a sample vial 13-mm inside diameter (see Figure 5) and a bracket for mounting an 8-mm movie camera perpendicular to a line between the spin axis and the vial.

The axis of the vial was displaced $\sim$ 41 mm from the spin axis reproducing the position of the sample relative to the rocket spin axis in SPAR II.

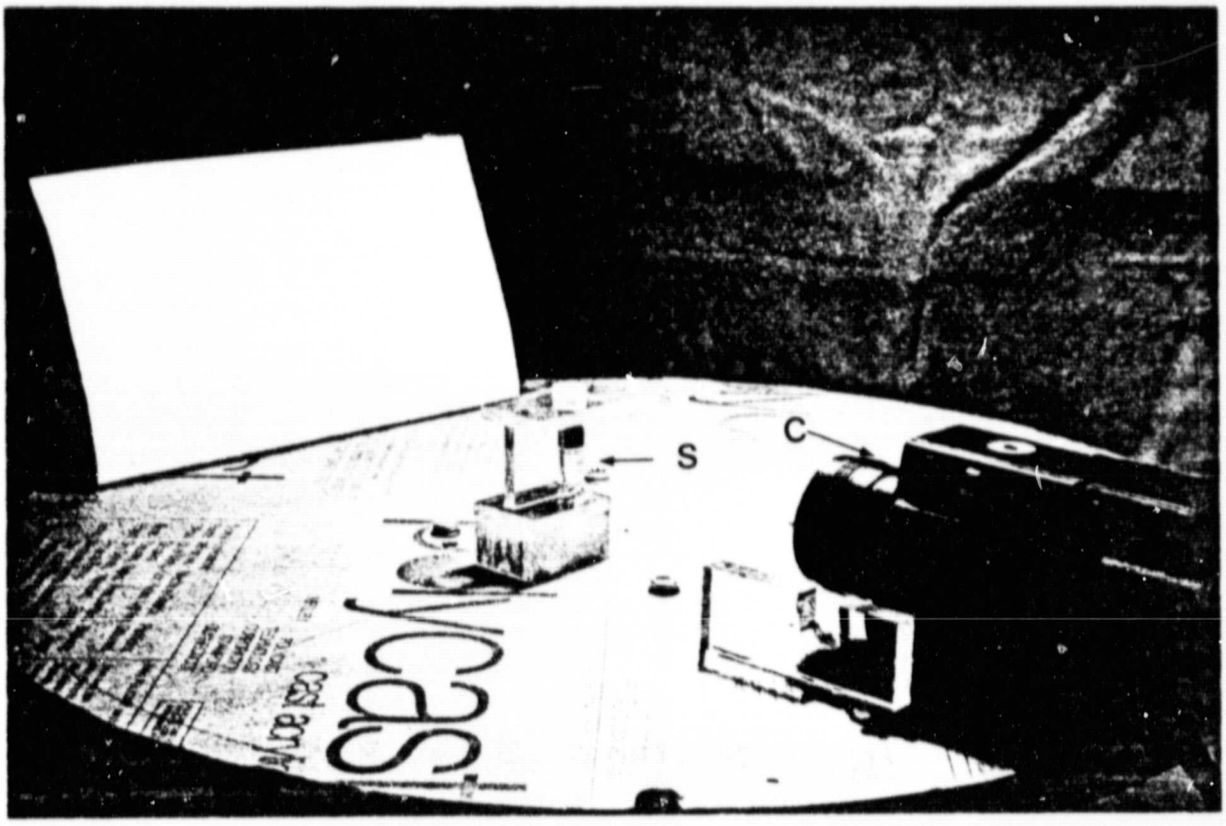

FIGURE 4. PHOTOGRAPH OF SPIN PLATFORM USED TO SIMULATE THE EFFECT OF ROCKET SPIN-UP AND DESPIN ON LIQUID MIXING. THE VIAL CONTAINING THE LIQUID SAMPLE IS DESIGNATED "S" AND THE 8mm MOVIE CAMERA IS MARKED "C".

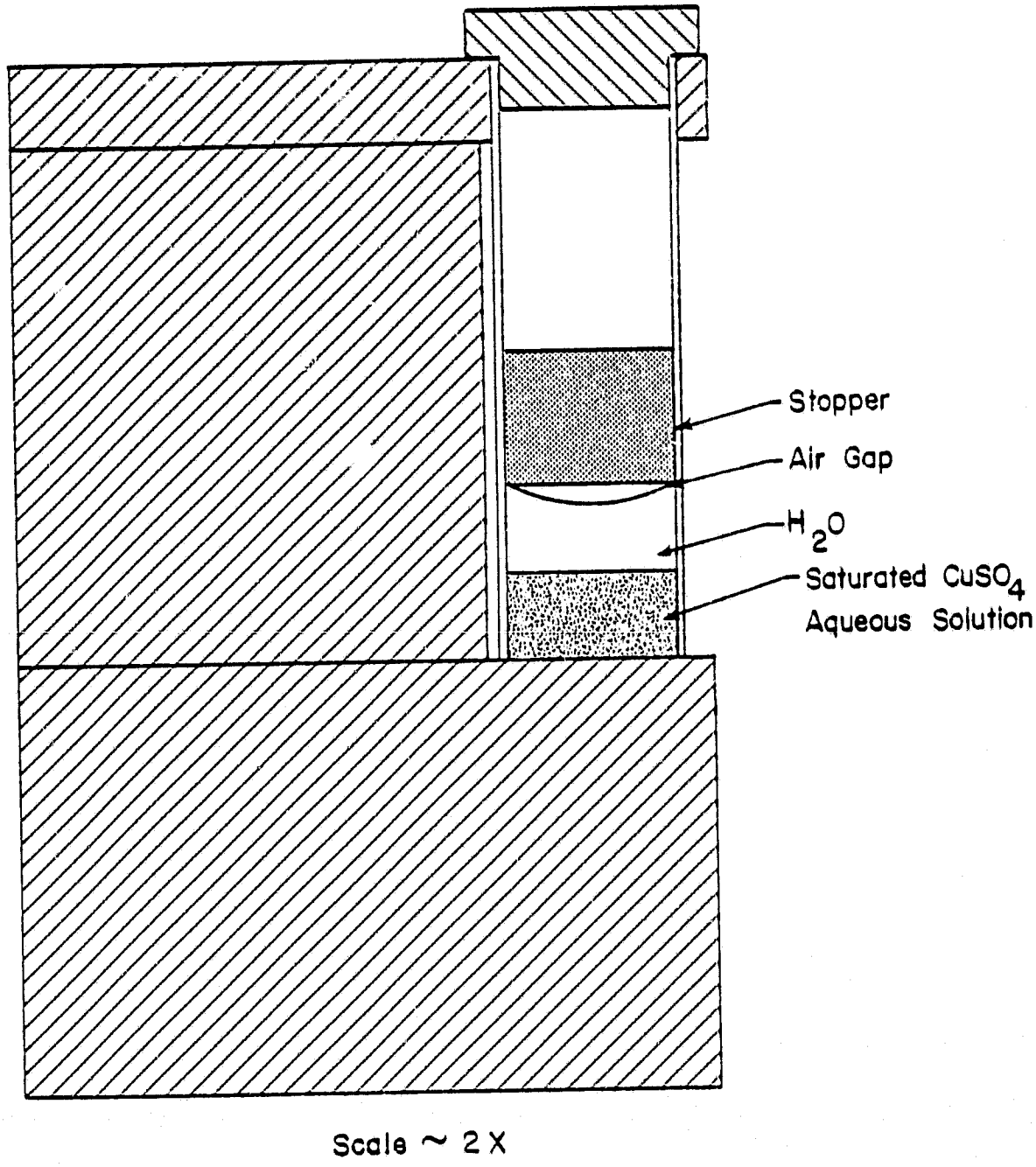

FIGURE 5. SCHEMATIC DRAWING OF SAMPLE AND HOLDER FOR SPIN-UP/DESPIN EXPERIMENTS

An aqueous solution of copper sulfate was chosen as the system to simulate the liquid Al-In alloys. The choice was based on consideration of viscosity level ($\sim$ 1 cp) and ease of photography (the blue colored copper sulfate provides excellent contrast with the colorless water).

In a typical experiment, the bottom of the vial was filled with the saturated aqueous solution of copper sulfate (calculated specific gravity 1.17) and a top layer of pure water was carefully added. A rubber stopper sealed the liquid into the vial either with or without a layer of air at the top of the liquid surface. The specimen was accelerated either directly to a speed of 246 RPM or accelerated to that speed after first pausing at the intermediate speed of 163 RPM. The specimen was continuously photographed at 18 or 36 frames/second during the process.

Among the investigated variables were the relative proportion of the overall height of the liquid occupied by the copper sulfate solution (0.25 and 0.5), the presence or absence of an air gap to simulate the presence of helium gas in the SPAR II experiment and the presence or absence of a wetting agent (1 drop of Kodak photoflow). A summary of the parameters used in the spin-up despin experiments is provided in Table 2.

Frames from Film Roll No. 2 are shown in Figure 6. They illustrate the position of the liquid and gas layers at the start of the experiment (Figure 6a), after acceleration to the intermediate speed of 163 RPM (Figure 6b), after acceleration to the maximum speed of 246 RPM (Figure 6c) and after deceleration to a rest position (Figure 6d). At the intermediate and highest rotational speeds, the higher specific gravity copper sulfate is forced up the vial wall to a height which increases with the rotational speed. The fluid motion produces a paraboloidal gas pocket at the top of the liquid adjacent to the vial surface closest to the spin axis.

The major point to be noted from these film strips is that after the spin-up and despin sequence is completed, the final configuration is altered little from the starting configuration. This demonstrates

TABLE 2. SUMMARY OF SPIN-UP/DESPIN EXPERIMENTS

Film Roll Number	Approximate Ratio of $CuSO_4$ Solution Height to Total	Other Conditions
1	.25	Air gap. No wetting agent.
2	.25	Air gap. No wetting agent.
3	.25	No air gap. Wetting agent present.
4	.25	Air gap. Wetting agent present.
5(a)	.50	Air gap. Wetting agent present.
5(b)	.50	Air gap. No wetting agent present.
6	.50	Air gap. No wetting agent.

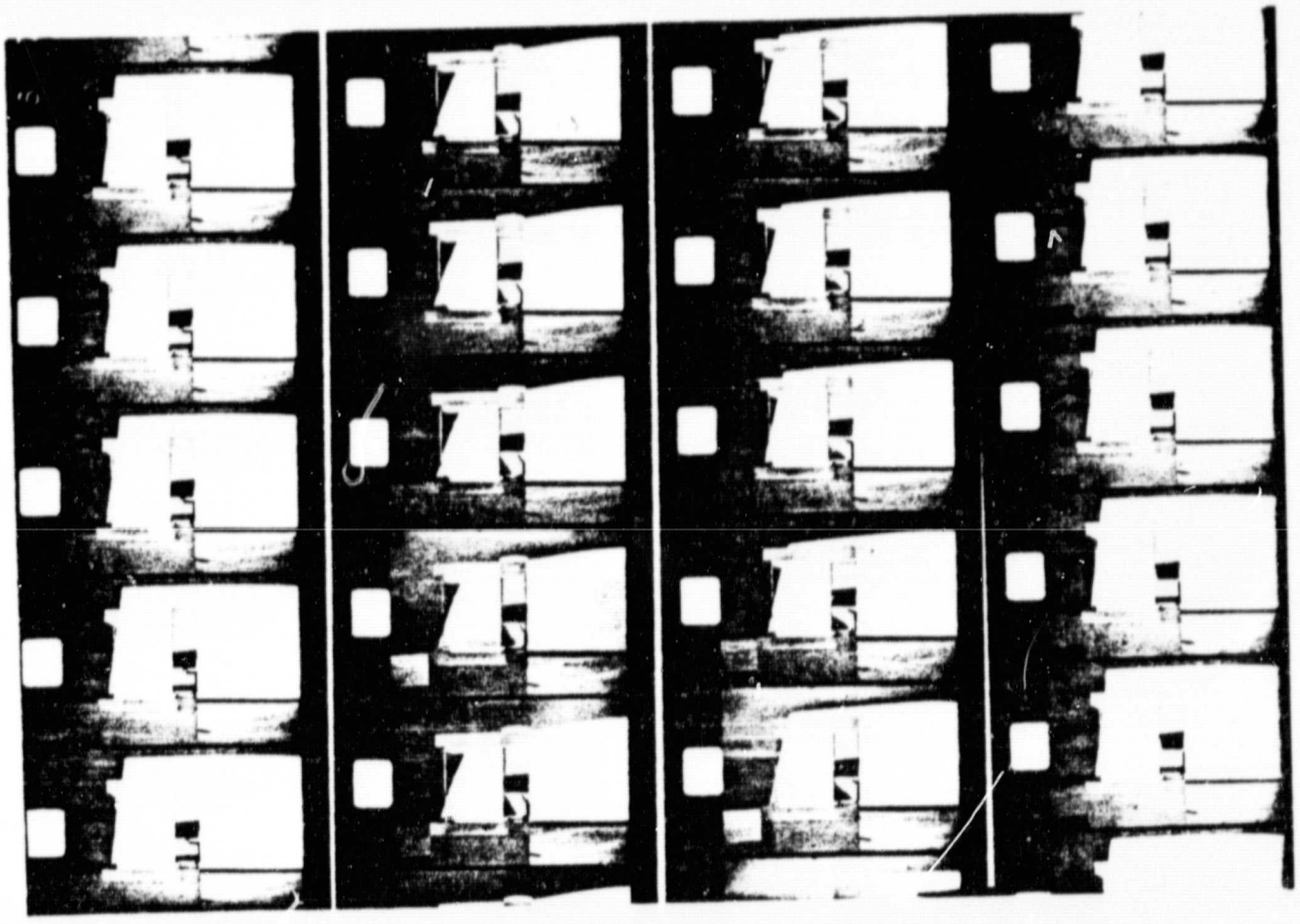

d c b a

FIGURE 6. SELECTED FRAMES FROM FILM NO. 2. (a) At Start (b) Rotating at 163 RPM (c) Rotating at 246 RPM, and (d) At rest after spin-up and despin.

the major conclusion of the experiment, that there is little mixing associated with the spin-up and despin of the rocket. (This conclusion neglects any mixing which may be induced by vibration during the various phases of the rocket flight.)

The following general comments can be made on the basis of all the films taken and analyzed.

(1) Although the liquid is a single phase, the region rich in copper sulfate behaves similarly to that expected in a multiphase material and is centrifugally accelerated up the vial on the side opposite the spin axis. The faster the rotational speed, the higher up the vial wall the copper sulfate is forced. This behavior appears to be independent of whether an air gap is present or not.

(2) When an air gap is present, it assumes a sectional shape which is approximately parabolic at the top surface nearest the spin axis. This is due to the acceleration of the heavier liquids to the outside of the vial. In the absence of a wetting agent, the configuration is stable (except for minor shape changes) even after motion has stopped. The presence of a wetting agent promotes the return of the air gap to its original configuration.

(3) The presence of the wetting agent appears to accelerate the movement of copper sulfate into the pure water portion of the sample either by enhanced diffusional or convective processes.

(4) The major turbulent disturbance of the liquid sample occurs during the rotational speed changes occurring during spin-up or despin and appears to be concentrated at the free

surface and in the area where the concentration gradient is the steepest.

Kinetics of Homogenization

Two methods were used to assess the rate at which homogenization of the pure aluminum and indium components took place at a temperature of 970 C, the target hold temperature for the SPAR II and SPAR V experiments. The first method, which was somewhat indirect, used differential thermal analysis (DTA) to measure the kinetic approach to homogenization by determining the time necessary to obtain a constant and reproducible measure of the consolute temperature for a given Al-In alloy. This technique also had the advantage of providing a check on the published results for the Al-In miscibility gap. The second method provided a direct measure of the interdiffusion coefficient in liquid Al-In alloys above the miscibility gap. Both methods provided sufficiently accurate, self-consistent data to select a hold time which would insure prequench melt homogeneity in the SPAR V experiment.

DTA Measurements

The DTA equipment used in the kinetic measurements is schematically shown in Figure 7. The heart of the apparatus consists of an alumina crucible capped with an alumina lid and containing the aluminum and indium components in the desired proportions. The crucible and its contents are in turn contained in an OFHC copper block which serves primarily as an untransforming standard with which the aluminum-indium alloys are compared. The copper block which has a heat capacity close to that of the alloys also serves to smooth out any non-uniformities in thermal conditions seen by the alloy samples.

The sample temperature and the differential temperature between the sample and the standard are measured by means of 1 mm outside diameter inconel sheathed chromel-alumel thermocouples. The sample thermocouple is positioned in an alumina well fabricated from tubing 1.2 mm ID x 1.9 mm OD cemented in the center of the crucible base and sealed at the top end with an alumina slurry. The crucible containing the

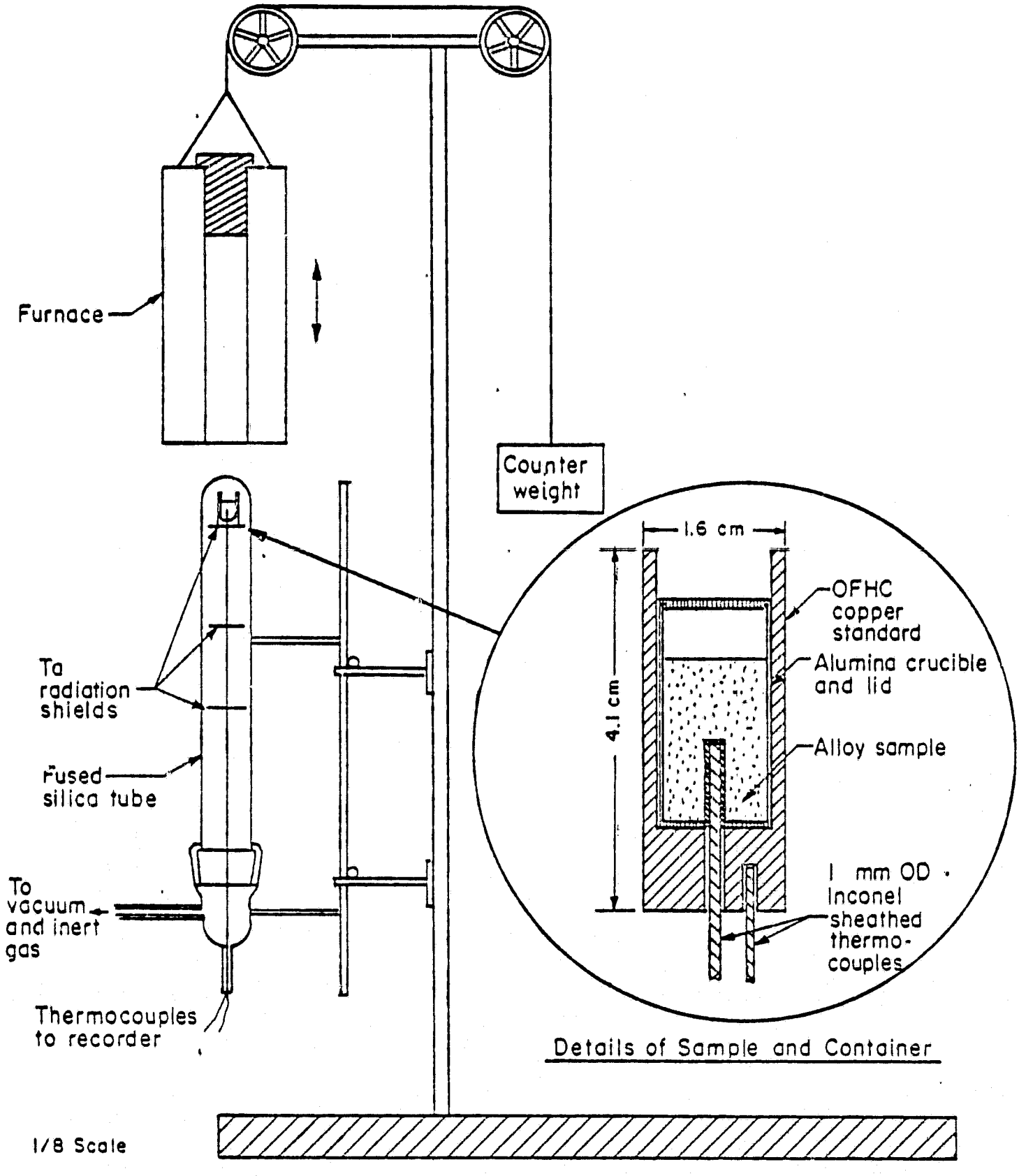

FIGURE 7. SCHEMATIC DRAWING OF THERMAL ANALYSIS EQUIPMENT

thermocouple well is fired at 1200 C before use. The "standard" thermocouple is positioned in a blind hole at the base of the copper block. Thermocouple calibration has been carried out at the melting point of pure aluminum, 660 C.

The direct and differential signals from the thermocouples are recorded on a two-channel millivolt recorder at a sensitivity of either 10 or 4 mV/in. (3.94 or 1.57 mV/cm) for the direct signal and 0.02 mV/in. (0.0079 mV/cm) for the differential signal.

The sample and copper block supported by a tantalum disc and by the thermocouples contained in an alumina tube are sealed in a fused silica tube capable of vacua of better than 1×10^{-5} Torr. Provision for the introduction of helium is also made. A resistance-heated furnace can be lowered around the fused silica tube and sample to provide heating and cooling rates in the temperature range of interest of approximately 7 and 6 C/minute, respectively.

In a typical experiment, the alumina crucible is loaded with pure aluminum and indium components in the proper proportions. The weights of the components are also chosen so as to fill approximately 75 percent of the crucible volume. After insertion of the alumina crucible and its contents into the apparatus, the fused silica tube is evacuated to $\sim 1 \times 10^{-5}$ Torr and the furnace is lowered around the fused silica tube and sample. Heating is carried out until the sample is completely molten (660 C) and any residual dissolved gas eliminated. At this point, helium at just below atmospheric pressure is introduced into the system in order to prevent excessive evaporation of the alloy components. When the sample reaches 970 C, it is allowed to remain at this temperature for a controlled time and then is cooled to below the monotectic temperature ($\sim$ 640) while the direct and differential temperatures are recorded. The sample is then usually reheated to 970 C and, after another hold period, is cooled again while the direct and differential temperatures are recorded as a function of time. The procedure is repeated in order to collect data for a number of hold-times.

The DTA studies were carried out on three alloys, 40.09, 70.06, and 76.02 weight percent In. The results of these studies are summarized in Table 3 and Figure 8. A typical differential temperature trace is shown in Figure 9.

Figure 8 shows the variation of the indicated miscibility gap boundary with hold time for the 40 weight percent In alloy. The data indicates that approximately 8 hours at 970 C is needed to produce a reliable value of the consolute temperature. Values for shorter hold times are presumed to be in error because of a lack of homogeneity in the alloy at the start of the DTA cooling experiment.

DTA data for all the alloys studied is presented in Table 3. All the measurements of consolute temperatures, have been made during cooling. However, measurements of the monotectic temperature have been made both during heating and cooling since this parameter is insensitive to compositional inhomogeneities. A best value for the monotectic temperature based on the present results is 640 C and is the average of the mean value obtained on heating and that obtained on cooling. The data for the 40 weight percent In alloys is by far the most sensitive of the three to hold time. The indicated miscibility gap boundary for the 70 weight percent In alloy still appears to be increasing up to four hours, while the data for the 76 weight percent In alloy does not appear to be at all sensitive to hold time. It should also be noted from Table 3 that there is a tendency for undercooling to occur at the monotectic temperature.

Consolute temperatures measured after 16 hours at 970 C for the 40 and 76 weight percent In alloys agree reasonably well with the equilibrium Al-In phase diagram published by Predel[1]. The data from the present investigation are compared with Predel's data in Table 4.

The DTA trace presented in Figure 9 for the 76 weight percent In alloy held at 970 C and cooled at a rate of 4 C/minute clearly shows the monotectic transformation at 637 C. Curiously, the initial heat effect is followed by temperature oscillations having an amplitude on the order or 0.05 C and a period of $\sim$ 20 seconds. The oscillations are presumably due to oscillatory convection currents which alternatively bring hot and cold fluid into the neighborhood of the measuring thermo-

TABLE 3. SUMMARY OF DTA RESULTS

Hold Time (hr)	Cooling Data: Miscibility Gap Boundary, °C	Cooling Data: Monotectic Temperature, °C	Cooling Data: Degree of Undercooling, ΔT, °C at Monotectic Temperature	Heating Data: Monotectic Temperature, °C
		Al-40.09 Weight Percent		
0	813	--	--	642
0	814	639	9	--
0	813	639	12	--
0	812	639	13	--
0	--	639	18	--
1	813	640	9	--
2.1	788	638	10	642
4.1	782	640	5	--
8.0	764	638	10	641
16.0	761	639	11	642
		Al-70.06 Weight Percent In		
0	812	638	5	641
0	--	638	6	644
1	813	638	3	--
2	--	--	--	--
4	816	639	9	--
		Al-70.02 Weight Percent In		
0	811	638	4	642
0	--	638	8	641
0.5	812	636	9	--
1.0	814	638	3	--
2.1	>812	637	8	641
4.0	813	636	9	--
16.0	811	637	13	644

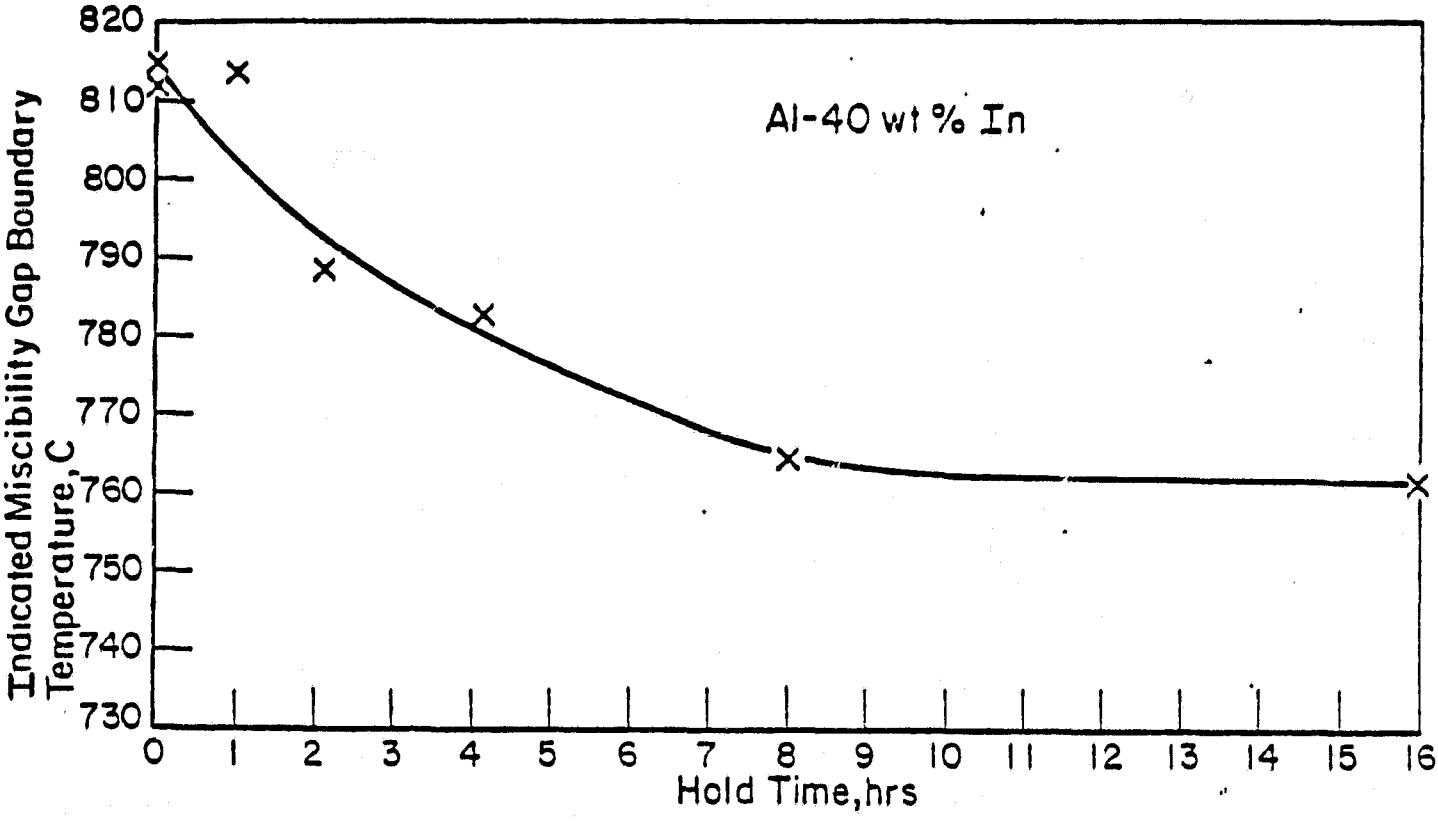

FIGURE 8. THE VARIATION OF INDICATED MISCIBILITY GAP BOUNDARY TEMPERATURE WITH HOLDING TIME AT 970 C

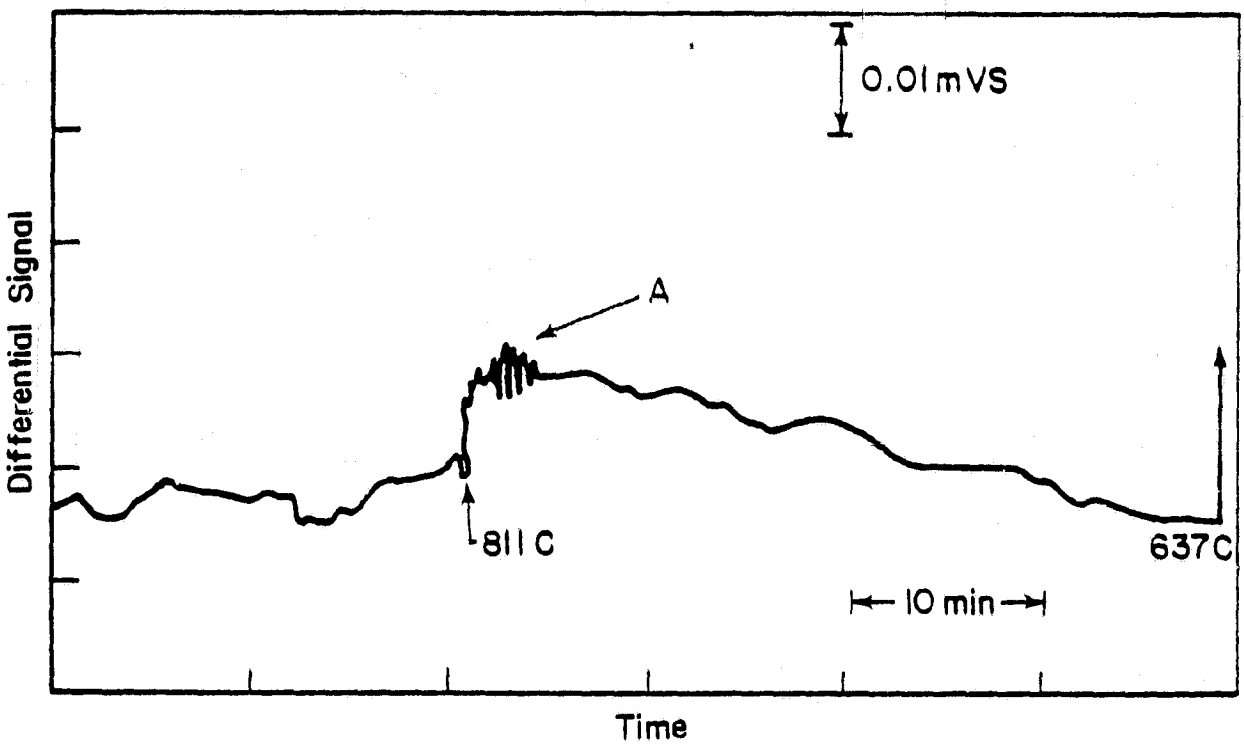

FIGURE 9. DTA TRACE FOR Al-76 WEIGHT PERCENT In ALLOY HELD 16 HRS AT 970 C AND COOLED AT ∿ 5C /MIN

Note cyclic differential signal at A having a maximum amplitude of ∿ 0.002 mv (0.05 C) and of frequency 3 cycles/min.

Table 4. COMPARISON OF DTA DATA FROM PRESENT WORK WITH PUBLISHED DATA OF PREDEL[1]

Predel Data		Present Investigation	
Composition, Wt. Pct.	Consolute Temperature, °C	Composition, Wt. Pct.	Consolute Temperature, °C
39.91	775	40.09	761
75.12	830	76.02	811
	Monotectic Temperature, °C		
	637		640

couple. Oscillations in liquid volume have recently been observed by Potard[12] during the cooling of Al-In alloys into the miscibility gap. His cooling rate was about one-tenth that used in the present investigation and the oscillation period was 600 seconds. Although the two oscillatory effects are possibly related, the relationship between them is not obvious. Oscillatory convection currents have also been observed to result from surface tension gradients arising from temperature variations in a liquid containing a free surface. Much more work is required in this area for a fuller understanding of these phenomena.

The conclusion to be drawn from the DTA experiments is that a hold time of at least 8 hours is necessary to yield a reproducible and equilibrium value of the consolute temperature. It is presumed that this time period is associated with the homogenization of the alloy above the miscibility gap. It should be noted that the homogenization time period for the DTA geometry would be appreciably longer than for the SPAR configuration owing to the longer diffusion distances in the DTA configurations. These factors will be discussed at length in the next section.

Diffusion Analysis

Introduction. In order to assess the results of SPAR II with regard to possible lack of homogeneity in the melt just before the cool-down and to provide design data for the SPAR V experiment, the diffusional characteristic of liquid Al-In alloys above the miscibility gap were assessed analytically and experimentally.

Analytical Calculations. The analytical calculations considered a simple one dimensional boundary-value problem based on Fick's formulation.

$$\frac{\partial C\ (x,t)}{\partial t} = D\ \frac{\partial^2 C\ (x,t)}{\partial x^2}\ , \qquad \text{Equation 1}$$

where

$$C\ (x,0) = \begin{cases} C_o \text{ for } 0<x<h \\ 0 \text{ for } h<x<1,\ 1>h \end{cases} . \qquad \text{Equation 2}$$

Here, C (x,t) is the composition at position x and time t, and D is the interdiffusion coefficient.

The solution of this boundary-value problem has been shown by Barrer[8] to be given by

$$C\ (x,t) = C_o \left\{ \frac{h}{\ell} + \frac{2}{\pi} \sum_{n=1}^{\infty} \frac{1}{n} \exp\left[-\left(\frac{n\pi}{\ell}\right)^2 Dt \right] \cos\left(\frac{n\pi x}{\ell}\right) \sin\left(\frac{n\pi h}{\ell}\right) \right\} ,$$

Equation 3

This expression has been used to describe the kinetics of homogenization, neglecting such effects as the possible concentration dependence of the interdiffusion coefficient and the somewhat undefined boundary conditions actually existing at t = 0.

Illustrated in Figure 10 is the manner in which C (ℓ, t), the composition at position ℓ, increases as a function of Dt from its initial value of zero and approaches its equilibrium level, $C_{eq} = C_o h/\ell$. The cases illustrated in this figure correspond to the three alloys run in the DTA and the two alloys run in the SPAR Rocket Flight configuration.

The principal feature of interest in this figure lies in the relatively strong dependence of C (ℓ, t) upon the value of ℓ itself. Decreasing ℓ from values a little over 2 cm for the DTA configuration to values just under 1 cm for the SPAR configuration results in a pronounced decrease in the time required to attain equilibrium. To further illustrate this fact, Table 5 presents the Dt values required to bring $C\ (\ell, t)/C_{eq}$ to within 1 percent of the asymptotic value of unity and the corresponding

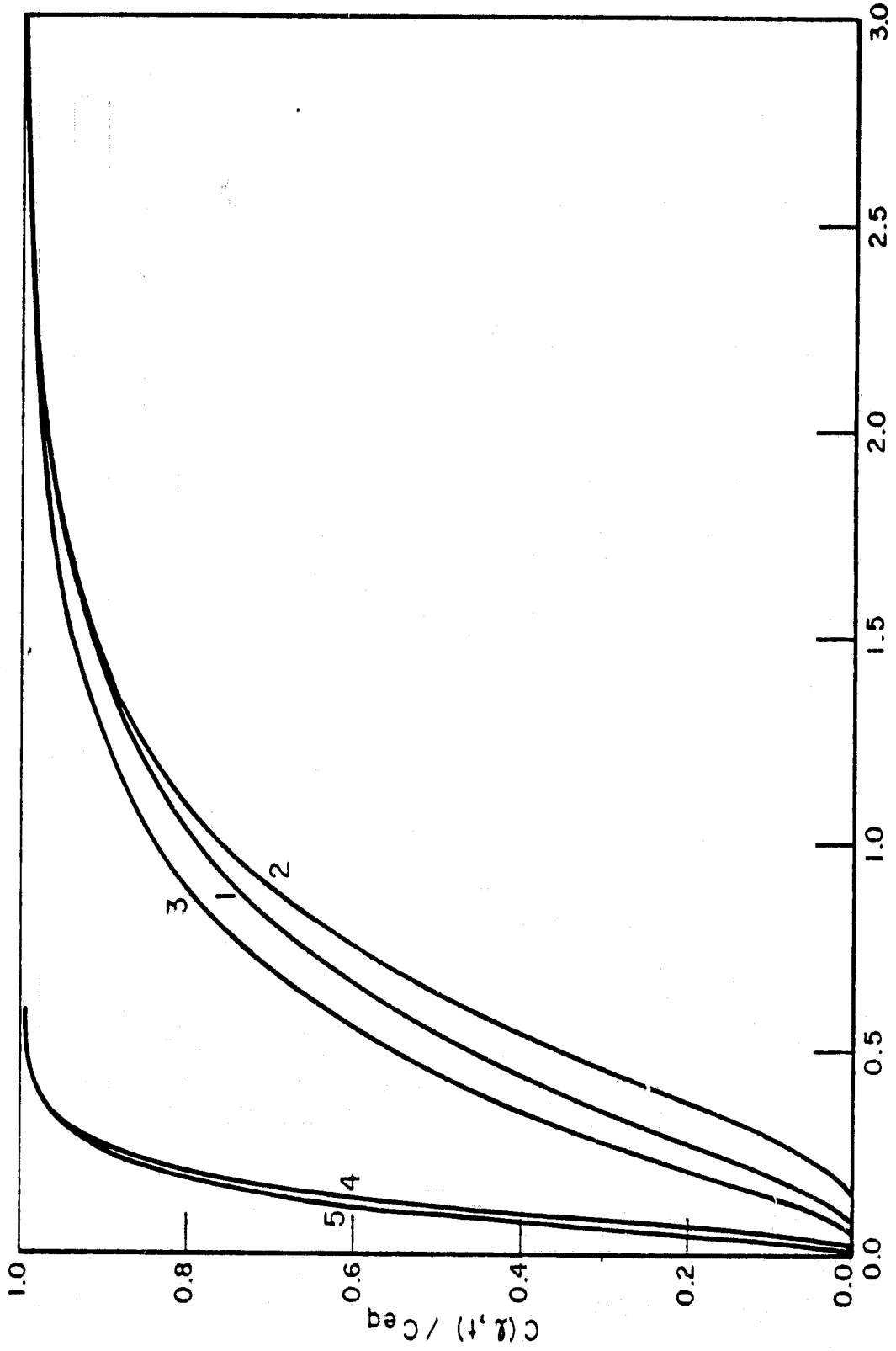

FIGURE 10. APPROACH OF C (ℓ,t) TO ITS EQUILIBRIUM VALUE FOR VARIOUS CONFIGURATIONS OF INTEREST

1--DTA Al-70 weight percent In, h = 1.04, ℓ = 2.29; 2--DTA Al-40 weight percent In, h = 0.421, ℓ = 2.19; 3--DTA Al-76 weight percent In, h = 1.18, ℓ = 2.22, 4--SPAR Configuration Al-40 weight percent In, h = 0.183, ℓ = 0.952; 5--SPAR Configuration Al-70 weight percent In, h = 0.446, ℓ = 0.9817; h and ℓ in units of cm.

times assuming a value of $D = 8 \times 10^{-5} cm^2/second$*. The more than 8 hours required to attain equilibrium in the DTA configuration is consistent with the experimental results presented in Figure 8. On this basis, $\sim$ 1.7 hours are required to homogenize the Al-In alloys in the SPAR configuration (see Table 5).

TABLE 5. VALUES FOR Dt REQUIRED TO BRING C (ℓ, t) TO WITHIN 1 PERCENT OF ITS EQUILIBRIUM VALUE

Case	Configuration	Composition Weight Percent In	Dt	$t^{(a)}$ (hr)
1	DTA	70	2.6	9.03
2	DTA	40	2.5	8.68
3	DTA	76	2.4	8.33
4	SPAR	40	0.5	1.74
5	SPAR	70	0.5	1.74

(a) Based on an assumed value of $D = 8 \times 10^{-5} cm^2/second$.

Finally, in Figure 11, we have presented the concentration gradients calculated for various values of Dt from 0.07 (t = 15 minutes, $D = 8 \times 10^{-5}$ $cm^2/second$) to that required to attain near uniform composition for the 40 and 70 weight percent In alloys in the approximate SPAR and DTA configurations. Based on these calculations and the ground base spin-up and despin studies, it was concluded that the SPAR II alloys were far from homogeneous after the 15-minute hold time assuming that fluid flow had not been induced by rocket vibration, etc.

---

* This value of D was chosen before measurements of D were made in the present study (see next section). The assumed value of $8 \times 10^{-5} cm^2/second$ based on measurements reported in the literature on the self diffusion of indium in an In-5 weight percent alloy[13] is somewhat higher than the value measured in the present study, $6.4 \times 10^{-5} cm^2/second$. However, the conclusions based on our calculations using the assumed value of D are still valid.

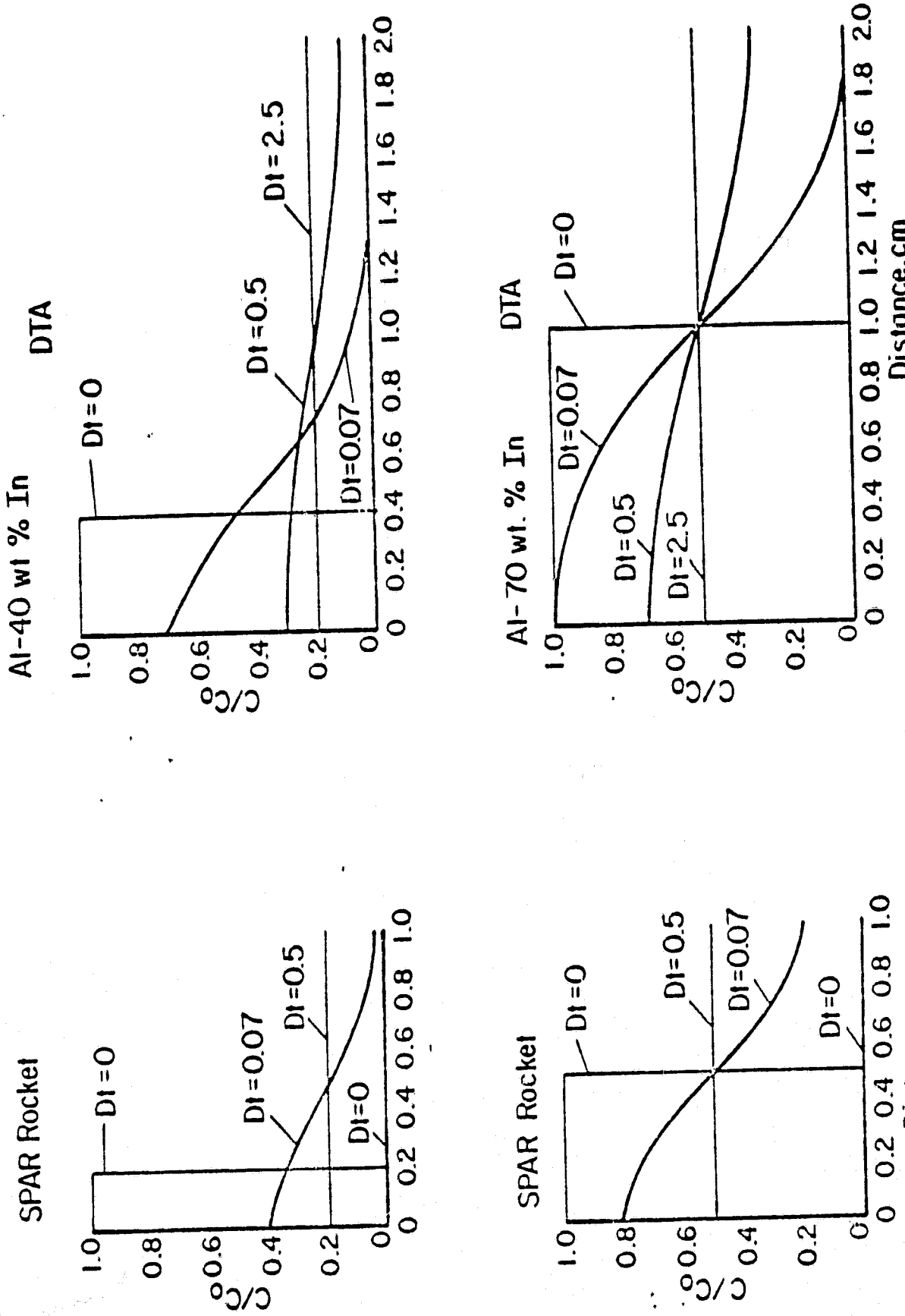

FIGURE 11. CALCULATED CONCENTRATION GRADIENTS IN THE Al-40 WEIGHT PERCENT In AND Al-70 WEIGHT PERCENT In ALLOYS IN THE DTA AND SPAR ROCKET CONFIGURATIONS

Direct Measurement of the Interdiffusion Coefficient, D. The purpose of this set of experiments is to determine the value of the interdiffusion coefficient in liquid aluminum-indium alloys at a temperature of 970 C in the homogeneous liquid region above the miscibility gap. These measurements were made to check the validity of the conclusions made in the previous section on the basis of an assumed value of D = $8 \times 10^{-5} cm^2/second$.

The results obtained thus far are still considered tentative since there are still some unsolved experimental difficulties associated with the technique. We feel, however, that when the method has been perfected, it will allow us to determine diffusion coefficients as a function of composition in liquid phase alloys. The technique has the added advantage that the microstructure of a continuous series of alloys can be conveniently prepared, examined and related to composition.

Three sets of experiments have been conducted thus far. In all cases two samples were involved, one for a diffusion time of 1 hour and the second for 4 hours.

The specimen design used in these experiments is shown in Figure 12. An alumina capillary tube, one end of which is sealed with a slurry made up of fine alumina in an H_3PO_4/H_2O solution, was utilized. The other end of the capillary incorporated a radial hole for suspending the sample in the furnace. These tubes were then fired by slowly heating in air to 1200 C* in order to drive off moisture and sinter the slurry. High purity In and Al wire, both of which were $\sim$ 1 mm in diameter and 3 cm long, were carefully inserted into the alumina tube after chemical cleaning of the indium and aluminum components in concentrated HCl and a 20 percent aqueous solution of NaOH respectively. After the capillaries were filled, they were suspended in a fused silica tube contained in a furnace as shown in Figure 13. The chamber was then evacuated to 1×10^{-5} torr and the samples heated to 800 - 900 C in approximately 30 minutes. At this temperature, helium was introduced into the system until a pressure level of slightly less than 1 atmosphere (0.1 MPa) was reached

---

* The tubes used in the first experiment were fired to only 700 C. Some gas evolution during the diffusion experiment is suspected. See text.

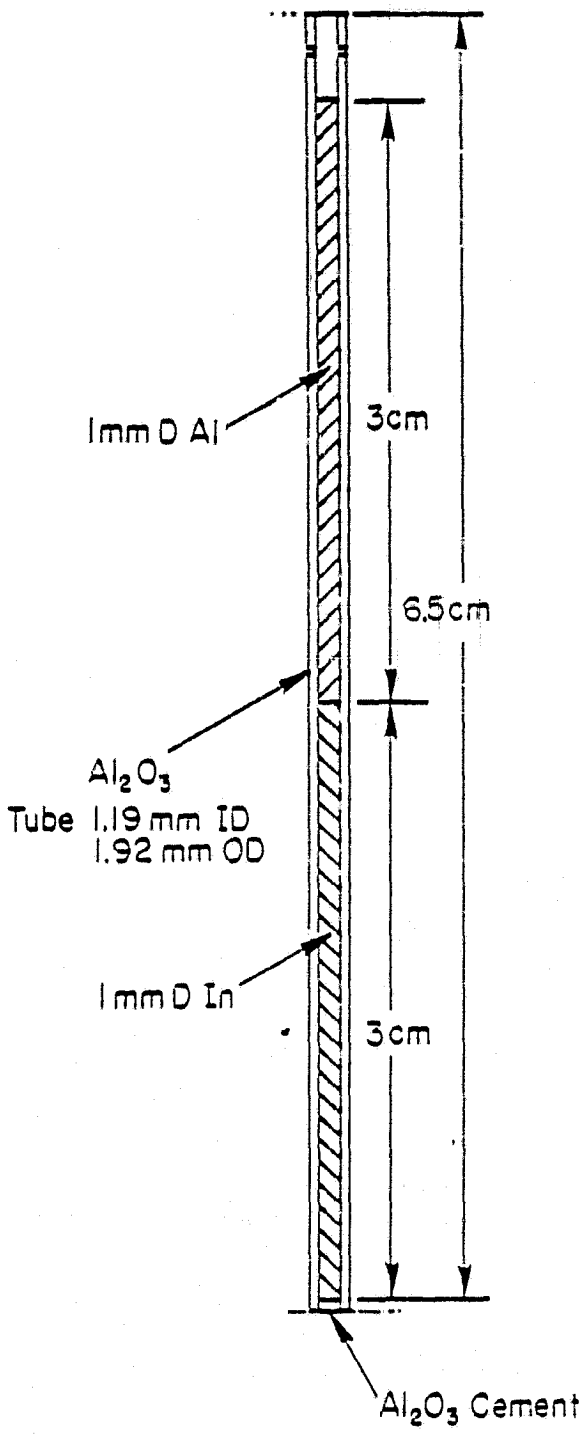

FIGURE 12. SPECIMEN DESIGN FOR Al/In LIQUID PHASE DIFFUSION EXPERIMENTS

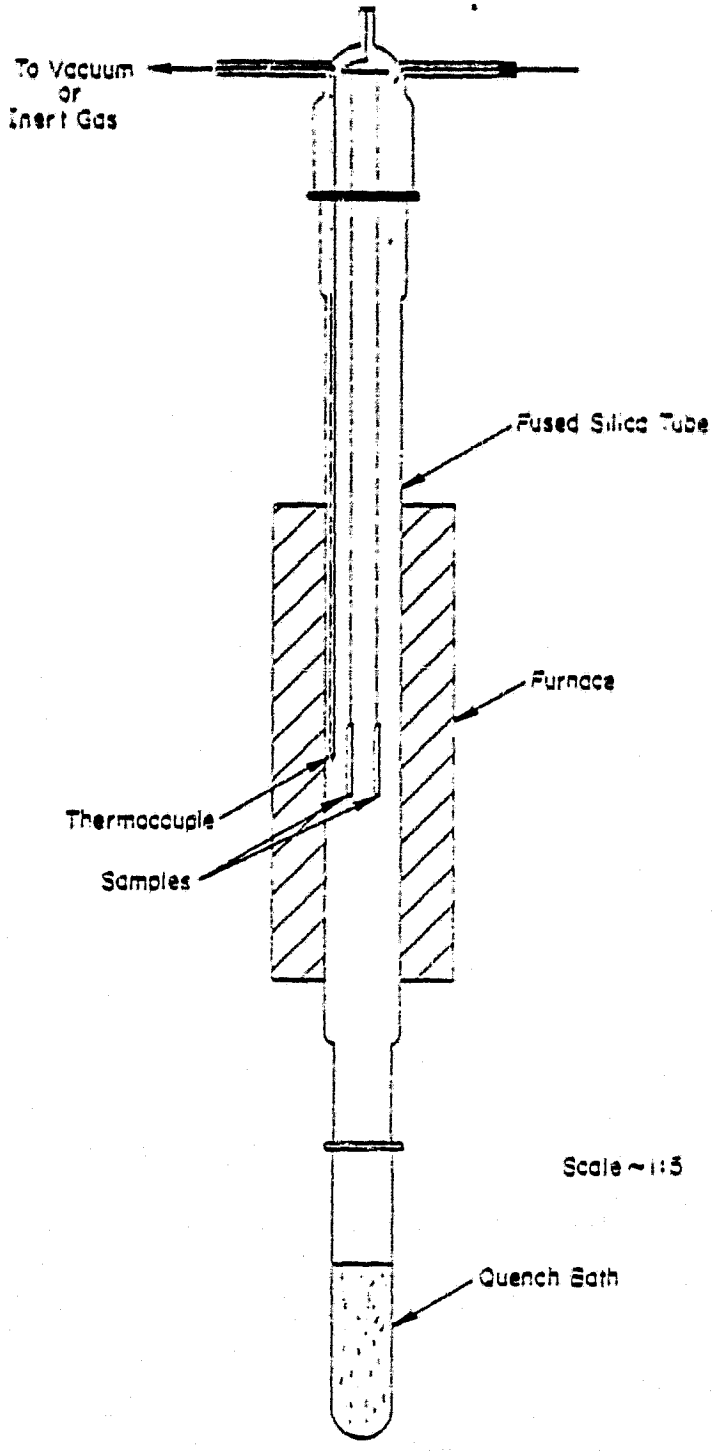

FIGURE 13. SCHEMATIC DRAWING OF APPARATUS USED IN LIQUID PHASE DIFFUSION EXPERIMENTS

while heating was continued to a temperature of 970 C. After the desired time at 970 C, the sample was dropped into a water-cooled siliconeoil quench bath where it was cooled to <20 C in ∿ 1 second.

Table 6 summarizes some of the experimental parameters used in the two diffusion experiments. It should be noted that the calculated length of the diffusion couple at 979 C (∿4.9 cm) is appreciably less than the 6 cm of original wire length because the wire diameter is somewhat smaller than the inside diameter of the capillary.

After the thermal treatment, the diffusion samples, while still in the Al_2O_3 capillaries, were metallographically polished down to the central longitudinal plane. Some difficulty was encountered in this procedure due to the presence of void regions and pull-out of portions of the specimen during polishing. Some macrostructural agglomeration was also observed which tends to complicate the composition analyses. Porosity and pull-out were so serious in Samples 1 and 2 that they were not analyzed.

The situation improved in the second experiment (DC 2), owing to a higher firing temperature (1200 versus 700 C) of the capillary and the maintenance of the vacuum environment to a higher temperature before introducing the inert gas. These procedures presumably allowed a greater proportion of the residual gases to be removed from the capillaries. Impregnation of the metallographic mounts with additional epoxy after the initial grinding was also found to be beneficial in retaining the bulk of the sample in the mount. However, even with these precautions, there were still some regions that suffered from pull-out. In addition, in the top portion of the specimen (the higher aluminum content portion) the metal only filled the capillary in isolated regions. The lack of complete filling is probably due to a combination of solidification shrinkage and the possible presence of gas bubbles.

Still another problem was encountered in the metallographic polishing of Samples 6 and 7. The presence of the alumina capillary tube interfered with the polishing of the appreciably softer metal and resulted in poorly prepared metallographic surfaces with the metal level substantially below the level of the ceramic.

TABLE 6. SUMMARY OF PARAMETERS USED IN Al-In LIQUID PHASE DIFFUSION EXPERIMENTS

Experiment No.	Sample No.	Diffusion Time (hr)	Wt. of In (gm)	Wt. of Al (gm)	L^*_{In} (cm)	L^*_{Al} (cm)
DC-1	1	4	0.1727	0.0603	2.401	2.349
	2	1	0.1827	0.0602	2.540	2.345
DC-2	6	1	0.1815	0.0584	2.523	2.275
	7	4	0.1830	0.0591	2.544	2.298
DC-3	8	1	0.1812	0.0636	2.519	2.477
	9	4	0.1769	0.0640	2.459	2.493

* L_{In} and L_{Al} are the lengths of In and Al at 970 C calculated on the assumption that the components fill the inside diameter of the capillary tube.

The preparation method described above was successfully applied to Samples 8 and 9. However, the polished sections revealed the presence of bubble-shaped void areas presumably due to gas bubbles.

The composition as a function of position in the diffusion couples was deduced for Samples 6, 7, 8, and 9 at 1.5 mm increments on an electron beam microprobe. The conditions used for these analyses are delineated in Table 7. Each of the diffusion couples was cut along its length into three approximately equal sections for these analyses. Pure aluminum and pure indium were used as standards. In a typical analysis of one of the section, the intensities from the aluminum and indium standards were first measured together with the background intensities determined on both sides of these peaks. The aluminum and indium peak and background intensities from positions along the diffusion couple section were then measured and finally a second set of intensity readings were taken on the aluminum and indium standards.

TABLE 7. PARAMETERS USED IN THE ELECTRON MICROPROBE ANALYSIS OF Al-In DIFFUSION COUPLES

Parameter	Sample			
	6	7	8	9
Approximate Spot Size, mm	0.13	0.13	0.4	0.4
Accelerating Potential, KV	25	25	15	15
Take-off Angle, deg.	20°	20°	20°	20°
Crystal	Mica	Mica	Mica	Mica
Al Line	Kα	Kα	Kα	Kα
In Line	Lα	Lα	Lα	Lα

The raw intensity data after background subtraction were converted to values of composition by means of MAGIC - Version 3[14], a computer program for quantitative electron microprobe analysis. This program calculates the values of $k = I_A/I_{A_o}$, the background subtracted intensity of the peak for element A in the sample divided by the corresponding peak intensity in the pure metal standard. The k values which represent a first approximation of the concentration of the element in the sample are then corrected for atomic number (Z), absorption (A), and fluorescence (F) effects to yield an independent aluminum and indium concentration for each position analyzed along the diffusion couple. The concentration-position relationships evaluated in the manner described above were used to determine the interdiffusion coefficients, D by the computer methods discussed below.

Computation of Interdiffusion Coefficients. A numerical procedure was constructed with which to determine the interdiffusion coefficients for liquid aluminum-indium alloys from the measured composition-distance data. A basic assumption of the analysis is that the spatial and time dependence of the concentration can be described by a solution of the one-dimensional, time-dependent diffusion equation, using an "effective" concentration-independent diffusion coefficient, and subject to the approximate initial and boundary conditions (see Equations 1 through 3). Since the experimental data were taken from solidified Al-In metal, account had to be taken of a number of factors, including shrinkage of the alumina container and net volume decrease of the Al-In liquid alloy upon cooling and solidification. An outline, in which the algorithm is summarized, is presented below.

Preliminary Steps.

A. Choose values for pertinent input parameters.
B. Choose an array of diffusion coefficients, relatively widely spaced, within which the "true" value is certain to be.
C. Read in experimental data for the weight-fraction of aluminum as a function of distance along the diffusion couple and the diffusion time. Convert the aluminum weight-fraction to indium weight fraction.

D. Compute the density of pure liquid aluminum and of pure liquid indium as well as the number of atoms per cubic centimeter in pure liquid indium, all corresponding to the temperature at which the diffusion experiment was performed.

E. Consider the liquid-metal system, which is shaped as a circular cylinder by the surrounding alumina crucible, to be divided (in a mathematical sense) into N "slices" (with N taken to be 100 in these computations), by "cutting" the cylindrical system along equally spaced planes perpendicular to the cylinder axis. This subdivision is assumed to represent the liquid metal at the diffusion temperature.

Computations.

A. Compute the thermal contraction upon cooling, of the inner cross-sectional area of the alumina cylinder, within which the liquid metal is contained.

B. For a given value of D and the diffusion time used in the experiment, compute the indium concentration at the center of each slice (assuming high-temperature conditions) using the solution of the diffusion equation (Equation 3).

It should be noted that the Barrer solution[8] involves evaluation of an infinite series; we retain up to some specified number (100) of terms in this series, but terminate the series before this point if the magnitude of the individual terms becomes very small.

C. Convert the concentration of indium calculated at the center of each slice to weight-fraction indium. This conversion not only makes the units of indium concentration the same as those for the experimental

data, but it also makes the calculated indium content of the slice invariant to the volume change undergone by the slice during cooling.

D. Compute the new thickness of each slice which exists after cooling from the test temperature (970 C) to room temperature.

1. Include the contribution due to contraction of alumina container.
2. Include also the volume contraction of the metal within each slice, calculated by simply summing the contractions that the constituent aluminum and indium would have undergone in the pure state. Assume that the net volume change of each slice is unaffected by interactions with any adjacent material (their slices or the container).
3. Note: the slices do not, in general, all have the same thickness after cooling, since the relative amounts of aluminum and indium that each slice contains varies from slice to slice.

E. Carry out a statistical analysis of the data.

1. Compute the sum of squares of the deviations of all values of indium concentration, measured on solidified material at room temperature, from the corresponding calculated indium concentrations. Each calculated value is obtained at the same spatial location as the corresponding data point. Each calculated value is determined by linear interpolation of values computed at midpoints of adjacent slices (with shrinkage due to cooling accounted for) such that spatial coordinate of the corresponding data point lies within the range of distance defined by these two midpoints.

2. Note: only data points lying within the spatial range from the midpoint of the first slice to the midpoint of the last slice are included in the analysis.

F. Repeat the previous computations for all diffusion coefficients in the "coarse" array chosen under B of "Preliminary Steps" described above.

G. From the results, determine the interdiffusion coefficient, D min, in the "coarse" array for which the calculated sum of square of deviations has the smallest value, and hence which constitutes the best estimate, obtained thus far at least, of the "true" diffusion coefficient.

H. Choose a more "finely" spaced array of diffusion coefficients about the value D_{min}.

I. Repeat the previous computation with the "fine" array of diffusion coefficients. In this manner, a more refined estimate of D_{min}, and hence of the "true" interdiffusion coefficient, is obtained.

Graphics Programming.

A. Carry out all procedures necessary to plot the experimental data as well as the theoretical concentration curve corresponding to the refined estimate of D_{min}.

Results. As described earlier, difficulties have been encountered in obtaining accurate values of the interdiffusion coefficient in liquid Al-In alloys above the miscibility gap (970 C). These impediments can be delineated as follows:

(1) Difficulties in the metallographic preparation of the diffusion couples (Samples 6 and 7)

(2) Less than optimum selection of the parameters used in the electron microbeam probe analysis (Samples 6 and 7)

(3) Problems associated with gas-bubble formation in the capillaries. Static bubbles would be expected to affect mass transfer in the liquid whereas moving bubbles may cause fluid flows and a disturbance of the diffusion induced concentration gradients (Samples 8 and 9). The formation of gas bubbles may be due to improper out-gassing of the capillary tubes.

Four diffusion couples, Samples 6, 7, 8, and 9 were subjected to electron microprobe analysis including the MAGIC corrections. The results from Samples 8 and 9 appear to be reasonably self consistent in terms of the independent determinations of aluminum and indium concentrations. However, the results from Samples 6 and 7 were very inconsistent presumably due to the combination of the poor metallographic polish and the less than optimum selection of electron probe parameters. Further diffusion analysis of these latter specimens does not appear to be warranted at this time.

Through use of the computer code described above, the concentration-position data from Samples 8 and 9 were compared with the theoretical diffusion relations corrected for solidification shrinkage and thermal contraction and the value of D providing the best fit with the data was determined for each couple. These values are summarized in Table 8, and the experimental data points are compared with the "best fit" theoretical curves in Figures 14 and 15 for Samples 8 and 9 respectively.

In an independent study with a similar objective, Dr. Lewis Lacy of MSFC[15] has conducted in situ diffusion experiments by an X-radiographic technique on samples in the SPAR configuration. His observations on the interdiffusion of aluminum and indium in the weight proportion 30:70 at 920 C indicated a concentration difference between the top and bottom of the sample amounting to 10 atomic percent after 1.4 hours and 6 atomic percent after 2.2 hours. Calculations of the interdiffusion coefficients have been made based on these observations and on the assumption that compositional differences correspond to concentrations at the extreme top and bottom of the alloy.

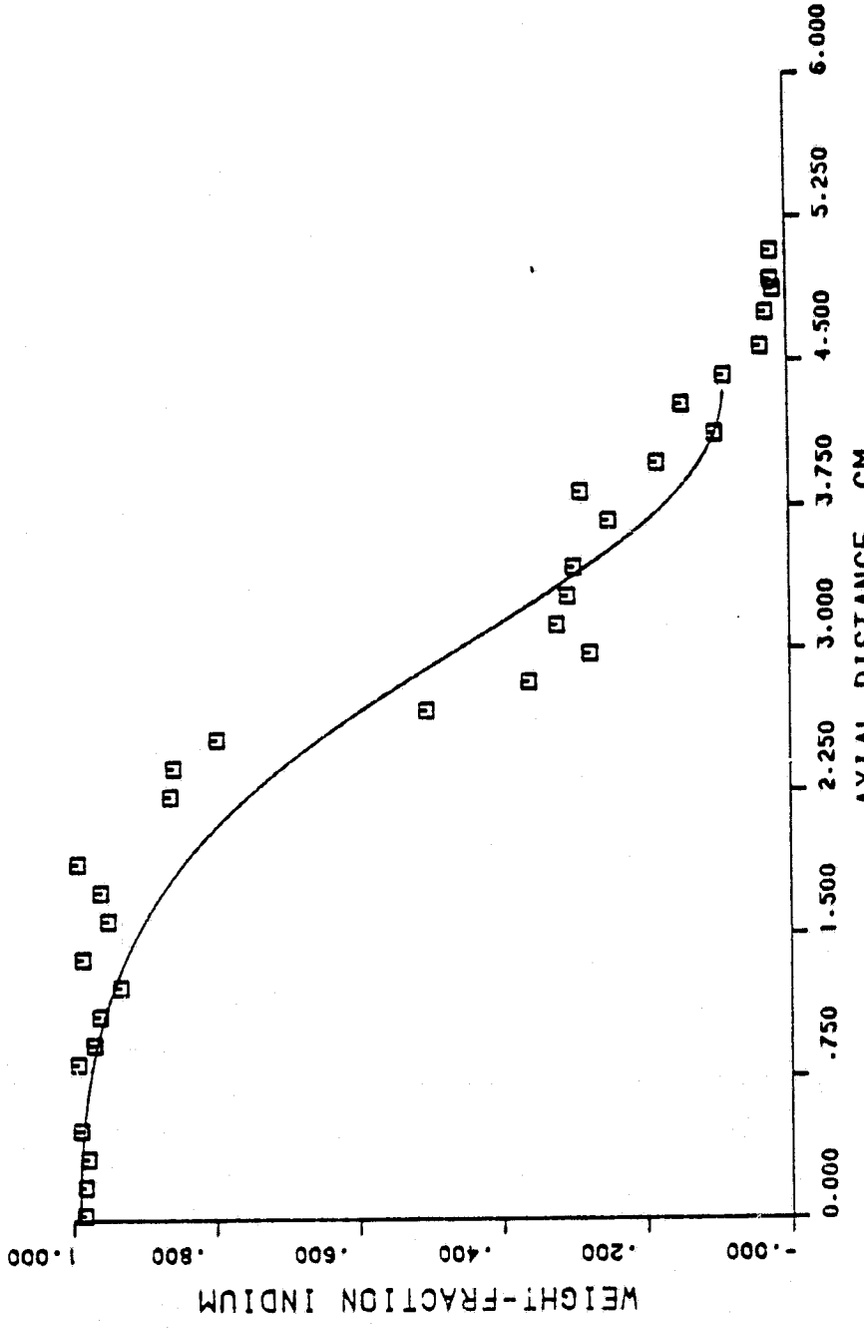

FIGURE 14. BEST LEAST SQUARE FIT OF THEORETICAL CONCENTRATION-DISTANCE CURVES WITH EXPERIMENTAL MEASUREMENTS.

Sample No. 8 – 1 hr at 970 C, D = 1.8×10^{-4} Cm^2/sec.

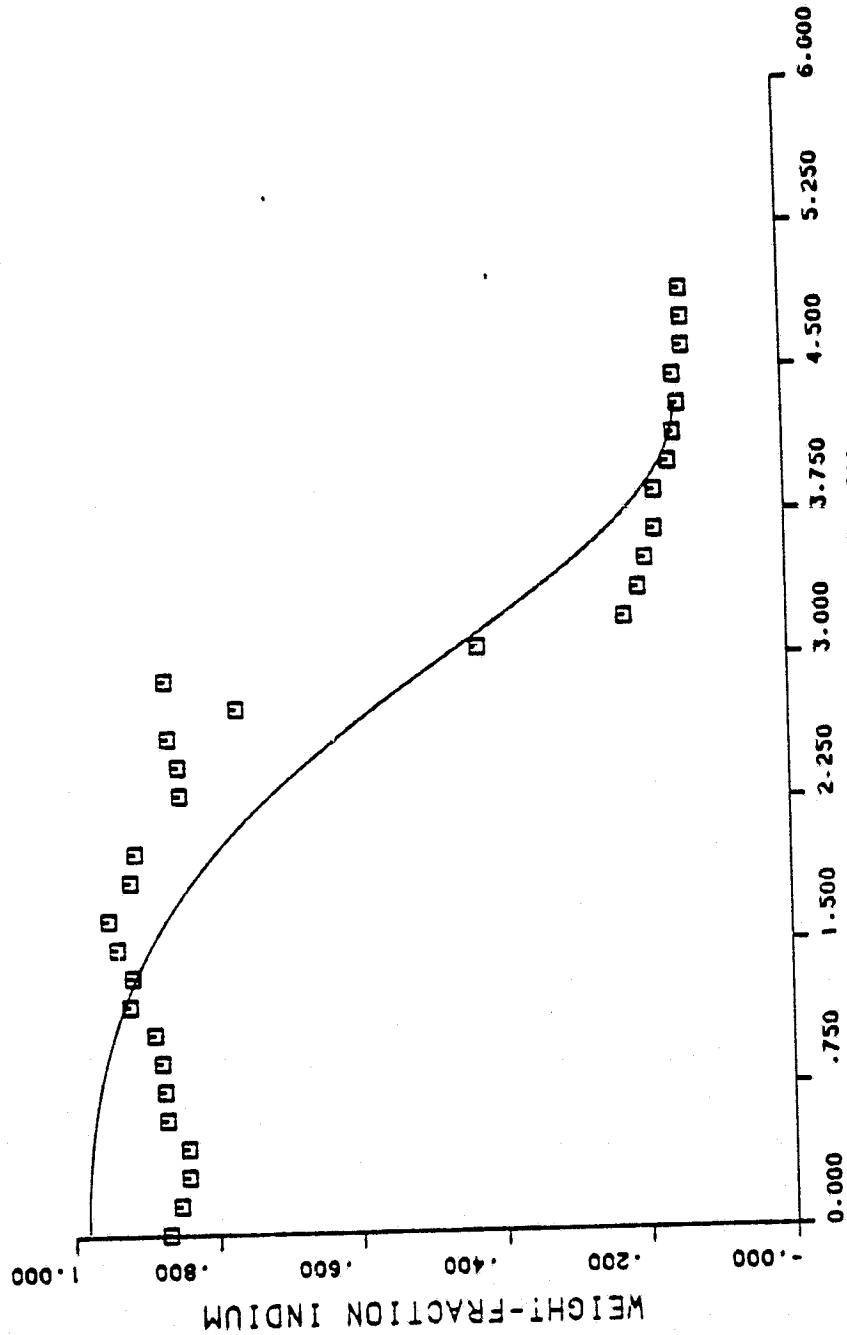

FIGURE 15. BEST LEAST SQUARE FIT OF THEORETICAL CONCENTRATION - DISTANCE CURVES WITH EXPERIMENTAL MEASUREMENTS

Sample No. 9 - 4 hrs at 970 C, D = 5.8×10^{-5} $cm^2/sec.$

TABLE 8. SUMMARY OF LEAST SQUARE DETERMINATION OF INTERDIFFUSION COEFFICIENTS

Sample No.	Diffusion Temp, C	Diffusion Time, Hour	D, cm^2/sec
8	970	1	1.8×10^{-4}
9	970	4	5.8×10^{-5}

Application of the solution of Fick's diffusion relations for the applicable boundary conditions (see Equation 3) provided a relationship between the concentration difference, ΔC, at the sample extremes and Dt. Table 9 lists the results of these calculations.

TABLE 9. CALCULATED DIFFUSION COEFFICIENT AS A FUNCTION OF COMPOSITIONAL DIFFERENCES AT THE SPECIMEN EXTREMES (a)

ΔC, Atomic percent	t, second	Dt, cm^2	D, $cm^2/second$
10.5	5040	0.25	5.0×10^{-5}
6	7920	0.30	3.8×10^{-5}

(a) SPAR configuration. Overall composition Al-70 weight percent In. Diffusion temperature 920 C.

Discussion and Conclusions. The technique utilized to evaluate diffusion in liquid Al-In alloys above the miscibility gap, in spite of the experimental difficulties which are expected to be eased with further development, has great potential as an experimental tool for characterizing liquid metal systems and their solid alloys. Two obvious attractions are as follows.

(1) The method allows the interdiffusion coefficient and its compositional variation to be determined by the same method (Matano-Boltzmann) as commonly used to characterize interdiffusion in the solid state.

(2) The technique produces a continuous series of rapidly cooled alloys whose microstructures can be related to composition. The method could also be applied to liquid phase miscibility gap systems cooled at slower rates but the processing would have to be conducted at low gravity to avoid segregation effects due to buoyancy.

An example of the metallographic potential of the technique is found in Figure 16, where the microstructure of a portion of Sample 7 is displayed. The photomicrograph shows that the separation process occurs extremely rapidly in this system as evidenced by the presence of well-developed droplets especially in the region of the critical composition. What is more, Figure 16a also shows a curious effect. In this low magnification photomicrograph, the size of the precipitating aluminum-rich droplets appears to vary in an almost continuous manner with composition. This effect will be discussed further in a later section dealing with interpretation of the SPAR V results.

The difficulties encountered with this method of determining the interdiffusion characteristics of liquids (electron probe analysis method, metallographic polishing technique, presence of gas bubbles) have largely been eliminated except for the presence of gas bubbles. These bubbles can probably be eliminated by outgassing the capillary tubes at high temperature and in high vacuum prior to filling. (The capillaries in the experiments to date have been baked in air rather than vacuum prior to the diffusion experiments.)

Two additional factors contributing to the uncertainty in the diffusion results to date are as follows:

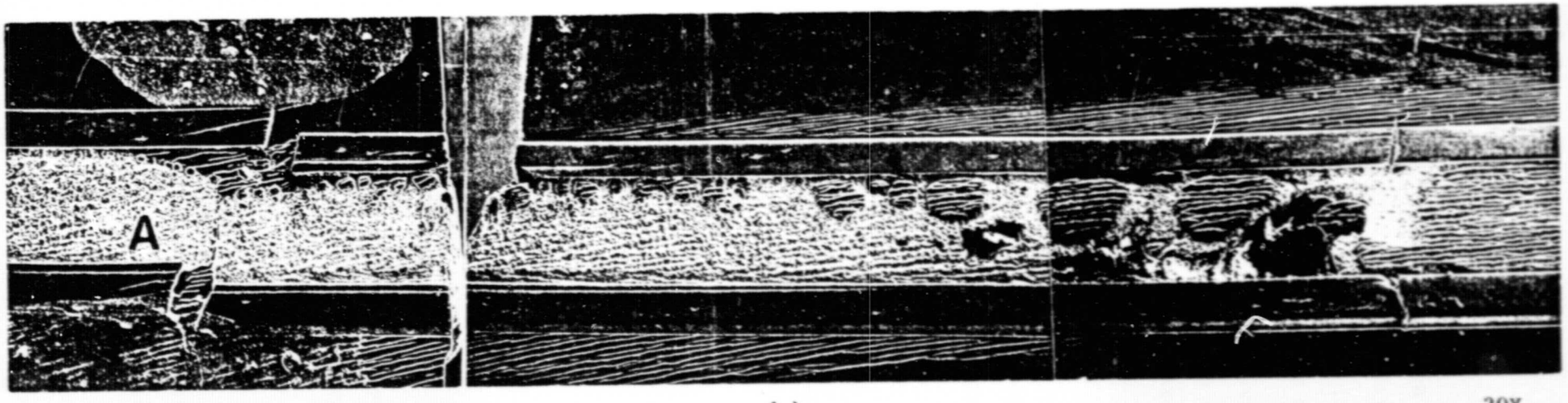

(a) 20X

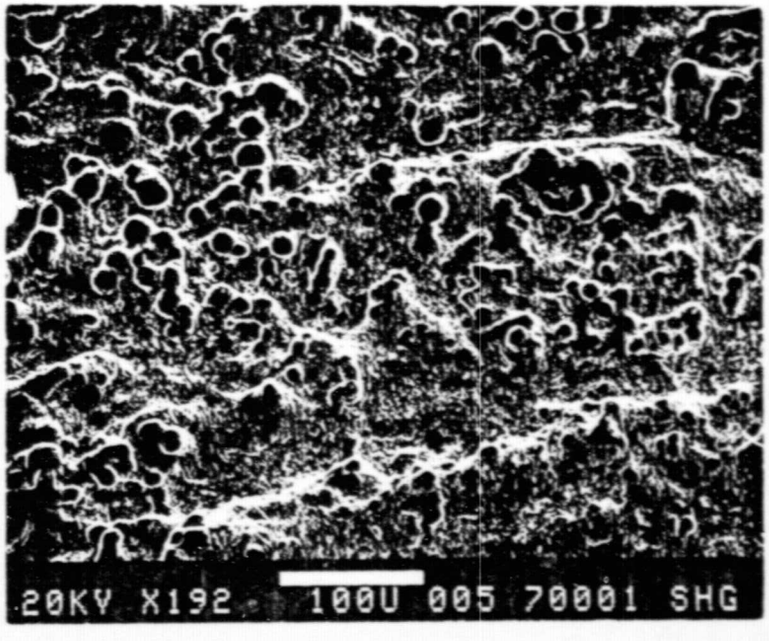

(b)

FIGURE 16. SEM PHOTOGRAPHS OF A PORTION OF SAMPLE 7, HEAT TREATED 4 HRS AT 970 C AND QUENCHED

(a) Macroview at 20X showing variation in size of aluminum-rich spheres, (b) higher magnification view of Area A in (a) showing finer Al-rich spheres.

(1) Diffusion occurring during the period of heating to the diffusion temperature

(2) The partial sinking of the solid aluminum wire into the molten indium at temperatures 155 C < T < 660 C.

Both of these factors lead to a deviation from the boundary conditions assumed in the solution of Fick's diffusion equation (Equations 1 and 2).

With regard to the diffusion occurring during the heat-up period, an estimate can be made for the contribution from this source by calculating a time-average interdiffusion coefficient that can be assigned to the period of heat-up from the monotectic temperature (640 C) to the desired diffusion temperature (970 C). This calculation assumes a value of 4.0 kCal/mole[16] for ΔH, the activation enthalpy which appears in the usual formulation describing the temperature dependence of interdiffusion coefficient:

$$D = D_o \exp [-\Delta H/RT] \qquad \text{Equation 4}$$

where

D_o is a constant
R is the gas constant
and T is the temperature in °K ;

and ignores the change in boundary conditions that occur in this temperature regime.

The temporal variation of temperature during the ∿ 38-minute heat-up period has been approximated by an analytical expression which closely fits the observed variation:

$$T = 913 + 427 \exp \{-9.82/t\} \qquad \text{Equation 5}$$

where

T is the temperature in °K
and t is the time in minutes .

By combining Equations 4 and 5, an expression is obtained for the average value of the interdiffusion coefficient during heating:

$$\overline{D} = \frac{D_o}{t_H}\int_o^{t_H} \exp\{-4000/[(R)(913 + 427 \exp(-9.82/t)]\}\, dt \quad \text{Equation 6}$$

where

t_H is the heat-up time in minutes.

By numerical integration, it is then found that

$$\overline{D} = 0.179\ D_o\ , \quad \text{Equation 7}$$

The corrected value of interdiffusion coefficients, D_c at 970 C is then found by applying the following relationship:

$$D_{LSF}t_D = \overline{D}t_H + D_c t_D \quad \text{Equation 8}$$

where D_{LSF} is the least square fit value of interdiffusion coefficient calculated from the computer codes previously described and t_D is the diffusion time at 970 C.

The values of D_c are compared with the respective values of D_{LSF} in Table 10 and show the corrections accounting for diffusion during heat-up are small and certainly do not account for the major difference between the measurements.

TABLE 10. COMPARISON OF CORRECTED AND LEAST SQUARE FIT DIFFUSION COEFFICIENTS

Sample Number	Diffusion Temp, °C	Time at Diffusion Temp	D_{LSF} cm^2/sec	D_c cm^2/sec
8	970	1	1.8×10^{-4}	1.0×10^{-4}
9	970	4	5.8×10^{-5}	5.1×10^{-5}

The change in boundary conditions due to the partial sinking of the solid aluminum into the molten indium during the heat-up period at temperatures between 155 C and 640 C are probably rather small and due largely to the dissolution of the solid aluminum in the molten indium. It is anticipated that when the aluminum melts, a redistribution of the liquid phases will take place which will tend to restore the original boundary conditions. It is not clear whether any of the diffusion couples that have been run have actually encountered this problem. It would be rather easy for the solid aluminum wire to be held from moving down the capillary by friction. We intend to avoid this experimental complication in the future by crimping the aluminum wire to prevent its moving until it is molten.

Based on these preliminary measurements and those of Lacy corrected to 970 C, our best estimate of the interdiffusion coefficient in liquid Al-In alloys at 970 C is $6.4 \pm 3.1 \times 10^{-5} cm^2/second$. This value agrees quite well with the $8 \times 10^{-5} cm^2/second$ value which has been found to be consistent with the DTA measurements. The value of $Dt = 0.5$ calculated as necessary to homogenize the SPAR alloys (see Table 5) allows us to calculate a value of the necessary homogenization time as 2.2 hours.

These diffusion measurements indicate that the SPAR II alloys were not homogenized sufficiently assuming that there are no other processes involved except diffusion.

It is recommended that additional work be conducted to perfect this technique which is well on its way toward full development. An improved method should allow more precise determination of the diffusion coefficient and allow the variation of D with composition to be characterized.

SPAR V Flight Experiment 74-30

Objective

The realization that the experimental alloys processed on SPAR II may not have been completely homogenized at the start of the cool-down period and that this factor might have lead to the massive separation

observed on SPAR II prompted the decision to repeat the SPAR II experiment but with a longer hold time at the 970 C homogenization temperature. A hold time of 16 hours was chosen providing a safety factor of approximately 7. The large safety factor was selected in light of some uncertainty in the value of the interdiffusion coefficient in the liquid Al-In alloys.

The specific objective of the SPAR V experiment was to determine whether the concentration gradients probably present in the SPAR II samples at cool-down were the cause of the observed massive separation. A secondary objective which developed as a result of an opportunity to fly an additional two alloys was to determine whether alloy compositions in addition to those flown on SPAR II would also show the massive separation. One of the alloys had a high indium content and was also chosen in order to determine whether there is a tendency during cool-down for the precipitating phase (in this case aluminum) to separate preferentially at the crucible walls.

Alloy Composition

Four Al-In alloy compositions, 30, 40, 70, and 90 weight percent In, were chosen for the SPAR V experiment. The 40 and 70 weight percent In alloys were the same compositions as processed in SPAR II. The 30 weight percent In alloy was chosen to determine the effect of a smaller concentration of indium droplets on the tendency toward massive separation. The 90 weight percent In alloy was selected for two reasons.

(1) This alloy should also produce a low concentration of precipitating phase and, in this respect, was chosen for the same reasons as the 30 weight percent In alloy.

(2) Aluminum droplets are expected to be the precipitating phase within the miscibility gap of this alloy. It is of interest to determine whether aluminum tends to precipitate preferentially at the crucible walls in a manner analagous to the precipitation of indium in the high aluminum concentration alloys.

Cartridge Design and Fabrication

The cartridges containing the components for the 40 and 70 weight percent In alloys were of the same design as used in the SPAR II flight and were fabricated in the same manner (see Figure 2). The capsules containing the components for the 30 and 90 weight percent In alloys were of similar design; the only changes being that no provision was made for an internal thermocouple to monitor the sample temperature and the aluminum components were fabricated from a different lot of 99.999 percent pure aluminum. The former change was prompted by a lack of capacity to accomodate another thermocouple, whereas the latter change was due to the depletion of the original lot of aluminum. It was not expected that these changes would impact the experiment significantly. The cartridge containing the 30 and 90 weight percent In alloys had the 90 weight percent alloy positioned at the bottom of the cartridge (see Figure 17). In all cases, the indium components were positioned above the aluminum.

The fabrication of the cartridges containing these alloys was performed in the same manner as the SPAR II capsule [6,7] with the exception that the capsules without internal thermocouples did not undergo the brazing operation. A listing of the component weights for the flight and ground-samples is presented in Table 11.

Samples Processing

Flight Samples 74-30-36 containing the 40 and 70 weight percent In alloys and 74-30-48 containing the 30 and 90 weight percent In alloys were processed on September 11, 1978, aboard SPAR V. Capsule 74-30-36 was equipped with a thermocouple designed to measure the internal temperature of the 40 weight percent In alloy. Unfortunately, the thermocouple failed by fracturing at the base of the cartridge during preparation for the flight. As noted above, capsule 74-30-48 did not contain an internal thermocouple. Although the information obtainable from the internal thermocouple is of great value, a reasonable estimate of the thermal history of each of the cartridges is available based on the

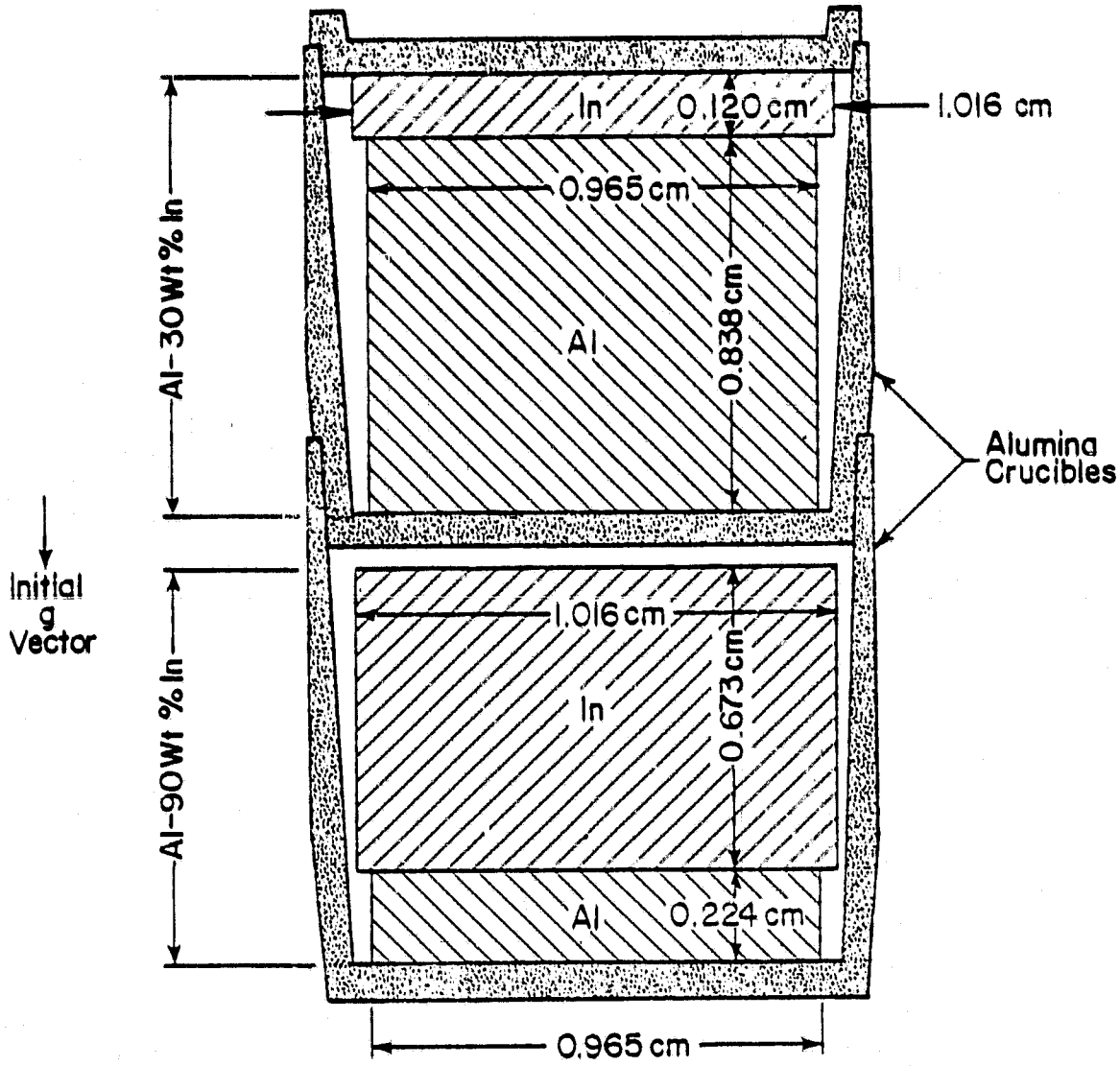

FIGURE 17. SCHEMATIC DIAGRAM SHOWING THE LAYOUT OF ALLOY COMPONENTS FOR Al-30 AND -90 WEIGHT PERCENT In ALLOYS FOR SPAR V EXPERIMENT CARTRIDGE (See Figure 2)

TABLE 11. WEIGHT AND COMPOSITION DATA FOR SPAR V FLIGHT AND GROUND BASE CARTRIDGES

Cartridge Number	Bottom Alloy			Top Alloy		
	Component Wt., gms		Composition	Component Wt., gms		Composition
	Al	In	Wt. Pct. In	Al	In	Wt. Pct. In
74-30-27GB	1.4234	0.9496	40.02	1.0083	2.3546	70.02
74-30-29GB	1.4264	0.9504	39.99	1.0078	2.3484	69.97
74-30-36FLT	1.4159	0.9439	40.00	0.9700	2.2635	70.00
74-30-38GB	1.3648	0.9104	40.01	0.9770	2.2805	70.01
74-30-48FLT	0.4024	3.6194	89.99	1.6027	0.6870	30.00
74-30-49GB	0.4140	3.7252	90.00	1.6190	0.6939	30.00

data from the furnace temperature thermocouple and past flight and ground base experiments. This data is summarized in Table 12.

In the SPAR V experiments, the samples were held at a temperature of ∿ 980 C (goal temperature of 970 C) for 16 hours on the ground before the flight. The rocket was launched after this hold period while the temperature was maintained at 980 C. Approximately 84 seconds after launch, the rocket entered a period of low g ($< 1 \times 10^{-3}$) and ∿ 76 seconds later the samples were rapidly cooled. Table 13 summarizes the sequence of events from the start of the hold period on the ground until the end of the low-g period. A plot of the furnace cavity temperatures and acceleration data as a function of time is shown in Figure 18.

It should be noted from Table 12 that the cooling rates experienced during SPAR V were somewhat lower than desired (∿10 C/second vs. the goal of 14 C/second). As may be seen from Table 12 and Figure 18, this factor has lead to the likelihood that the indium-rich phase was still liquid at the end of the low-g ($<1 \times 10^{-3}$g) period.(a) Although this factor is not expected to alter the general conclusions of the study, it does introduce some uncertainty in the results. The absence of a thermocouple internal to the melt adds further to the degree of uncertainty in the results. In other respects, the processing of the flight samples proceeded as planned.

Specimen Characterization - Method and Results

The two flight samples, 74-30-36 and 74-30-48, as well as two ground control samples, 74-30-29 and 74-30-49 were characterized by radiography and metallography. In addition, ground base sample 74-30-38 which had been held for 16 hours at 970 C and cooled through the miscibility gap at a rate of 3.5 C/second was examined metallographically and provided some understanding of the effect of cooling rate on the evolution of microstructure in the 40 and 70 weight percent In alloys.

(a) This conclusion is based on the assumption that when the furnace temperature reaches 120 C, the sample has completely solidified. The relationship between furnace temperature and specimens temperature is approximate and is based on previous comparisons of the two temperatures.

TABLE 12. FLIGHT AND GROUND CONTROL SAMPLE PROCESSING CONDITIONS

	Flight Sample 74-30-36	Flight Sample 74-30-48	Ground Base Sample 74-30-29	Ground Base Sample 74-30-49
Hold Temperature, C				
Furnace	1036	1040	1061	1060
Specimen	979[a]	980[b]	982	983[b]
Hold Time, hours	16	16	16	16
Cooling Rate,[c] C/sec				
Furnace	12	13.2	15.4	12.8
Specimen	10.0[a]	10.6[b]	10.0	10.4[b]

(a) Specimen thermocouple failed. Value is estimated.

(b) Specimen did not have an internal thermocouple. Value is estimated.

(c) Average cooling rate from hold temperature to monotectic temperature.

TABLE 13. SPAR V LAUNCH COUNTDOWN

Time	Event
T - ∿ 16 hours	Specimens at hold temperature
T = 0	Launch
T + 66 Sec	Nose tip eject
T + 68 Sec	Motor despin
T + 70 Sec	Payload separation and RCS enable
T + 71 Sec	RCS enable (Back-up)
T + 84 Sec	Estimated low-g period start
T + 160 Sec	Start of cooldown
T + 329 Sec	Estimated low-g period end (10^{-3}g)
T + 352 Sec	Estimated complete solidification in 74-30-48
T + 392 Sec	Estimated complete solidification in 74-30-36

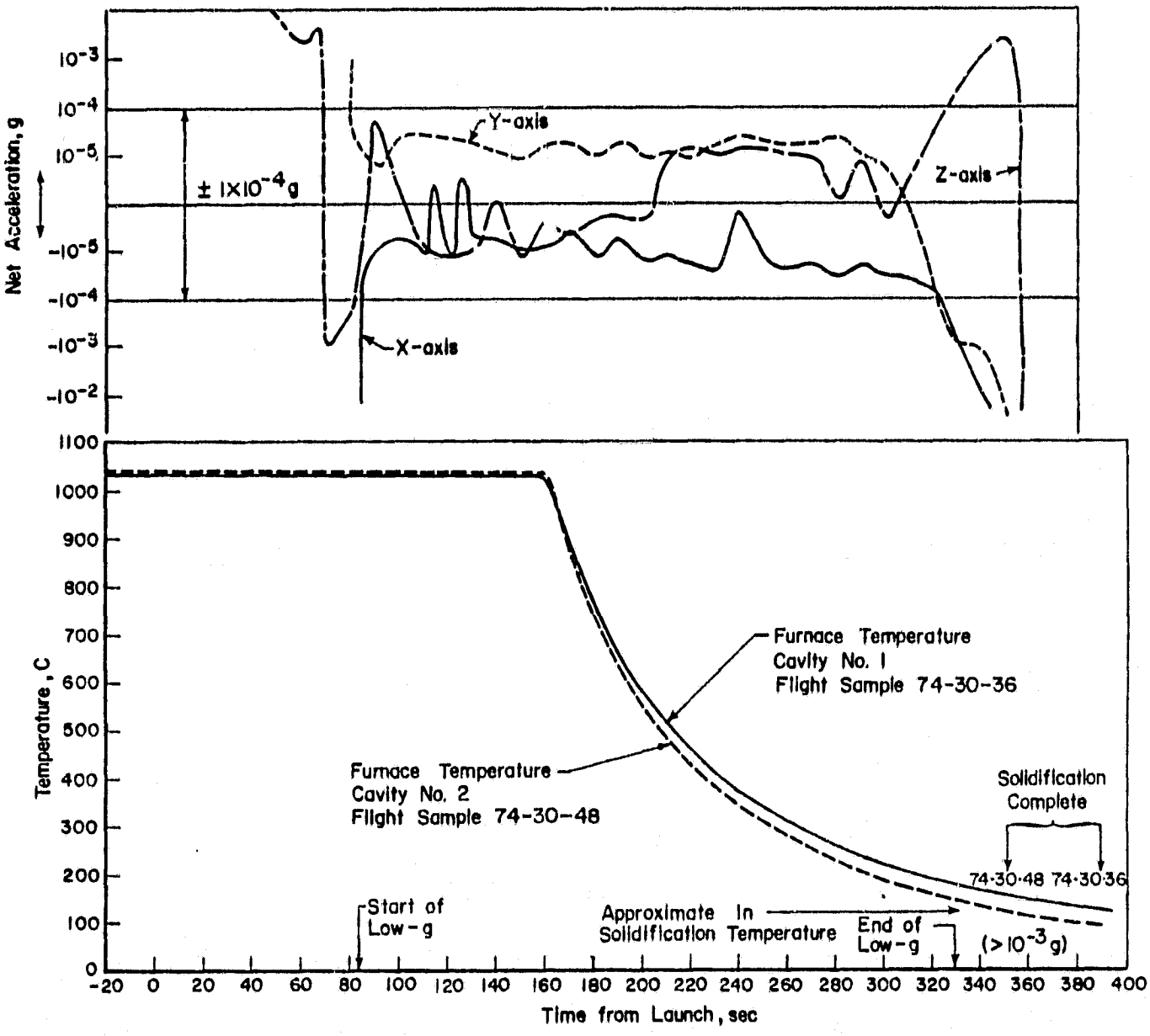

FIGURE 18. PLOT OF SPAR V ACCELEROMETER AND FURNACE CAVITY TEMPERATURE DATA VS TIME FROM LAUNCH

Radiography. Radiographs were taken of the two ground control samples and the two flight samples at kilovoltages ranging from 80 to 245 and at various sample orientations relative to the beam. The kilovoltage was varied in order to study various features of the sample. For example, 80 KV radiographs were utilized to examine the perfection of the alumina containers, whereas the higher kilovoltages were used to examine the macro-distribution of phases within the alloys. The highest kilovoltage (245 KV) was used in order to penetrate the alloy containing the highest indium content. The radiographs indicated that the samples were free of major flaws after thermal processing and demonstrated phase layering in the 1-g processed samples and massive separation in some of the flight samples. Some of the radiographs are presented in Figures 19 and 20 for the ground control and flight samples respectively.

Metallographic Examination. The two flight and two ground control samples after removal from the stainless steel container were sectioned along a longitudinal diametrical plane by first slitting the alumina crucibles with a diamond cut-off wheel and then carefully cutting through the alloys with a jeweler's saw. This technique avoids the usage of a SiC cut-off wheel and the associated problem of silicon carbide embedment in the soft alloy. After metallographic polishing, the samples were examined on both a macroscopic and microscopic level. Figures 21 through 28 show the macroviews as well as typical microstructures related to their positions in the macroview.

Aluminum-30 Weight Percent In Alloy. The macroviews and photomicrographs of this alloy processed at 1-g and in the microgravity environment are shown respectively in Figures 21 and 22. The macrograph of the 1-g processed alloy consists of a layered structure made up predominantly of the less dense aluminum-rich layer above a thin indium-rich layer. The settling of indium-rich droplets in the aluminum-rich layer is clearly observable in Figure 21 a-f. The top of this alloy is made up of an extremely fine distribution of indium droplets in the aluminum-rich matrix (Figure 21a-c) but as the interface between the aluminum-rich and indium-rich materials is approached, coarsening of the indium-rich droplets to

FIGURE 19. CONTACT PRINTS OF 200 KV RADIOGRAPHS OF GROUND CONTROL SAMPLES 74-30-29 AND 74-30-49

Al-70 Wt. Percent In

Al-40 Wt. Percent In

200 KV

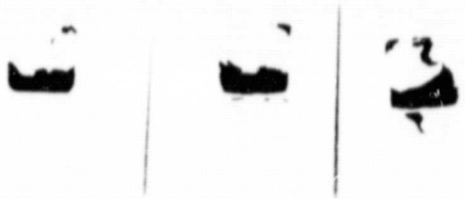

Al-70 Wt. Percent In

245 KV

74-30-36

0° 120° 240°

Al-30 Wt. Percent In

Al-90 Wt. Percent In

200KV

Al-90 Wt. Percent In

245KV

74-30-48

FIGURE 20. CONTACT PRINTS OF RADIOGRAPHS OF FLIGHT SAMPLES 74-30-36 AND 74-30-48

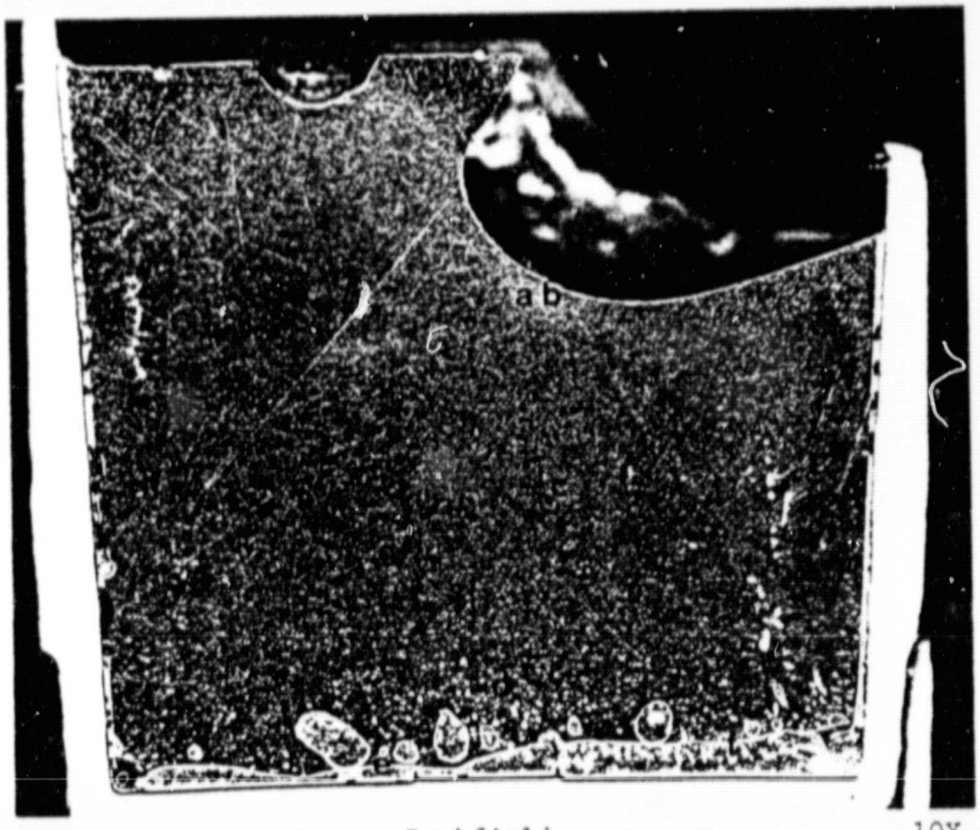

Darkfield 10X

7J664 (a) 100X 7J665 (b) 500X

FIGURE 21. MACROVIEW AND MICROSTRUCTURE OF Al-30 WEIGHT PERCENT In ALLOY FROM GROUND CONTROL CAPSULE 74-30-49

Note: Photomicrographs labelled (a) through (f) correspond to the regions similarly marked on macroview above.

7J666 (c) 100X

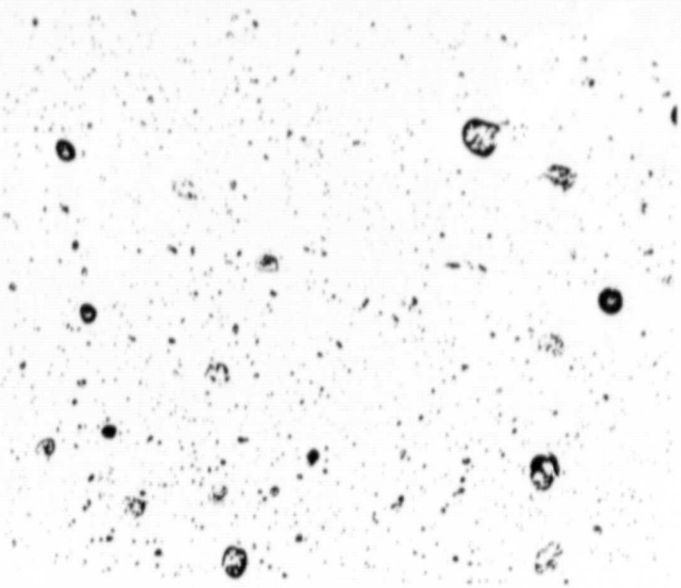

7J667 (d) 100X

7J669 (e) 100X

7J671 (f) 100X

FIGURE 21. (Continued)

Darkfield

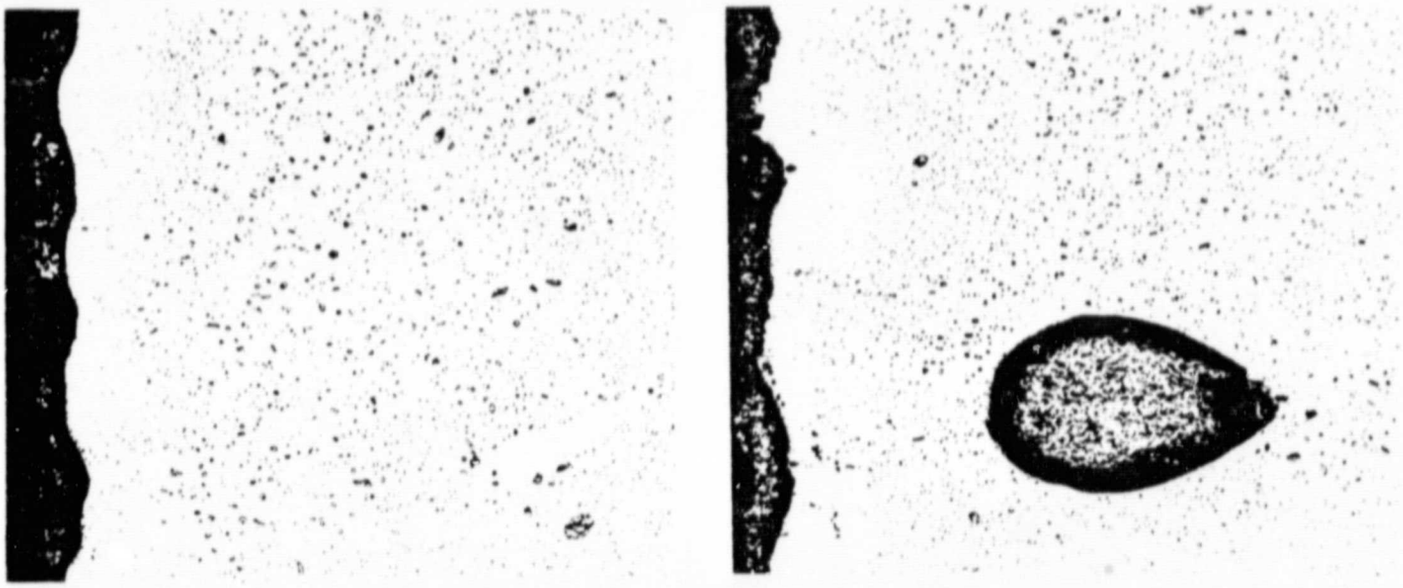

7J112 (a) 100X 7J111 (b) 100X

FIGURE 22. MACROVIEW AND MICROSTRUCTURE OF Al-30 WEIGHT PERCENT In ALLOY FROM FLIGHT SAMPLE 74-30-48

Note: Photomicrographs labelled (a) through (f) correspond to the regions similarly marked on macroview above.

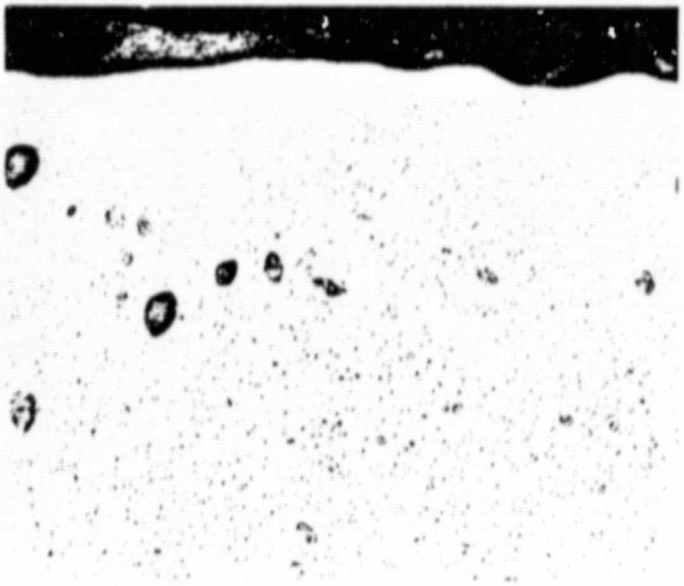

7J110 (c) 100X

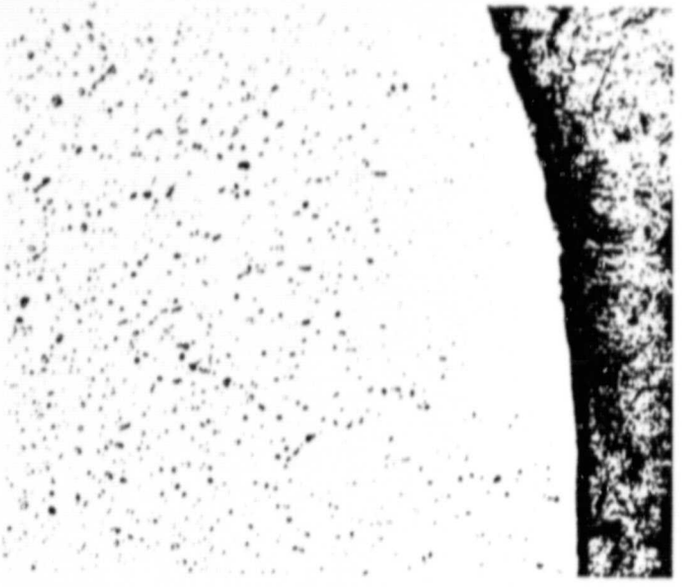

7J115 (d) 100X

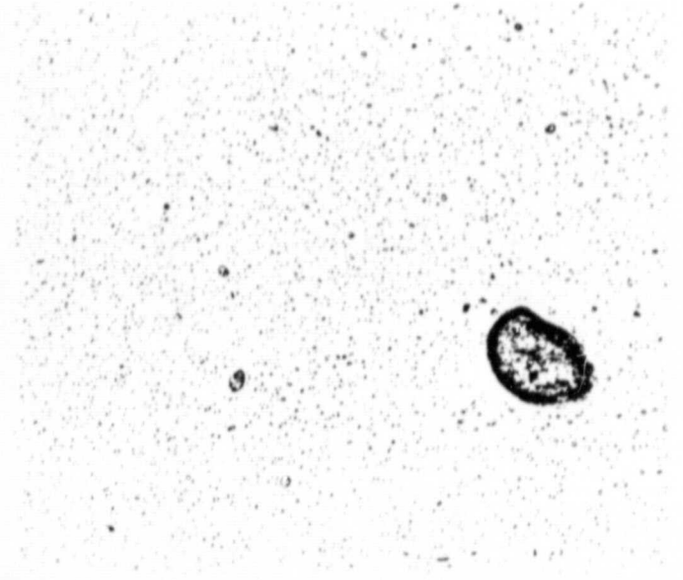

7J114 (e) 100X

7J113 (f) 100X

FIGURE 22. (continued)

sizes on the order of 1 mm is evident (Figures 21d-f). The structure of the indium-rich phase consists primarily of aluminum-rich dendrites in an indium-rich matrix. There is little evidence for the presence of aluminum-rich spheres as seen in alloys of this system with higher indium concentration.

The macroview of the 30 weight percent In flight sample shows a predominant aluminum-rich phase surounded by a very thin layer of indium-rich alloy (see Figures 22a-d). It should be noted that the interface between the aluminum-rich core and the surrounding indium-rich material is somewhat wavy. The aluminum-rich core contains in addition to a fine distribution of indium droplets, a distribution of coarse ($\leq$ 0.4 mm diameter) indium droplets which appears to be concentrated in the region extending from the upper left to the lower right of the macroview. The shrinkage cavity in the upper right portion of the macroview presumably is the last portion of the alloy to solidify because of the presence nearby of the low conductivity helium gas phase. The indium-rich phase surrounding the aluminum-rich core appears to be devoid of second phase aluminum.

Aluminum-40 Weight Percent In Alloy. The macroviews and microstructural features of the 40 weight percent In alloys processed on the ground and in the micro-gravity environment are shown respectively in Figures 23 and 24.

The macroview of the sample processed at 1-g possesses a layered structure typical of this type of alloy. The major differences between this alloy and 30 weight percent In alloy previously described are the relative thickness of the indium and aluminum-rich layers, the presence in the indium-rich layer of second phase aluminum-rich dendrites and droplets and the finer size of the indium-rich droplets settling within the aluminum-rich host.

The photomicrographs presented in Figures 23 a-d of the aluminum-rich portion of the alloy reveal a microstructure similar to that of the 30 weight percent In alloy. The photomicrographs of the indium-rich portion, Figure 23 d-f, show a relatively narrow region near the interface between the aluminum-rich and indium-rich portions of the alloy

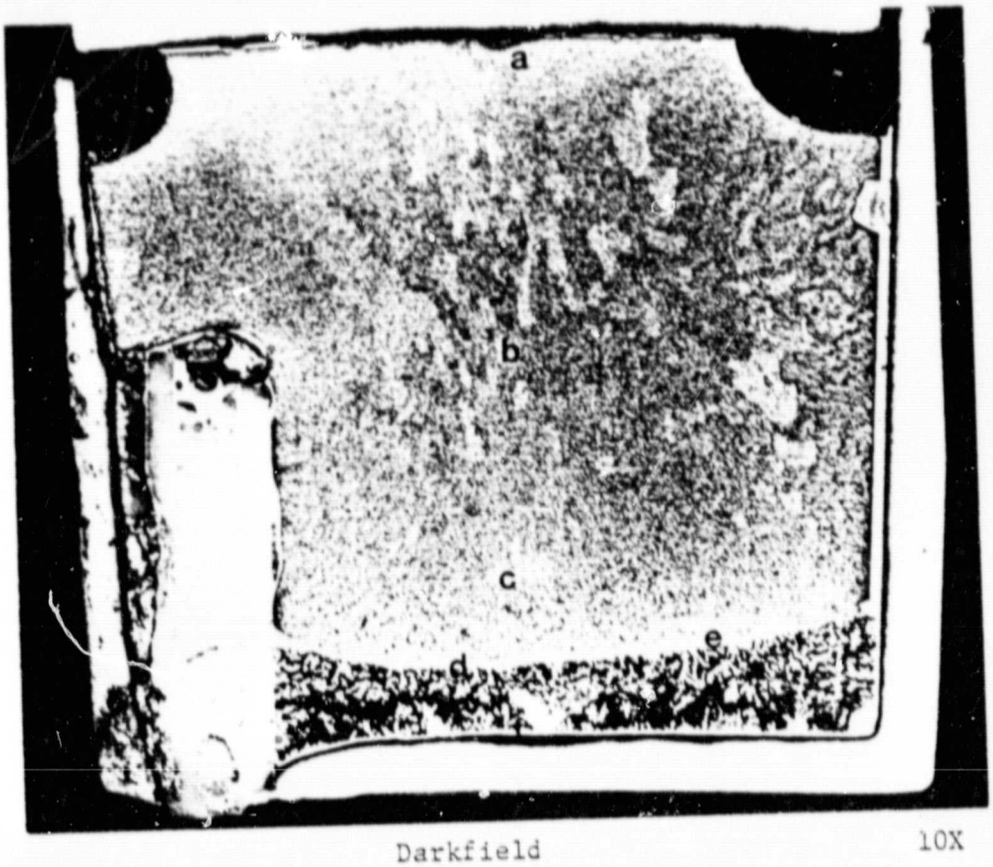

Darkfield 10X

7J657 (a) 100X

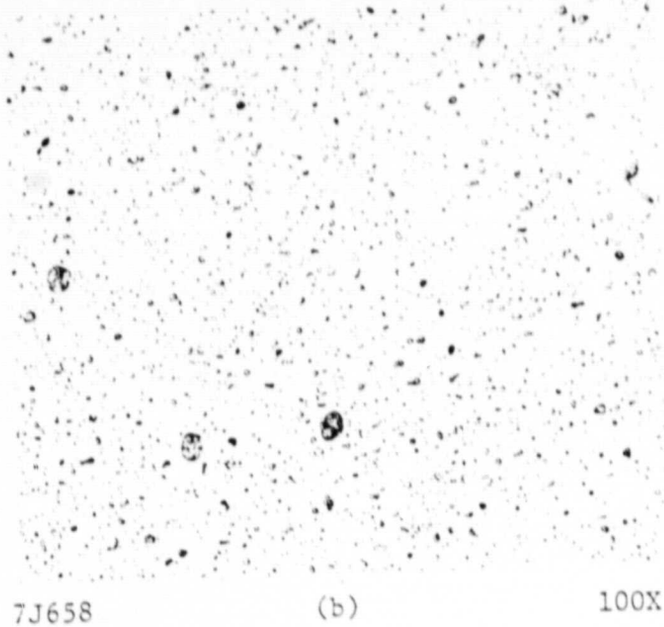

7J658 (b) 100X

FIGURE 23. MACROVIEW AND MICROSTRUCTURE OF Al-40 WEIGHT PERCENT In ALLOY FROM GROUND CONTROL CAPSULE 74-30-29

Note: Photomicrographs labelled (a) through (f) correspond to the regions similarly marked in the macroview shown at the top.

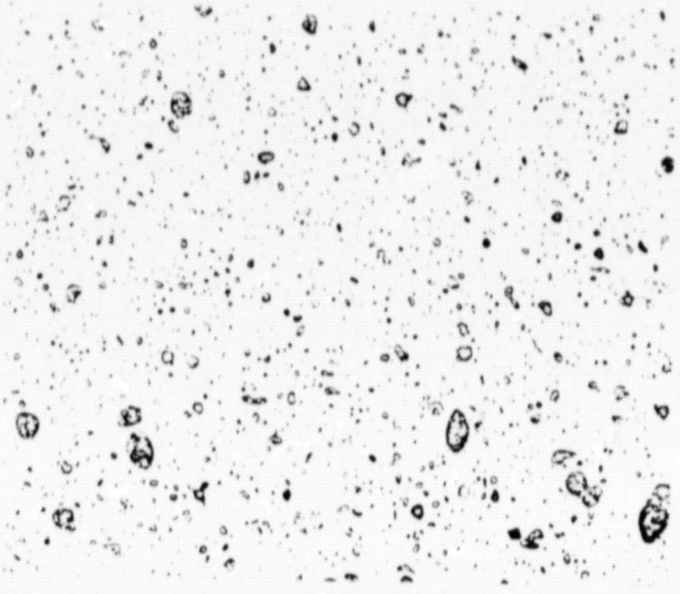

7J659 (c) 100X

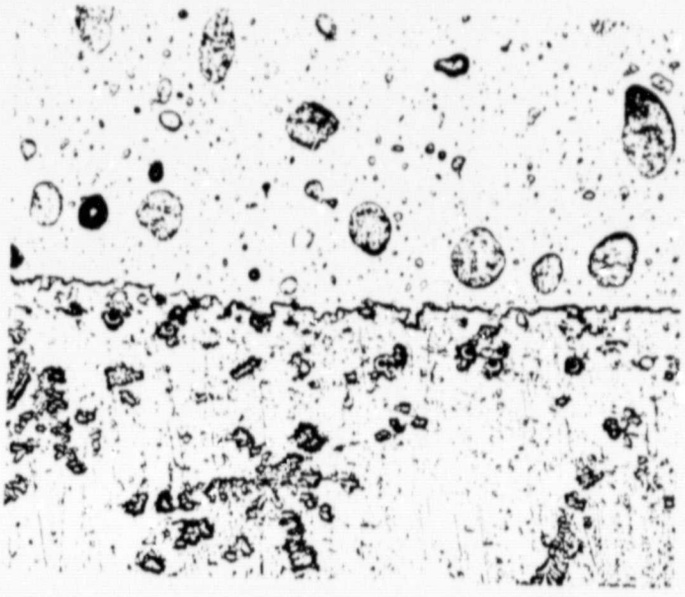

7J660 (d) 100X

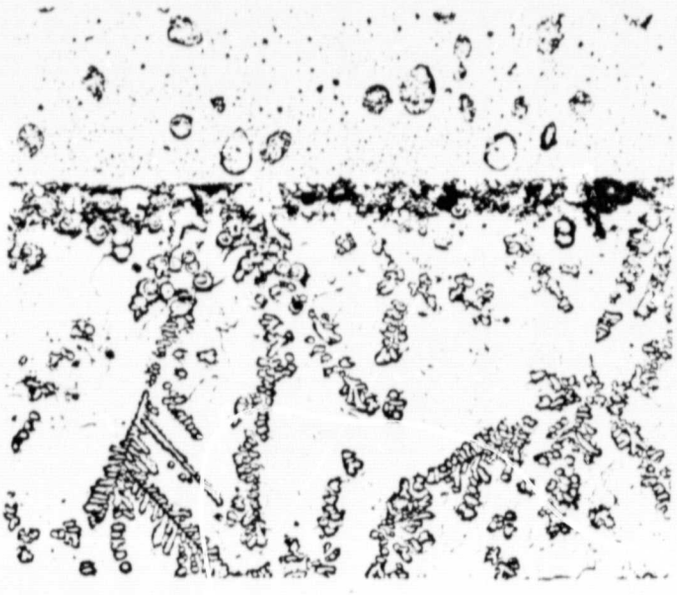

7J661 (e) 100X

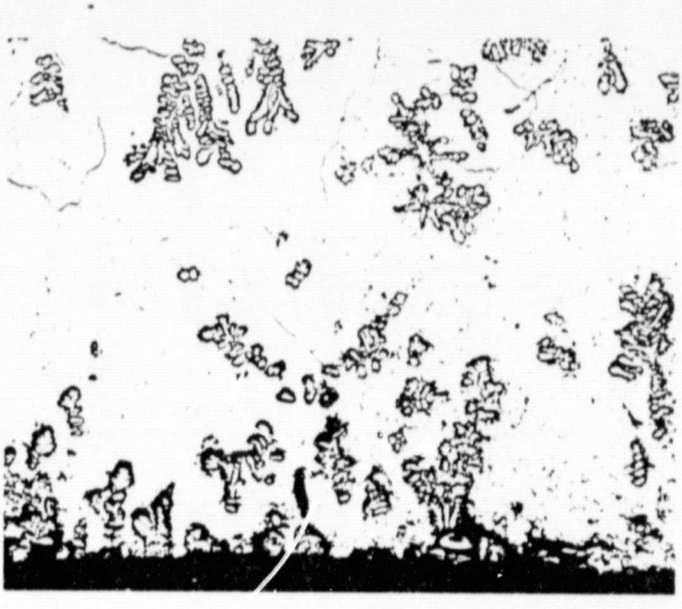

7J662 (f) 100X

FIGURE 23. (continued)

Darkfield

7J108 (a) 100X

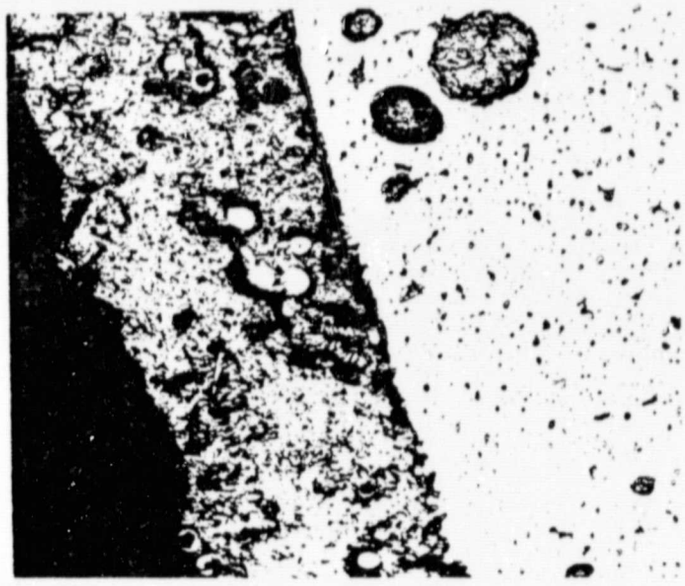

7J104 (b) 100X

FIGURE 24. MACROVIEW AND MICROSTRUCTURE OF Al-40 WEIGHT PERCENT In ALLOY FROM FLIGHT SAMPLE 74-30-48

Note: Photomicrographs labelled (a) through (f) correspond to regions similarly designated in macroview above

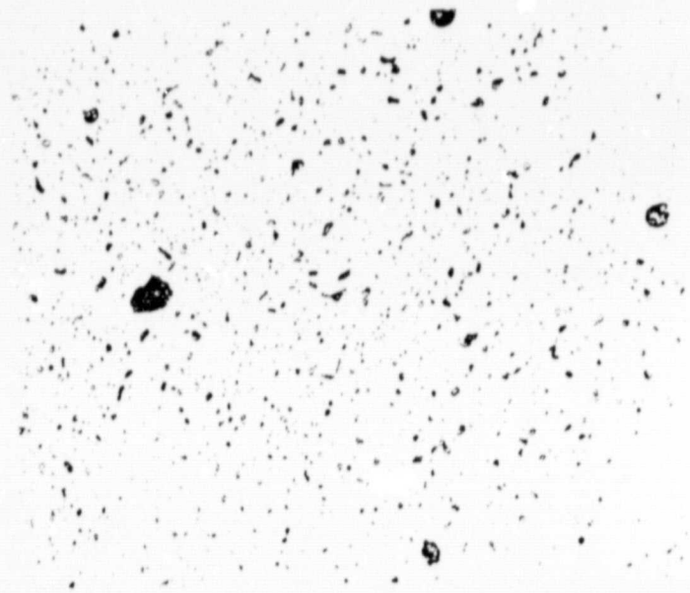

7J102 (c) 100X

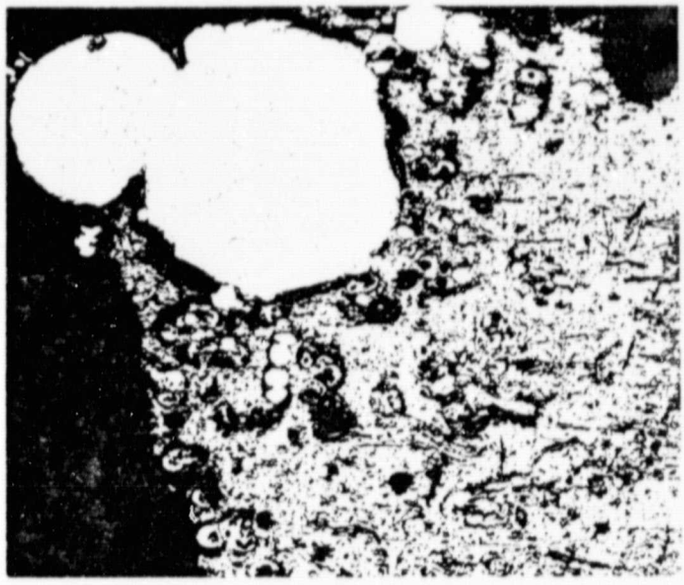

7J109 (d) 100X

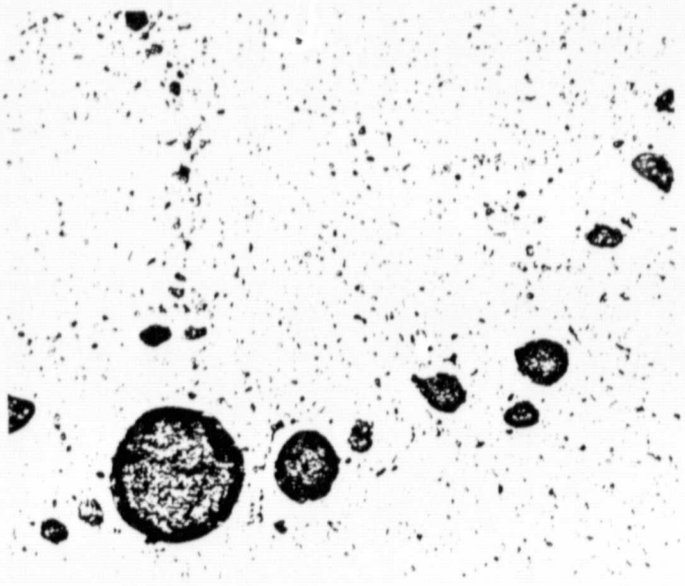

7J107 (e) 100X

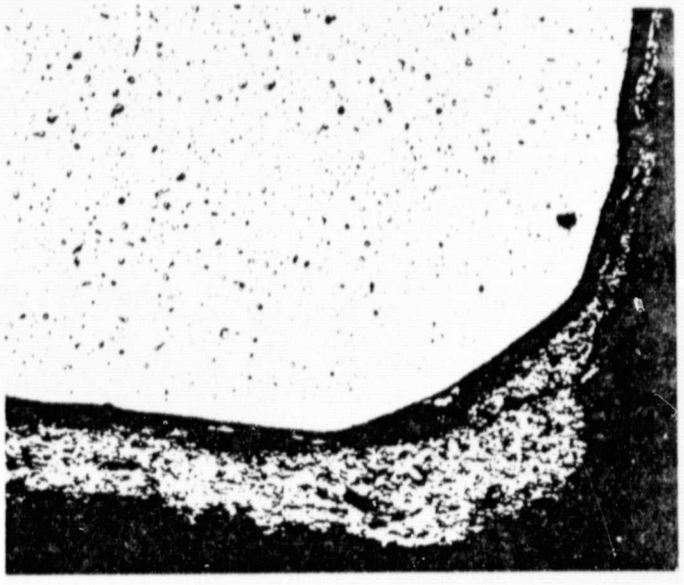

7J106 (f) 100X

FIGURE 24. (Continued)

that contain aluminum-rich spheres. Some aluminum-rich spheres have also been found at the bottom crucible wall (Figure 23f). The major portion of the indium-rich region has a microstructure consisting of an indium-rich matrix containing a high volume fraction of aluminum-rich dendrites.

The 40 weight percent In flight sample shown in Figure 24 has a macrostructure consisting of an aluminum-rich core region surrounded by an indium-rich region of much greater thickness than observed in the 30 weight percent In flight sample. The microstructures of the aluminum-rich regions are quite similar. However, the 40 weight percent In alloy appears to contain a somewhat more homogeneously distributed indium-rich phase. On the other hand, the microstructure of the indium-rich region differs significantly from its counter-part in the 30 weight percent In alloy in that aluminum-rich spheres and dendrites are present in this alloy and absent in the 30 weight percent In alloy. The aluminum-rich spheres appear to be concentrated near the aluminum-rich core in most cases. However, a region shown in Figure 24d shows larger aluminum-rich spheres surrounded by concentrations of smaller spheres.

Aluminum-70 Weight Percent In. Macroviews and photomicrographs of the ground control and flight samples are shown respectively in Figures 25 and 26. The ground control samples is very similar to the 40 weight percent In ground control sample with the following exceptions.

(1) The proportion of indium-rich to aluminum-rich material is larger.
(2) A larger number of aluminum-rich spheres are present along the interface between the indium-rich phase and alumina crucible (see Figure 25 f).
(3) A number of larger aluminum-rich spheres ($\sim$ 0.2-mm in diameter) are present at the interface between the aluminum-rich and indium-rich phases in addition to a concentration of relatively small spheres.

7J649 Darkfield 10X

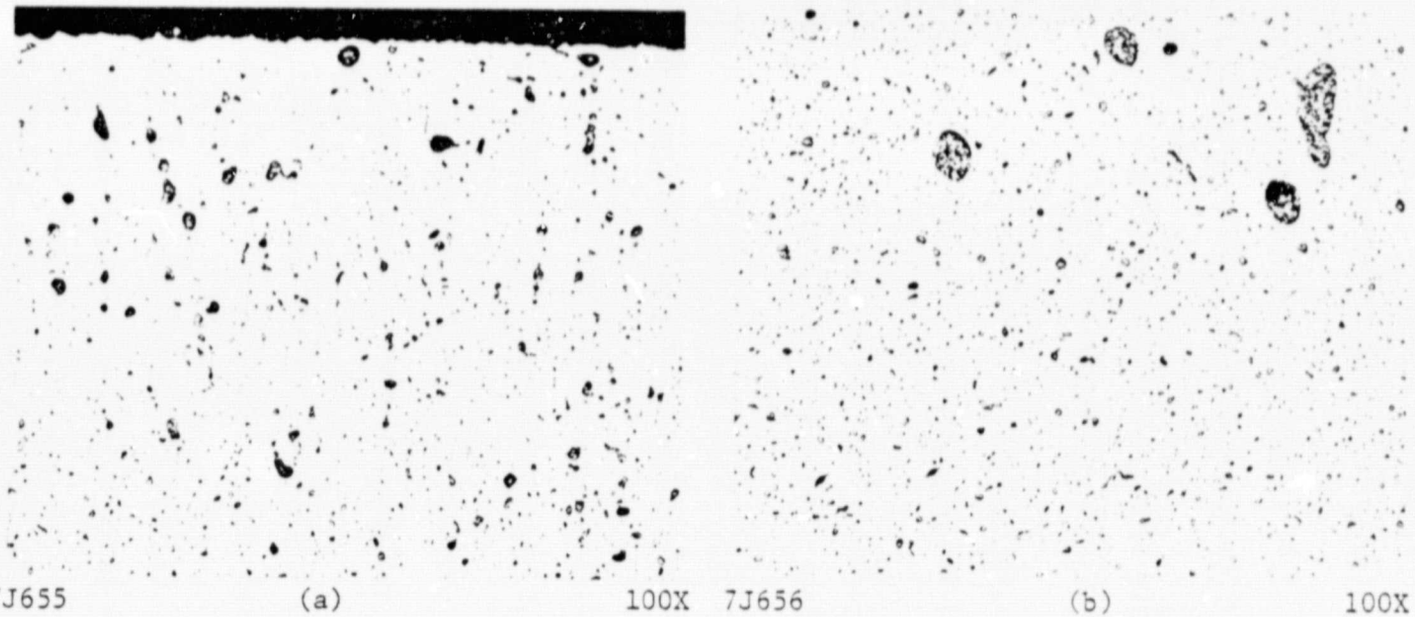

7J655 (a) 100X 7J656 (b) 100X

FIGURE 25. MACROVIEW AND MICROSTRUCTURE OF Al-70 WEIGHT PERCENT In ALLOY FROM GROUND CONTROL CAPSULE 74-30-29

Note: Photomicrographs labelled (a) through (f) correspond to the regions similarly marked in the macroview shown at top

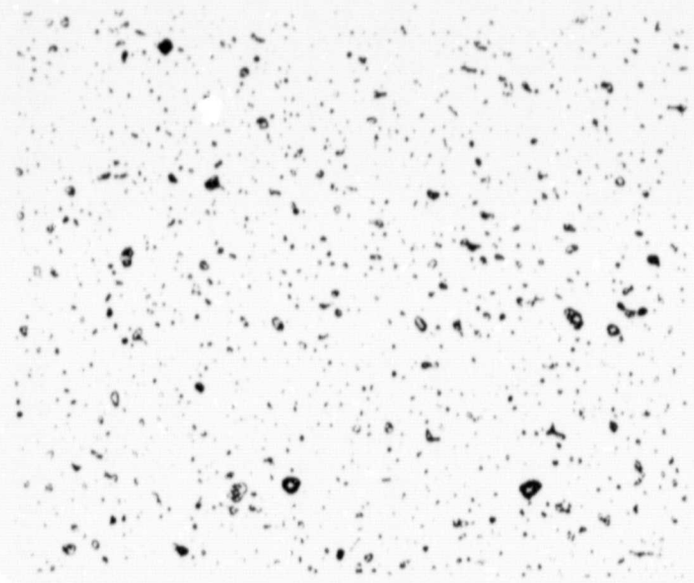

7J652 (c) 100X

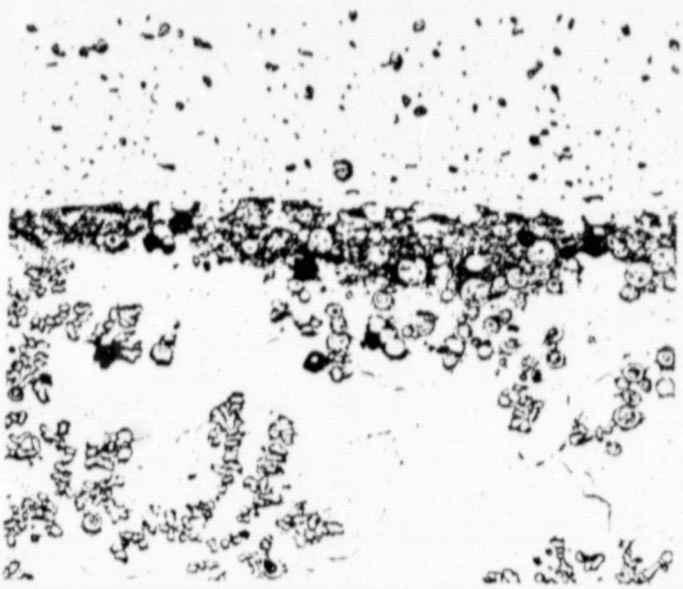

7J654 (d) 100X

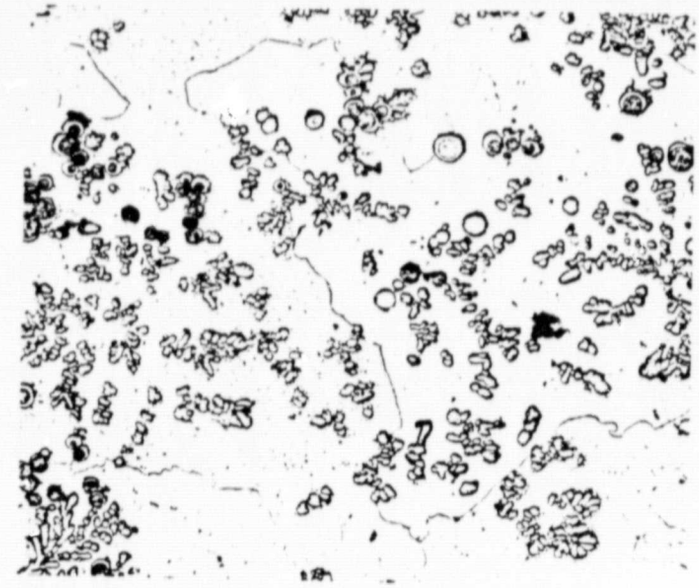

7J655 (e) 100X

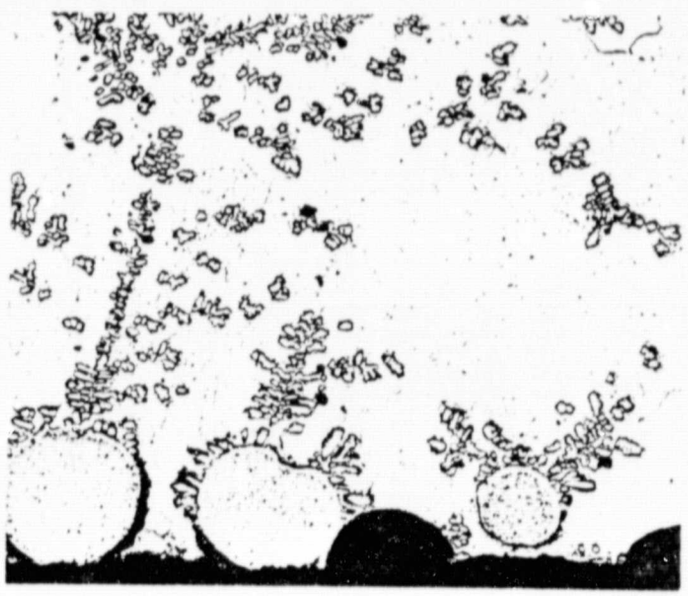

7J656 (f) 100X

FIGURE 25. (Continued)

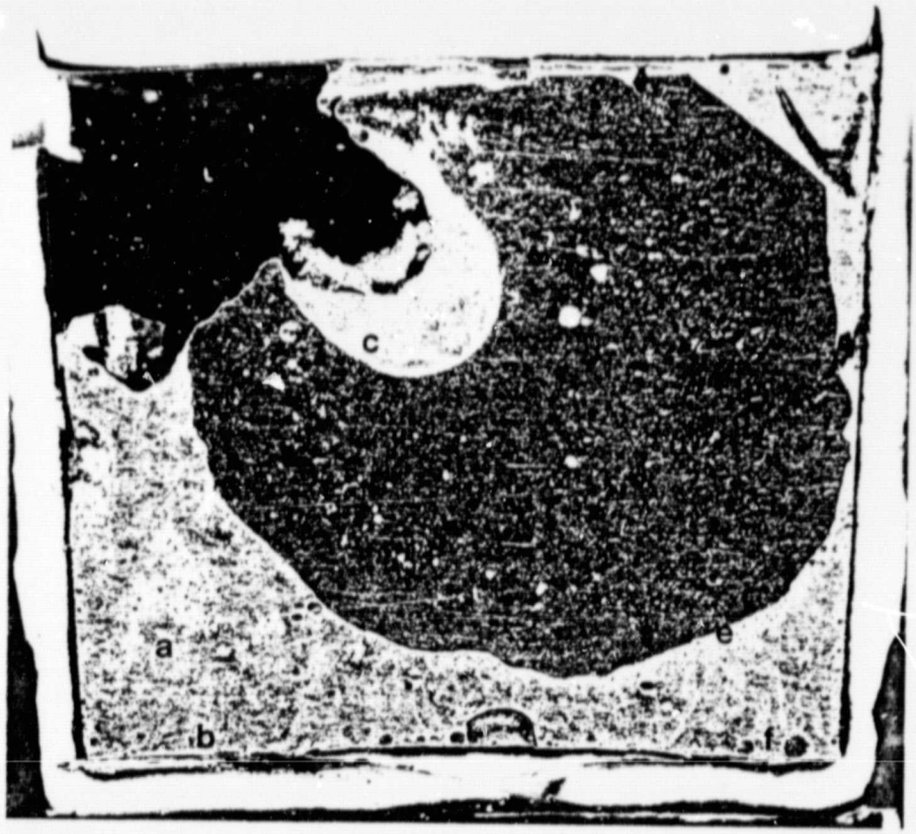

Darkfield 10X

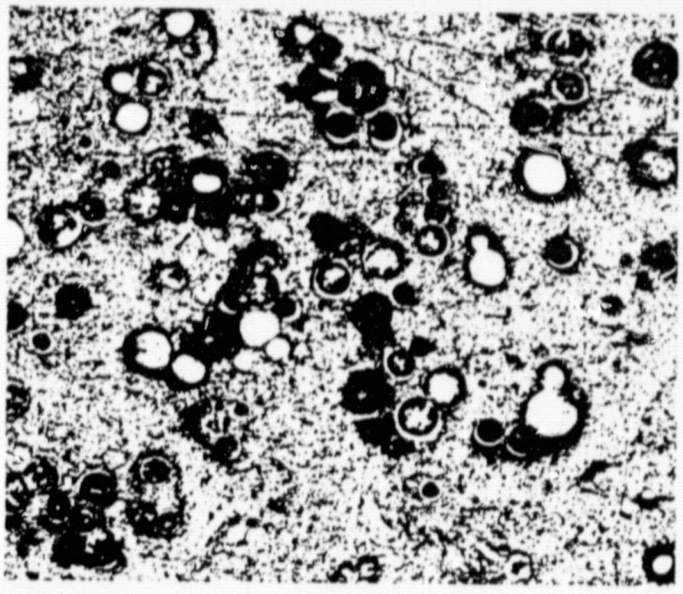

7J098 (a) 100X

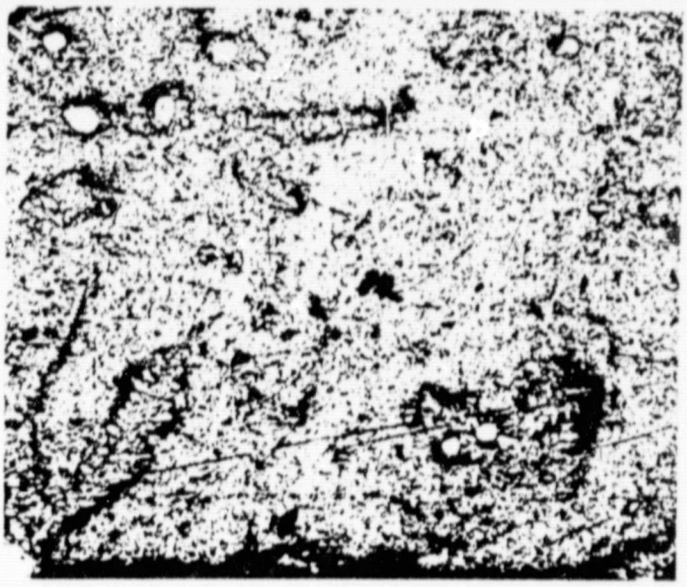

7J101 (b) 100X

FIGURE 26. MACROVIEW AND MICROSTRUCTURE OF Al-70 WEIGHT PERCENT In ALLOY FROM FLIGHT SAMPLE 74-30-36

Note: Photomicrographs labelled (a) through (f) correspond to regions similarly marked in the microviews shown at top

7J100 (c) 100X

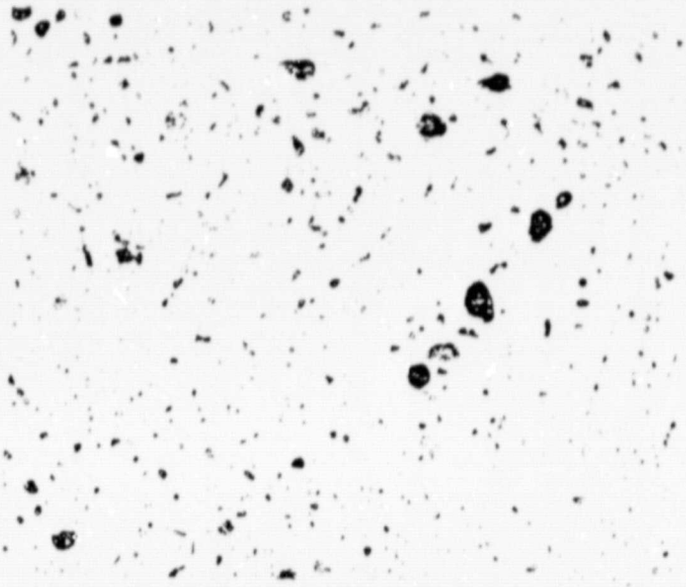

7J097 (d) 100X

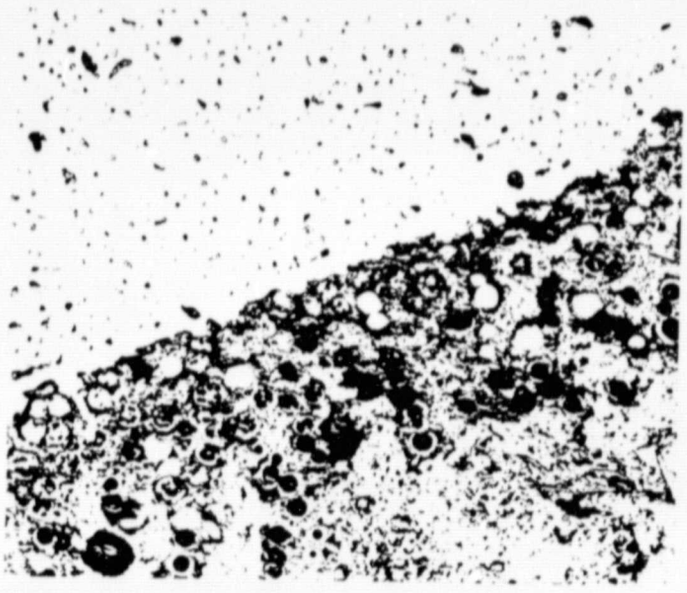

7J096 (e) 100X

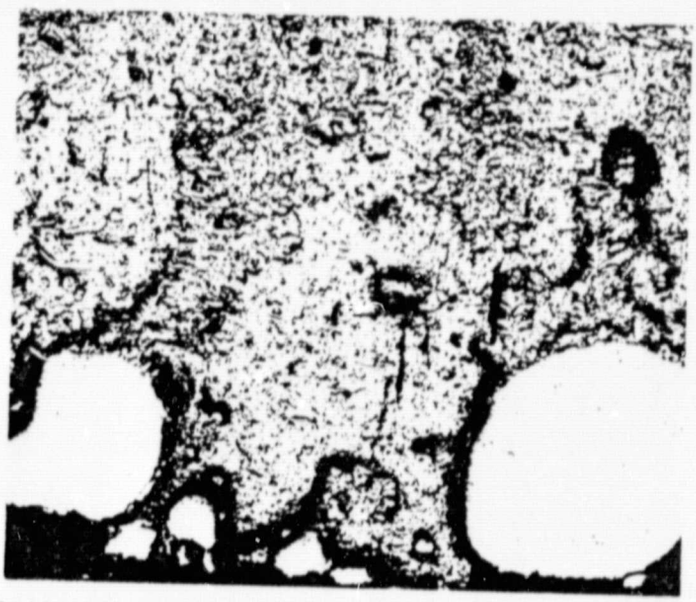

7J099 (f) 100X

FIGURE 26. (Continued)

The 70 weight percent In alloy flight sample has a macrostructure very similar to that of its SPAR II counterpart. Since the volume of the aluminum-rich phase is now small enough not to be restricted by the crucible, this phase is able to assume a roughly spherical shape while being surrounded by the indium-rich metal. The indium-rich droplets contained within the aluminum-rich core appear to be of approximately the same size distribution as in the 70 weight percent In ground control sample and in the 40 weight percent In alloys and is much more homogeneously distributed than in the ground control samples.

As may be seen from photomacroviews shown in Figure 26 and the photomicrograph of Figure 26f, there is a great tendency for the aluminum-rich spheres in the indium-rich alloy to concentrate at the crucible walls. In addition, as may be seen in Figure 26e, there is adjacent to the aluminum-rich core a concentration of small aluminum-rich spheres which appear, in some cases, to be in the process of being absorbed at the periphery of the central core. Aluminum-rich spheres of somewhat larger size and, in some cases, seemingly frozen while in the process of coalescence were also found in isolated regions within the indium-rich region (see Figure 26a). As previously observed in the 40 weight percent In alloys and in the SPAR II samples, aluminum-rich dendrites have also formed in this sample.

Aluminum-90 Weight Percent In. Macroviews and photomicrographs of the 90 weight percent In ground control and flight samples are shown in Figures 27 and 28.

The ground control sample shows a layered structure consisting of a relatively small lenticular shaped aluminum-rich phase above the indium-rich layer (see macroview, Figure 27). The indium droplets are fairly uniformly distributed in the aluminum-rich host phase and appear to have a size distribution which is somewhat smaller than that observed in the previous alloys. The settling action of the indium droplets due to gravity is not evident in the macroview of Figure 27.

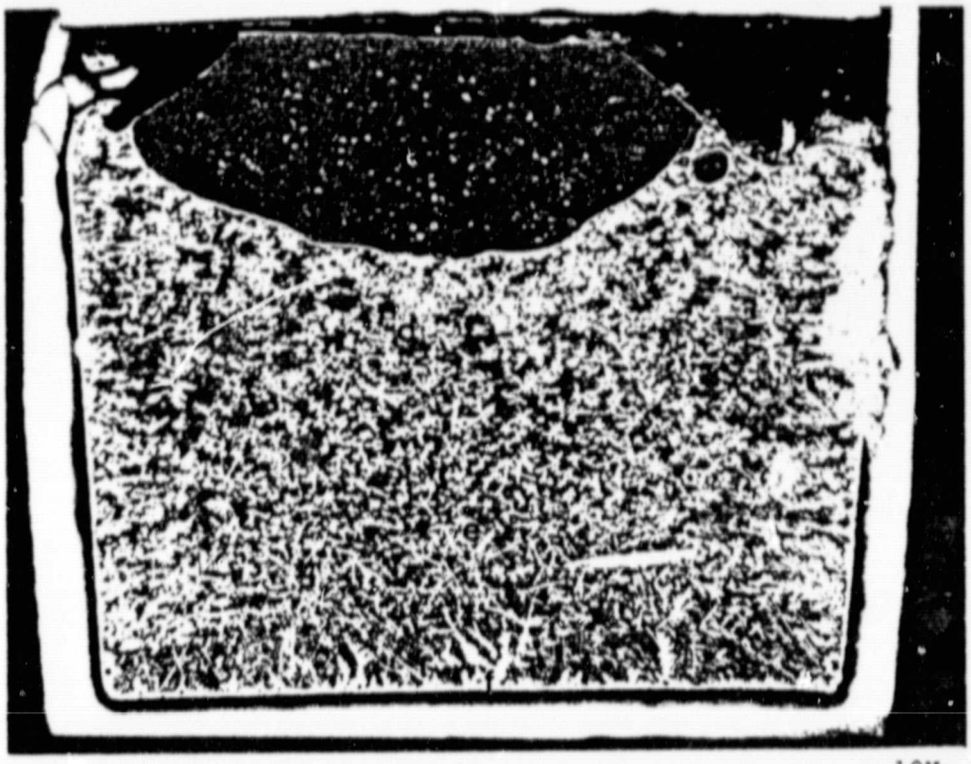

10X

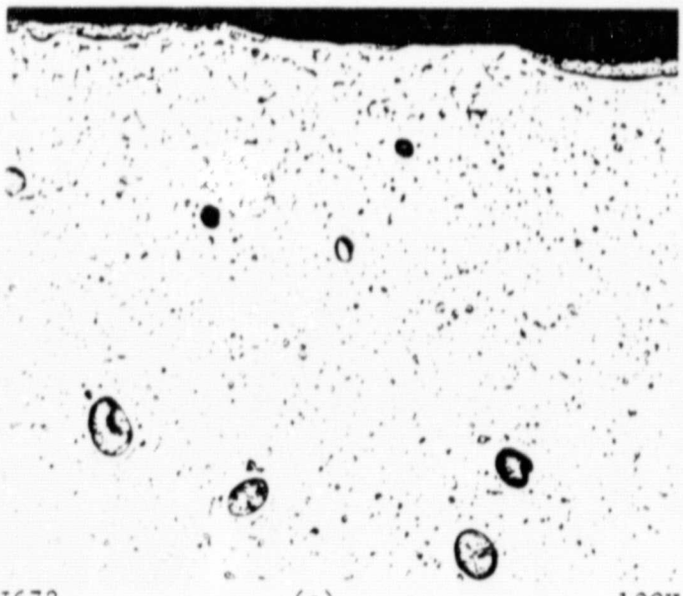

7J672 (a) 100X

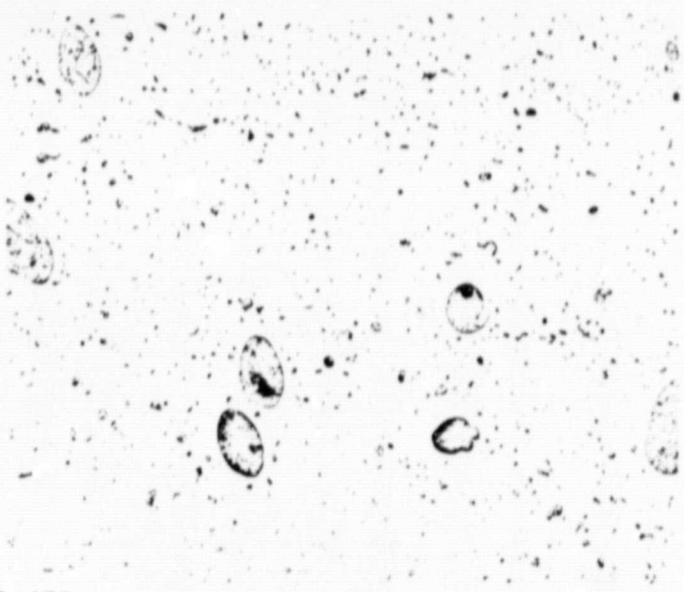

7J673 (b) 100X

FIGURE 27. MACROVIEW AND MICROSTRUCTURE OF Al-90 WEIGHT PERCENT In ALLOY FROM GROUND CONTROL CAPSULE 74-30-49

Note: Photomicrographs labelled (a) through (f) correspond to regions similarly marked on macroview above.

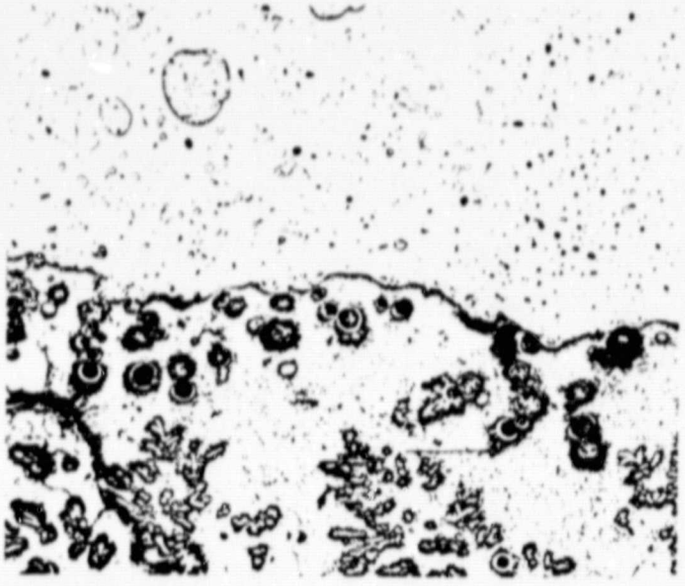

7J674 (c) 100X

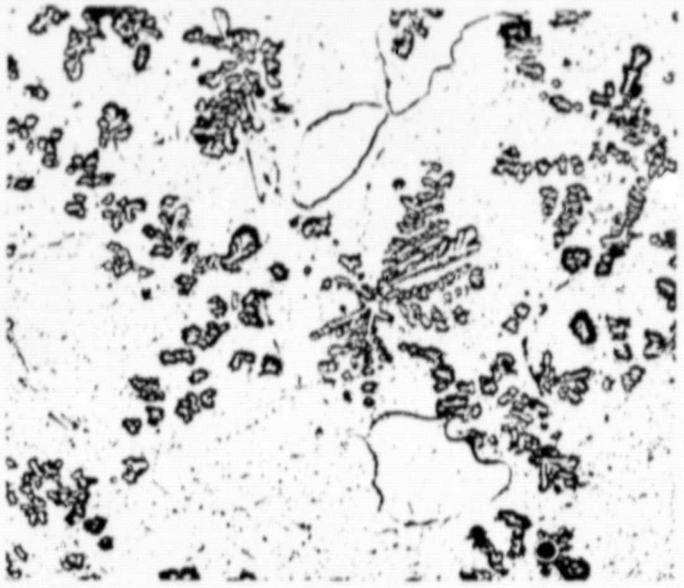

7J675 (d) 100X

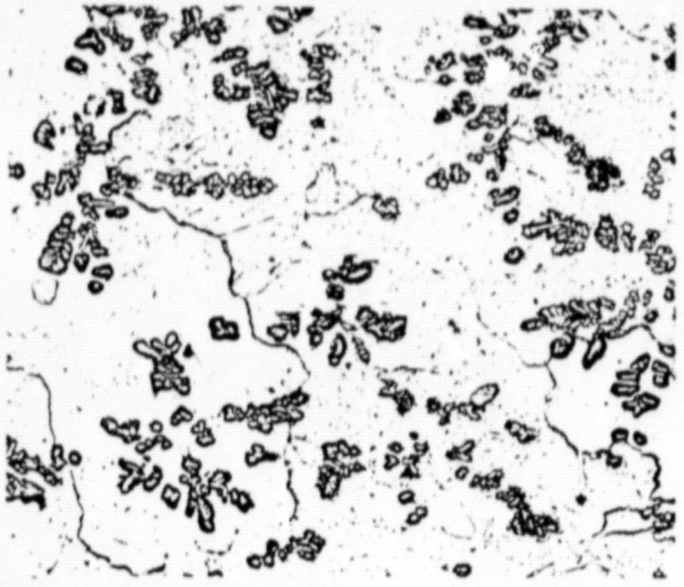

7J676 (e) 100X

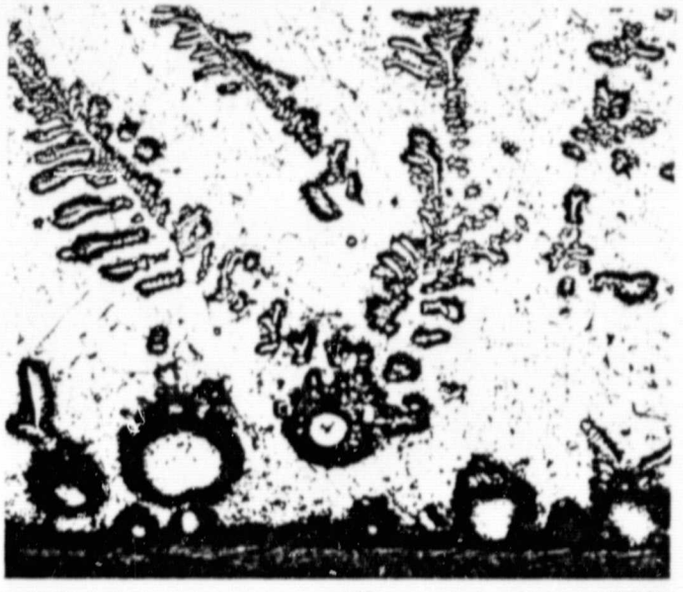

7J677 (f) 100X

FIGURE 27. (Continued)

Darkfield 100X

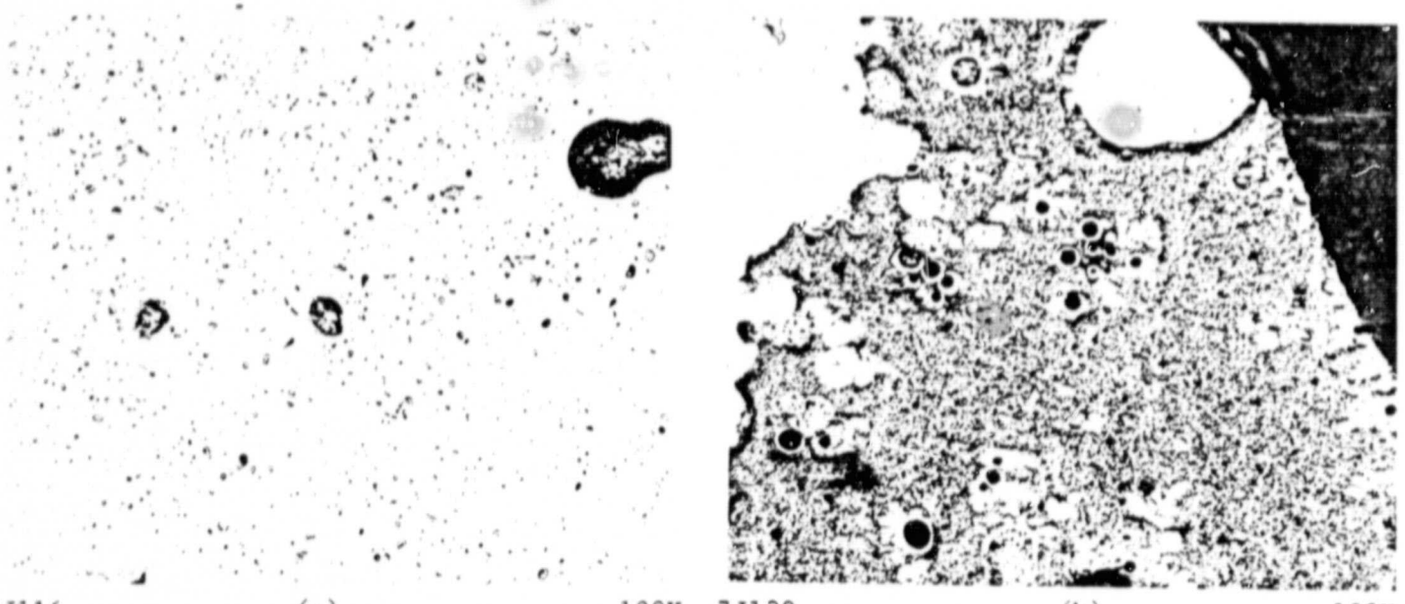

7J116 (a) 100X 7J120 (b) 100X

FIGURE 28. MACROVIEW AND MICROSTRUCTURE OF Al-90 WEIGHT PERCENT In ALLOY FROM FLIGHT SAMPLE 74-30-36

Note: Photomicrographs labelled (a) through (f) correspond to the regions similarly marked on macroview above.

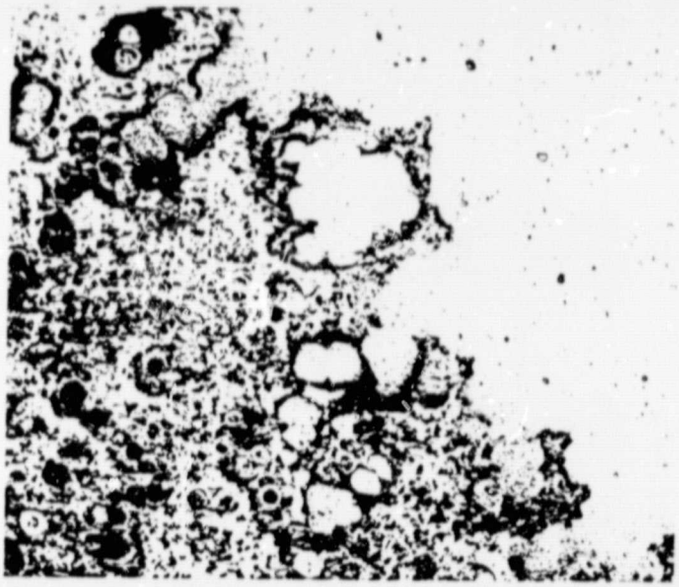

(c) 100X

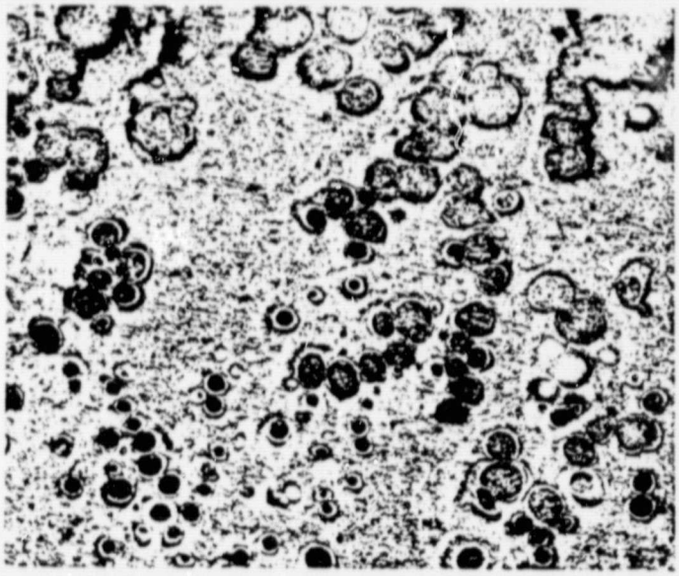

(d) 100X

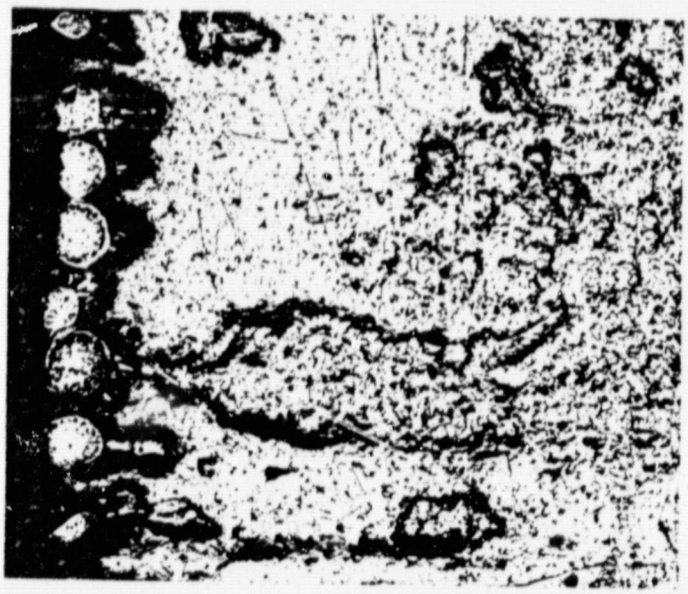

7J123 (e) 100X

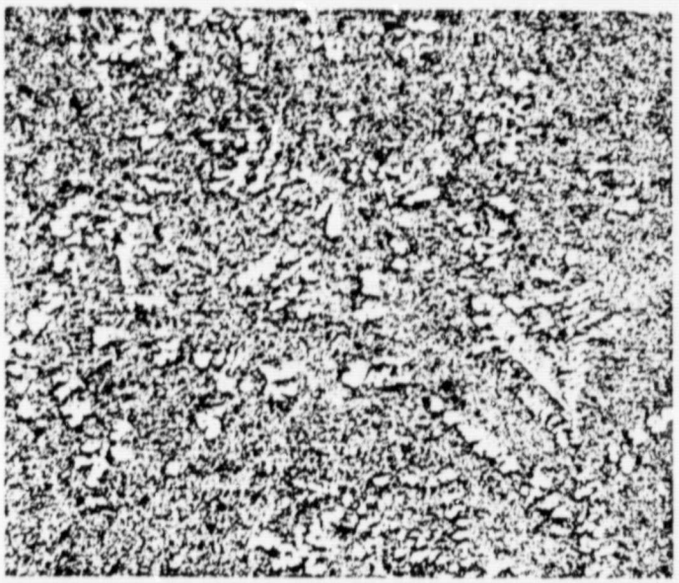

7J124 (f) 100X

FIGURE 28. (Continued)

The indium-rich portion of the 90 weight percent In ground base alloy consists of an indium-rich matrix containing a fairly uniform distribution of aluminum dendrites. The aluminum-rich spheres also present in this portion of the alloy appear to be concentrated along the crucible walls at the bottom of the sample and near the interface between the aluminum-rich and indium-rich portions of the alloy.

The 90 weight percent In flight alloy shown in Figure 28 was by far the most informative of the samples. As may be seen from the macroview shown in this figure, the structure consists of two aluminum rich regions (dark colored) surrounded by indium-rich metal. The aluminum-rich portion of the alloy shows features which are similar to those in the other alloys previously described (see Figure 28 a). The indium-rich portion, however, did reveal rather unusual macro- and microstructures. The region immediately surrounding the aluminum-rich phase (see macroview in Figure 28 and Figure 28b-d) contains a high concentration of aluminum spheres which appear to increase in size by a coalescence process as they approach the massive aluminum-rich phase. This process can be clearly seen in Figure 28c and 28d. (Note the macroscopic aluminum-rich phase is at the top right of Figure 28 and above Figure 28.) This annular region containing a high concentration of aluminum-rich spheres and surrounding the massively agglomerated aluminum-rich core is in itself surrounded by a region devoid of aluminum-rich spheres. The microstructure of this region, shown in Figure 28 consists of an indium-rich matrix containing aluminum dendrites. Aluminum-rich spheres are also found to be concentrated in the indium-rich region at the crucible bottom and walls (see macroview of Figure 28 and Figure 29).

Discussion of SPAR V Results

Comparison with the Results of Spar II

The major differences in the processing of SPAR II versus SPAR V samples were in the homogenization time (0.25 vs. 16 hours), cooling rate (17.9 C/second vs. 10.4 C/second for the ground control

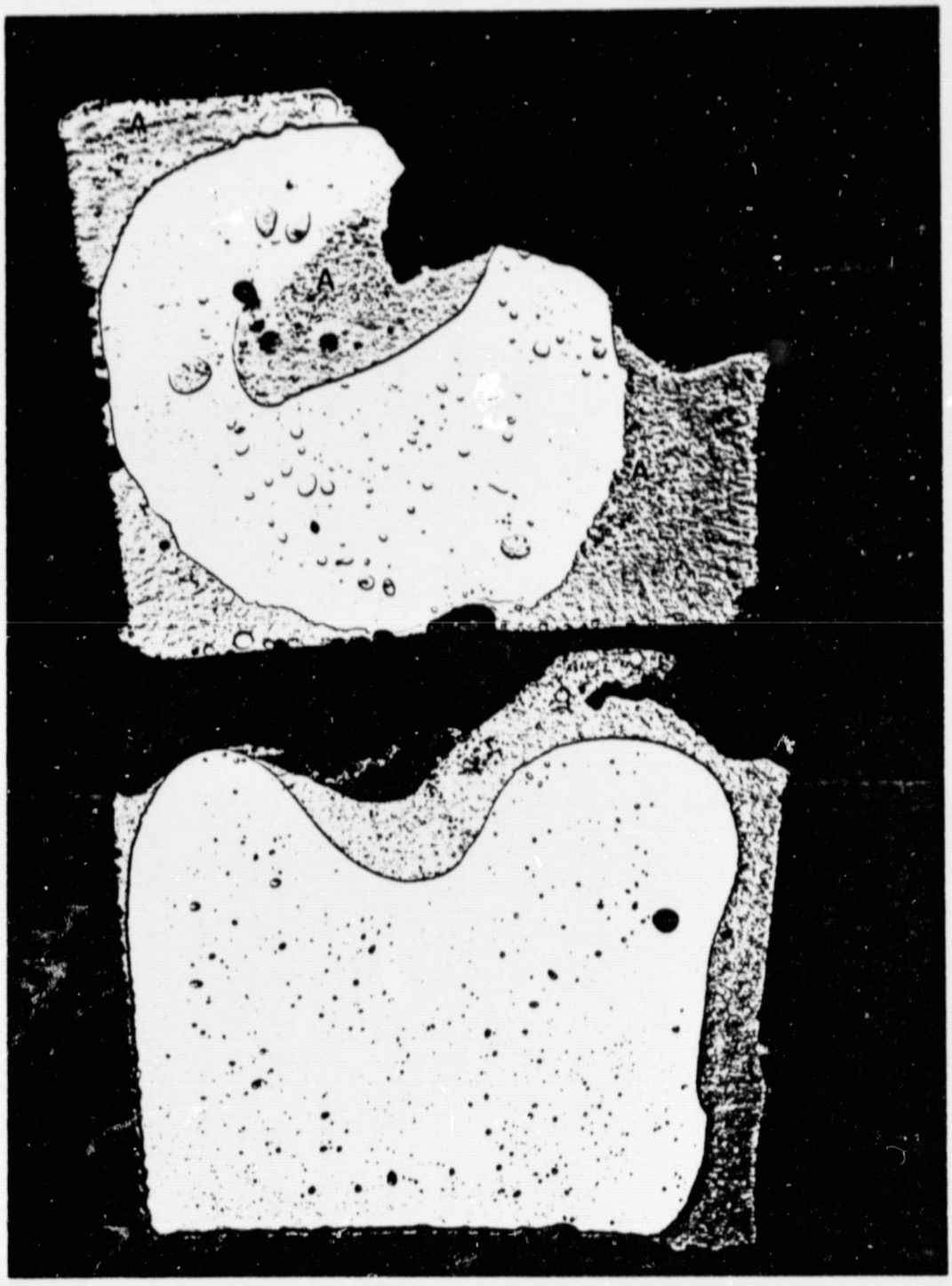

FIGURE 29. MACROVIEW OF CENTRAL POLISHED LONGITUDINAL SECTION FLIGHT SAMPLE 74-30-21 (SPAR II)

This section is the opposite half of that shown in Figure 3.

samples, 14.7 vs. 10.0 C/second for the flight samples) and the likelihood that the indium-rich portions of the SPAR V flight samples had not completely solidified while in the microgravity environment.

In spite of these seemingly large differences in processing conditions, the macro and microstructures of the 40 and 70 weight percent In ground control and flight samples from SPAR II and SPAR V were surprisingly similar. The only differences noted were rather subtle and can be attributed primarily to differences in cooling rate. Some of these microstructural variations are discussed below.

In the ground base 40 weight percent In alloys, the degree to which the indium-rich droplets have settled in the aluminum-rich host phase appears to be appreciably less in the SPAR II sample as evidenced by a wider band of coarse indium-rich droplets near the interface between the bulk phases. Likewise, the band containing aluminum-rich spheres appears to be wider in the SPAR II 70 weight percent In ground base sample than in its SPAR V counterpart. There are comparatively fewer aluminum-rich dendrites in both SPAR II ground base alloys. The wider extent of the indium-rich particles and aluminum-rich spheres in the SPAR II ground alloys may be attributed to the faster cooling rates and thus, the shorter times allowed for buoyancy forces to float or settle out the precipitated droplets. The more rapid cooling rate also restricts the time during which the aluminum dendrites can precipitate in the indium-rich phase of these samples.

The SPAR II and SPAR V flight samples were found to have very similar macro- and microstructures. There were some subtle differences seen however. For example, the indium-rich droplets in the aluminum-rich core of the SPAR II 70 weight percent In alloy appeared to be more highly coalesced. (Compare the macroview of Figure 26 with that of the SPAR II 70 weight percent In alloy shown in Figure 29.) These microstructural differences which may be in the realm of statistical variations cannot be readily interpreted at this time.

The close similarity between the structures of the SPAR II and SPAR V ground control and flight samples and the fact that most differences could be attributed to differences in cooling rates lead to the following possible conclusions.

(1) The SPAR II samples were more homogeneous at the start of cool-down than would be theoretically predicted based solely on diffusion considerations.
(2) The structures are insensitive to the degree of homogeneity, or
(3) Both the SPAR V samples were inhomogeneous at the start of cool-down.

On the basis of the diffusion experiments previously described, we would rule out the third possibility. The second possibility also does not appear viable since variations in structure associated with compositional variations would be expected. For example, in the SPAR II 40 weight percent In alloys, hypomonotectic compositions ($C/C_o < 0.07$ corresponding to compositions < 17 weight percent In) and structures would be expected at the top of the ground control sample (see Figure 11) and within the aluminum-rich portion of the flight sample. Since no evidence of hypomonotectic structures (primary aluminum plus monotectic) has been observed in the SPAR II 40 weight percent In samples, it would indicate that the first possibility is most probable and that convection currents appear to have played a substantial role in homogenizing the alloys. Since conventional convection is not expected to contribute significantly in this process owing to the compositionally stabilized configuration at 1-g, surface tension driven convection due to thermal or solutal gradients is suspected.

No differences in the macro- or microstructures between the SPAR II and SPAR V samples could be attributed to the likelihood that solidification of the indium-rich portions of the SPAR V alloys was not completed while in the micro-gravity environment. The 90 weight percent In alloy processed on SPAR V is the one expected to be most affected by this complication, but none of its structural features could be attributed to this effect. Further analysis, however, is necessary concerning the magnitude and direction of the acceleration present during the solidification of the indium-rich liquid. Some thermal analysis is also required to determine the extent of the solidification at the end of the low-g period. It should be noted that all of the aluminum-rich portion of this alloy had solidified under microgravity conditions.

Mechanisms of Massive Separation

As discussed in the review of the SPAR II experiment and delineated in Table 1, a number of mechanisms leading to fluid flow and droplet coalescence are possible. Additional observations made on SPAR V samples have added support for some of the suggested mechanisms.

Thermocapillary Convection. As previously discussed, the relatively large values for the Marangoni number, Ma, calculated on the basis of the thermal environment present during cool-down and the estimated variation of the liquid-vapor interfacial energy with temperature (-0.15 dynes/cm-deg C), has suggested that extensive fluid flows could result from this effect.

Since the time of the original analysis, there has been mounting evidence to suggest the presence of surface tension driven convection. In another NASA sponsored program[17], it has been calculated that the interfacial energy between the equilibrium aluminum-rich and indium-rich liquid phases has a variation with temperature of ∿-0.2 dyne/cm-deg C, somewhat larger than the gas-liquid interfacial tension variation with temperature. Thus, it is expected that thermocapillary flows might originate at liquid-liquid interfaces. Moreover, it is likely that such surface tension drive fluid flows might develop as a result of solutal gradients in the region of liquid-liquid interfaces. The change in liquid-liquid interfacial energy with composition, $\frac{d\gamma_{12}}{dC}$, is expected to be relatively large in the Al-In system since the liquid-vapor surface energies for aluminum and indium are quite different (850 vs. 490 ergs/cm^2).[17] These considerations hold equally well for solutal capillary flows due to liquid-vapor interfaces. Further analyses are necessary to quantify these effects.

Additional evidence to support the supposition that surface tension drive convection significantly contributes to fluid flows in this system is delineated below.

(1) Wave-like structures at former liquid-liquid interfaces have often been observed in the Al-In system.

This effect is readily seen in the SPAR II 40 weight percent In flight sample and in the 70 weight percent In ground sample shown respectively in Figures 3 and 30. Such behavior has also been previously noted in the photomicrographs of Figures 22a and b.

(2) As noted in Figure 9, temperature oscillations occur in DTA samples during cooling from a single phase liquid field into the liquid-liquid miscibility gap. Such oscillations could be produced as a result of thermal or solutal surface tension driven convection cell formation. However, there is some evidence that they may be due to transformational volume changes.[12]

(3) The presence of convection currents induced by surface tension gradients can also explain the apparent homogeniety of the SPAR II alloys prior to cool-down in spite of the expectation to the contrary based purely on diffusional considerations.

Droplet and Particle Movement. We have found evidence in the 90 weight percent In flight sample (see Figures 28c and d) that there has been a movement of aluminum-rich liquid droplets in the indium-rich liquid host phase during the cool-down process. The fact that these droplets appear to have readily coalesced supports the hypothesis that they were molten at the time of migration. This observation precludes the possibility that this effect results from solid aluminum particles being pushed by an advancing indium-rich solidification front at ∿155 C.

The hypothesis that the aluminum-rich spheres were molten during their migration and the observation that migration appears to be toward the hottest portion of the melt indicate that these droplets have migrated as a result of thermocapillary forces.

A treatment of thermocapillary migration has been reported by Bewersdorff[9] for Al-In alloys. We repeat here his calculations, but with the introduction of some refined values for the applicable physical parameters.

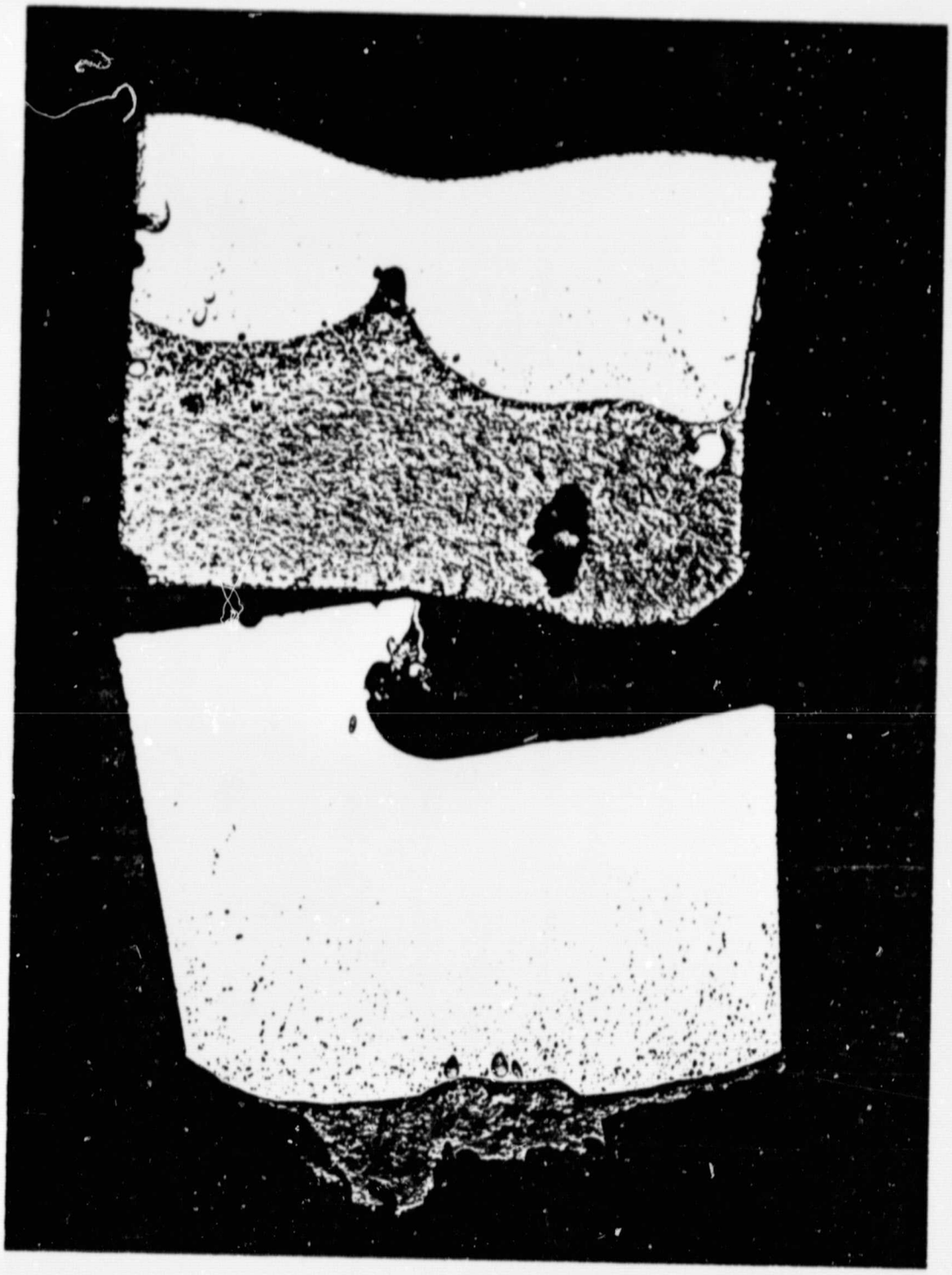

FIGURE 30. MACROVIEW OF SPAR II GROUND CONTROL SAMPLE 74-30-18

Note: Highly wavy interface between the aluminum-rich and indium-rich phases in the 70 weight percent In alloy.

The relationship for thermocapillary migration velocity, V has been formulated as follows:

$$V = \frac{-2R \frac{d\gamma_{12}}{dT} \frac{dT}{dx}}{3(2\mu_M + 3\mu_p)} , \qquad \text{Equation 9}$$

where:

R is the droplet radius,

$d\gamma_{12}/dT$ is the change in interfacial energy with temperature,

$\frac{dT}{dx}$ is the temperature gradient, and

μ_M and μ_p are the kinematic viscosities of matrix and droplet fluids, respectively.

Values of these parameters are given in Table 14 assuming that the liquids are pure aluminum and pure indium at 800 C. The results of the calculation predict the following droplet migration velocities:

Indium Droplets in an Aluminum Matrix

$$V_{In} = 16.9 \text{ R/second}, \qquad \text{Equation 10}$$

Aluminum Droplets in an Indium Matrix

$$V_{Al} = 19.1 \text{ R/second}. \qquad \text{Equation 11}$$

On the basis of Equation 11, the extent of droplet migration in 10 seconds (corresponding to the approximate time in the miscibility gap for the SPAR V alloys) for different size droplets has been calculated and is summarized in Table 15.

The aluminum-rich droplets shown in Figure 28d have radii ranging in size from approximately 10μ to more than 50μ. The corresponding expected movements are respectively 0.19 and > 0.96 cm. From the macroview of Figure 28, it may be seen that the zone relatively free of aluminum-rich droplets is approximately 0.3μ wide, a value which is consistent with the proposed mechanism. Thus, it appears to be highly probably that thermocapillary migration of aluminum-rich droplets in an indium-rich host fluid has occurred during the SPAR V experiments. Controlled ground

TABLE 14. VALUES OF PHYSICAL PARAMETERS AT 800 C USED IN THERMOCAPILLARY DROPLET MIGRATION CALCULATIONS

μ_{Al}	1.1×10^{-2} Poise
μ_{In}	5.8×10^{-3} Poise
dT/dx (6)	7 C/CM
$d\gamma_{12}/dT$ (17)	-0.17 ergs/cm^2 - °C

TABLE 15. MIGRATION DISTANCE FOR VARIOUS SIZE ALUMINUM DROPLETS IN AN INDIUM HOST FLUID

Droplet Radius, μm	Movement in 10 seconds, cm
1	0.02
10	0.19
20	0.38
50	0.96
100	1.91

base experiments aimed at studying this effect in Al-In alloys will help to further elucidate this phenomenon.

It is interesting to note that although expected, there was little evidence to support the analagous movement of indium-rich droplets toward the warmer regions of the aluminum-rich host fluid. Localized precipitation accompanied by spreading of indium-rich fluid along the crucible walls may in part have interfered with indium-rich droplet migration.

Some of the macro- and microstructures of the SPAR II and SPAR V flight samples provided evidence that some of the agglomerates of aluminum-rich spheres may be the result of particle pushing by the advancing indium-rich solidification front. These particles would be solid at the solidification temperature of the indium-rich metal. Evidence for particle pushing is especially clear in the macroview of the 70 weight percent In alloy flight sample shown at the top of Figure 29. Concentrations of fine particles (marked A in Figure 29) may be seen in the indium-rich regions. In contrast to the coalesced agglomerates described earlier, these particles, although in close proximity, show much less tendency to coarsen (see Figure 26c and e). Controlled experiments on the pushing of solid aluminum-rich particles by an advancing solidification front and the subsequent coarsening process should shed additional light on this process.

Diffusional Growth of Liquid Droplets

At the suggestion of Dr. L. Lacy of MSFC, a calculation was made to determine the droplet size at the end of the diffusion growth period for aluminum-indium alloys of various compositions. Previous calculations have shown that the diffusional growth period is extremely short (on the order of 10^{-2} to 10^{-1} seconds, depending on the number of particles per unit volume).[6] Thus, diffusional growth is complete early in the phase separation process.

We have calculated the droplet radius of the precipitating phase for various Al-In alloys at the end of the diffusional growth period using a rather simple approach. The calculation starts with a

determination of the volume fraction of the precipitating phase at the monotectic temperature as a function of alloy composition on the basis of the phase rule and equilibrium diagram.[1] The calculation is completed by dividing the volume fraction by the number of particles per unit volume and converting the resultant average particle volume to an average particle radius. Results of this calculation for the alloys of interest in this study are presented in Table 16. The particle radius is based on an assumed concentration of 2×10^7 particles/cm^3. This latter figure has been obtained from measurements made on Figure 16b, a photomicrograph of a portion of an aluminum-indium diffusion couple which had been cooled at a rate of approximately 1000 C/second.

TABLE 16. EQUILIBRIUM PARTICLE SIZE AND SPACING RESULTING FROM DIFFUSIONAL GROWTH

Alloy Composition Weight Percent In	Volume Fraction of Droplets, percent	Particle Radius[a] μm	Interparticle Spacing[b]
30	7.5 In	9.6	1.95R
40	14.6 In	12.0	1.44R
70	45.8 In	17.6	0.35R
90	17.9 Al	12.9	1.21R

(a) Based on a droplet concentration of 2×10^7 droplets/cm^3

(b) Based on close packing of spherical drops

The distance between particles, d, is also listed in Table 16. This parameter has been calculated assuming that the centers of the droplets lie on a close-packed cubic grid of spacing a. It then follows that

$$d = \frac{a\sqrt{2}}{2} - 2\,r_p \qquad \text{Equation 12}$$

where

r_p is the droplet radius.

a and r are related to the volume fraction of droplets, V_f by the relation:

$$V_f = \frac{16r_p^3}{3a^3} \qquad \text{Equation 13}$$

By combining Equations 12 and 13 in such a way as to eliminate a, it follows that the ratio, d/r_p, is related to V_f by the equation:

$$\frac{d}{r_p} = \sqrt{\frac{2}{2}} \left(\frac{16\pi}{3V_f}\right)^{1/3} - 2. \qquad \text{Equation 14}$$

It should be noted that Equation 14 is independent of the number of droplets per unit volume.

The effect of composition may be clearly seen from Table 16. For a given assumed droplet density, and for the compositions treated, the particle radius at the end of the diffusional growth process is largest for the 70 weight percent In alloy. What is more important is that the spacing between droplets at this composition is extremely small being only 0.35 r_p. The small distance between droplets, especially if the droplets are very fine, can lead to gross instability of the droplet dispersion since only small movements are required for two droplets to collide and coalesce. Based on these consideration, it is not suprising that alloys of approximately this composition show massive separation even if they are in the miscibility gap for only a fraction of a second.

CONCLUSIONS

The following conclusions are based on our SPAR II and SPAR V flight studies and the supporting ground base experimentation:

(1) The results of SPAR V have established that the massive phase separation observed in both SPAR II and SPAR V was not caused by a lack of homogeneity in the molten liquid at the start of the cool-down portion of the experiments.

(2) It is highly probable that surface tension drive flows are active and significantly contribute to the observed structures in the SPAR II and SPAR V samples. This is evidenced by the presence of wavy interfaces between the aluminum-rich and indium-rich phases, the homogeneity of the SPAR II alloys at the start of cool-down and the presence of oscillatory flows in DTA experiments.

(3) It is highly likely that thermocapillary migration of aluminum-rich droplets has occurred in the indium-rich flight samples. The observation of particle coalescence distinguishes thermocapillary migration from particle pushing by an advancing liquid-solid interface. Some evidence is also presented for this latter mechanism, but it contributes little to the observed massive separation.

(4) The SPAR V flight samples had not completely solidified at the end of the low-g period ($< 10^{-3}$g). However, no macrostructural or microstructural features have been found that can be attributed to this effect.

(5) Ground-based experiments conducted on rapidly cooled aluminum-indium alloys have shown the phase separation to be extremely sensitive to composition with regions near the critical composition providing massively separated phases which nucleated and grew in much less than a second. A high volume fraction of second phase and the close proximity of neighboring droplets in this composition range has been used to explain the basic instability of these structures.

(6) We have found evidence to support the hypothesis that in the aluminum-rich region of the miscibility gap, the indium-rich phase nucleates at the crucible walls during cool-down and because of its wetting properties, spreads out along the walls. As the indium-rich content of the miscibility gap alloys increases, there is a greater tendency for aluminum-rich spheres to nucleate at the crucible walls.

(7) Additional work is required to corroborate and confirm some of the mechanisms thought to be important in the phase separation process. Additional analysis is also required to assess the possible role other mechanisms may play in the phase separation of the aluminum-indium alloys and other miscibility gap systems.

RECOMMENDATIONS FOR FUTURE WORK

Based on the results of our SPAR II and SPAR V ground base and flight experiments, we would recommend the following areas for futher investigation:

(1) Conduct confirming ground base work on the thermocapillary migration of aluminum droplets. This work should include thermocapillary migration experiments parallel and anti-parallel to gravity and studies aimed at providing an understanding of the role of liquid-liquid interfacial energy on this behavior. It will also be necessary to obtain measurements of these energies to compare with the theoretical calculations and for use in checking the thermocapillary migration predictions.

(2) Conduct further work on surface tension drive convecation currents induced either by temperature

gradients or concentration gradients. Analysis and measurement of the change of surface energy for both liquid-gas and liquid-liquid interfaces with temperature and composition a.e necessary. Direct observations of surface deformation and flow during the phase separation process should provide some insight into the presence of surface tension drive flows and/or spreading. A space experiment in which the gas-liquid interface is eliminated would provide information on the relative roles played by the gas-liquid vs. liquid-liquid interfaces on surface tensior driven fluid flows.

(3) Perform research work on transparent miscibility gap systems having various interfacial energies and physical properties in order to directly observe fluid flow phenomena that might be leading to massive separation. Extensive grov-d base study should be conducted initially and then extended to the low gravity environment.

(4) Perform particle pushing experiments on aluminum-rich solid spheres in an indium-rich host liquid in order to confirm the interpretation of various aspects of the microstructure attributed to the interaction of the solid-liquid indium interface with the solid aluminum-rich spheres.

(5) Conduct experimental work on other metallic miscibility gap systems in order to obtain a range of physical parameters so as to provide insight into their effect on the phase separation process. Theoretical analyses on the interfacial behavior of these systems should be conducted to aid in their selection. Both ground base and flight studies will be necessary.

(6) Determine the influence of container-liquid interactions on the evolution of the final micro- and macrostructures. A containerless experiment will provide one extreme of behavior while other containers of various wetting characteristics will provide additional information.

(7) Continue the work on the diffusion behavior above the miscibility gap in order to both obtain accurate measurement of the diffusion coefficients in the aluminum-indium system as well as in other metallic miscibility gap systems. In addition, the close examination of the microstructures thus produced will provide insight into the initial stages of the phase separation for the different systems as a function of composition.

REFERENCES

1. B. Predel, "Beitrag Zur Konstitution und Thermodynamik von Entmischungssystemen", Zeitschrift fur Metallekunde, 56 (1965) 791.

2. J. L. Reger, "Study of Processing Immiscible Materials at Zero-G", Interim Report to NASA-MSFC, Contract NAS8-28267 (May, 1973).

3. A. J. Markworth, W. Oldfield, J. Duga, and S. H. Gelles, "Investigation of Immiscible Systems and Potential Applications", Final Report to NASA-MSFC, Contract NAS8-29748 (April, 1975).

4. S. H. Gelles, E. W. Collings, W. H. Abbott, and R. E. Maringer, "Analytical Study of Space Processing of Immiscible Materials for Superconductors and Electrical Contacts", Final Report to NASA-MSFC, Contract NAS8-31445, (September, 1976).

5. A. J. Markworth, S. H. Gelles, J. J. Duga, and W. Oldfield, "Immiscible Materials and Alloys", in Proceedings of the Third Space Processing Symposium, NASA Report No. 74-5, p. 1003 (June, 1974).

6. S. H. Gelles and A. J. Markworth, "Final Post Flight Report on SPAR II Experiment No. 74-30, Agglomeration in Immiscible Liquids", Report to NASA-MSFC, Contract NAS9-31543 (December, 1976).

7. S. H. Gelles and A. J. Markworth, "Microgravity Studies in Liquid Phase Immiscible System: Aluminum-Indium", AIAA Journal, 16 (1978) 431.

8. R. M. Barrer, Diffusion in and through Solids, University Press, Cambridge, 1951, p 14.

9. A. Bewersdorff, "A Mechanism for Macroscopic Phase Separation in Emulgated Liquid Systems" Paper VIII 2.2, COSPAR Meeting, 1978.

10. E. W. Otto, "Static and Dynamic Behavior of the Liquid-Vapor Interface during Weighlessness", Aerospace Chemical Engineering, 62 (1966) 158.

11. J. T. Neu and Robert J. Good, "Equilibrium Behavior of Fluids in Containers at Zero-Gravity", AIAA Journal, 1 (1963) 814.

12. C. Potard, "Directional Solidification of Aluminum-Indium Alloys at Microgravity: Results of Basic Preparatory Investigations", Presented at the 17th Aerospace Sciences Meeting AIAA held in New Orleans, January 15-17, 1979.

13. S. T. Zamarca, L. Ganovici, and I. Ganovici, "Self-Diffusion of Indium and Liquid Indium-Aluminum Alloys", Revue Roumaine de Chimie, 14 (1969) 35.

14. J. W. Colby, "MAGIC-Computer Program for Quantitative Electron Microprobe Analysis", Advances in X-Ray Analysis (J. B. Newkirk, G. R. Mallett, and H. G. Pfeiffer, Editors) Vol. II, Plenum Press, 1968, p 287.

15. L. Lacy, personal communications, 1978.

16. C. J. Smithells, Metals Reference Book 5th Edition, Buttersworth, London, 1976, p. 939.

17. "Experiments for Materials Processing in Space, Liquid Phase Miscibility Gap Materials, Eleventh Monthly Progress Report to NASA-MSFC, S. H. Gelles Associates, Contract NAS8-32952, March, 1979.